Rapid Quantitative and Qualitative Screening of Naphthenic Acids in Contaminated Waters Using Condensed Phase Membrane Introduction Mass Spectrometry

by

Dane René Letourneau
BSc, from Vancouver Island University, 2013

A Thesis Submitted in Partial Fulfillment
of the Requirements for the Degree of

MASTER OF SCIENCE

in the Department of Chemistry

Supervisory Committee

Rapid Quantitative and Qualitative Screening of Naphthenic Acids in Contaminated Waters Using Condensed Phase Membrane Introduction Mass Spectrometry

by

Dane René Letourneau
BSc, Vancouver Island University, 2013

Supervisory Committee

Dr. Erik Krogh, Co-Supervisor
(Department of Chemistry, Vancouver Island University)

Dr. Tom Fyles, Co-Supervisor
(Department of Chemistry)

Dr. Chris Gill, Departmental Member
(Department of Chemistry, Vancouver Island University)

Abstract

Supervisory Committee

Dr. Erik Krogh, Co-Supervisor
(Department of Chemistry, Vancouver Island University)

Dr. Tom Fyles, Co-Supervisor
(Department of Chemistry)

Dr. Chris Gill, Departmental Member
(Department of Chemistry, Vancouver Island University)

Naphthenic acids (NA) are a highly complex mixture of aliphatic carboxylic acids that may contain multiple rings and unsaturated double bonds, and are a subset of the naphthenic acid fraction components (NAFC), which can contain heteroatoms, unsaturations, and aromatic structures. Mono-carboxylated NAs can be classically represented by $C_nH_{2n+z}O_2$ where z is a negative integer representing the hydrogen deficiency. NAs and NAFCs are components of the acid extractable organics (AEO) frequently associated with increased toxicity and observed at elevated concentrations in oil sands process waters (OSPW). Numerous chromatographic and mass spectrometry techniques have recently emerged to probe the composition and concentrations of these components. This thesis reports the use of a capillary hollow fiber polydimethylsiloxane (PDMS) membrane mounted on a probe interface that can be immersed directly into an aqueous sample. A methanol acceptor phase passing through the lumen transports analyte to an electrospray ionization source and a triple quadrupole mass spectrometer. This technique, termed condensed phase membrane introduction mass spectrometry (CP-MIMS), allows for rapid screening of *m/z* profiles and on-line quantification of NAs in complex samples within minutes. This thesis reports parametric studies of several model carboxylic acids and a standard naphthenic acid mixture (Merichem) involving the effect

of sample pH on membrane transport and acceptor phase pH on ionization enhancement. Several quantitative strategies are explored including the use of an internal standard in the acceptor phase to correct for ionization suppression and variations in instrument sensitivity, and the use of selected ion monitoring (SIM) experiments to increase analytical sensitivity and potentially target specific NA isomer classes for quantitation. Analytical performance measures such as the linear dynamic range (1-2300 ppb $[NA]_T$ as Merichem), sensitivity (~1 ppb $[NA]_T$ as Merichem detection limit), precision (~20 %RSD for replicates of a single OSPW) and accuracy are reported. Quantitative results for various OSPW samples in the ppb to ppm range are reported as equivalents of several surrogates, including 1-pyrenebutyric acid (PyBA), Merichem, and a large-volume extract of northern Alberta OSPWs. The variety of quantitation strategies allows results to be compared with several other published methods. CP-MIMS results for three mid-range northern Alberta OSPWs are compared to analysis by Environment Canada with an average -21% bias. Results for five archived OSPWs spanning a wider concentration are compared to data from AXYS Analytical, with an average -49% bias. Applications of CP-MIMS as an *in-situ* monitor of removal efficiencies of NAs on adsorbents and real-time mass profile changes are also presented, along with some interpretation of the resulting high-resolution kinetic data to obtain decay constants. Using the targeted SIM method, adsorption decay can be followed in real-time for various isomer classes within the Merichem mixture, and kinetic data extracted to obtain decay constants for each. CP-MIMS is also used to characterize adsorption behavior for two activated biochars, including % removals for various loadings of each when added to stirred Merichem solutions. Preliminary multi-loading experiments are conducted with one biochar, and the ability of CP-MIMS to characterize adsorbent behavior by constructing adsorption isotherm plots is demonstrated.

Table of Contents

List of Tables

List of Figures

List of Abbreviations

AEO: acid extractable organics

API: atmospheric pressure ionization

APCI: atmospheric pressure chemical ionization

APPI: atmospheric pressure photoionization

CP-MIMS: condensed phase membrane introduction mass spectrometry

DA: decanoic acid

ESI: electrospray ionization

GC-MS: gas chromatography-mass spectrometry

HPLC: high-performance liquid chromatography

I.S.: internal standard

LC-MS: liquid chromatography-mass spectrometry

M.C.: Merichem naphthenic acid mixture

MeOH: methanol

MIMS: membrane introduction mass spectrometry

MS: mass spectrometer

NA: naphthenic acids

NAFC: naphthenic acid fraction components

OSPW: oil sands process-affected waters

PDMS: polydimethylsiloxane

PPB: parts-per-billion (μg/kg)

PPM: parts-per-million (mg/kg)

PyBA: 1-pyrenebutyric acid

QqQ: triple-quadrupole mass spectrometer

SIM: selected ion monitoring

SPE: solid phase extraction

SVOC: semi-volatile organic compound

SW: surface water

TIC: total ion count

VOC: volatile organic compound

Acknowledgments

The author would like to acknowledge the contributions and support from fellow AERL colleagues, particularly Gregory Vandergrift, Kyle Duncan, Daisy Feehan, and Larissa Richards. This work would not have been possible without the excellent supervision and inspiration of Dr. Erik Krogh and Dr. Chris Gill at the AERL, and Dr. Tom Fyles at UVic Department of Chemistry. The author gratefully acknowledges Vancouver Island University and the University of Victoria for their ongoing support of students in the Applied Environmental Research Laboratories. Special thanks to Harold Malle, John Headley and Kerry Peru at Environment Canada and David Layzell at University of Calgary for providing samples, and Coreen Hamilton, Million Woudneh and John Cosgrove at AXYS Analytical Services, Sidney, BC for performing the SPE-LC-MS/MS analyses used in the comparison studies. The author is grateful for the financial support of this work provided by the Natural Science and Engineering Research Council (NSERC) of Canada through the CGS-M, Discovery, and USRA programs.

Chapter 1: Introduction

1.1 Naphthenic Acids

1.1.1 Athabasca Oil Sands

The oil sands (or 'tar sands') in northern Alberta, Canada represent the second largest oil deposit in the world, containing 1.7 trillion barrels of oil as bitumen.[1] Primarily contained in three locations (Athabasca, Cold Lake and Peace River), these oil sands cover an area the size of the province of New Brunswick. The Athabasca area is the largest of these at 40,000 km^2, with many deposits located close enough to the surface (< 75 m) to be mined. The remaining deeper deposits are located between 300 and 700 meters below the surface,[2] and require other, *in-situ* techniques to recover the bitumen from its sand and clay matrix. The extraction, refining, and transport of this valuable resource represents a vast, growing industry centered around Fort McMurray, Alberta, with hundreds of billions of dollars invested in the last 15 years alone.[3] Employing thousands of Canadians and generating around a quarter of Alberta's GDP, the oil sands are a major contributor to Canada's economy, with continued growth planned – according to the Alberta government, oil sands production is expected to increase from 2.3 million barrels per day in 2014 to 4 million barrels per day in 2024.[3] Indeed, considering the huge variety of industrial and consumer products made from crude oil, including fuels, plastics, solvents, waxes, lubricants, and dyes (to name just a few),[4] it seems that this demand will continue for the foreseeable future until sustainable alternatives are realized. Fig. 1 highlights the general location of the major oil sands deposits in northern Alberta.[5]

Figure 1: Map of Athabasca, Peace River, and Cold Lake oil sands, northern Alberta, Canada (Wikimedia Commons)

Concurrent with the growth of industry, concerns about the environmental impact of oil sands extraction operations have been at an all-time high in the public conversation, with issues such oil pipeline projects and contaminated waters regularly making headlines in news sources and on social media.[6, 7] Issues such as the controversial Northern Gateway pipeline proposed by Enbridge have sparked significant concerns about oil spills, both on land and at sea, particularly in areas such as the northern BC coast. Contaminated waters

in the Athabasca oil sands area have also raised many concerns, including potential health issues in First Nations communities and local wildlife populations.[8-10]

The Athabasca oil sands bitumen is located underground, although there are naturally occurring deposits visible along the banks of the Athabasca river and roadway outcrops.[11] Bitumen can be recovered from the shallower deposits by open-pit surface mining, but deeper deposits require underground (or *in-situ*) techniques, such as toe-to-heel air injection (THAI), vapour extraction (VAPEX), or cyclic steam stimulation (CSS). One of the most common *in-situ* techniques is steam-assisted gravity drainage (SAGD), which uses high-pressure steam to heat the bitumen, reducing its viscosity and making it easier to pump out of the ground as a heterogeneous emulsion.[2] There are a variety of strategies for separating hydrocarbons from the sand and clay formations they are naturally found in. For surface mining operations, large quantities of caustic warm water are used (i.e. in the Clark hot water process), consuming two to four barrels of water for every barrel of oil extracted.[12] During its contact time with the bitumen, the alkaline water can accumulate a variety of organic compounds, including naphthenic acids (NA). These resulting oil sands process waters (OSPW) are highly saline, and after use, they are stored in huge tailings ponds because their release into the environment is strictly prohibited under a zero-discharge policy.[12] Collectively, these tailings ponds comprise an area of approximately 130 km^2 and are now a major feature of the northern Alberta landscape.[12]

1.1.2 Oil Sands Process Waters

Oil sands process waters are complex mixtures, and can contain a variety of hydrocarbons, salts, suspended solids, residual bitumen, and fine silts as well as the water-soluble naphthenic acids.[1, 13] OSPWs have been found to be both acutely and chronically toxic, with salinity levels, pH, and dissolved organics contributing to overall mixture toxicity.[14] However, the acid extractable organics (AEO) including naphthenic acids have been suggested as the primary agents of OSPW toxicity, with known toxic effects on various organisms including algae, protozoa, bacteria, invertebrates, fish, and mammals,[14-16] and suspected endocrine disrupting activity.[17] In particular, the lower

molecular weight NAs (< 22 carbons) have been observed to have the highest potency.[15] Although NAs can be found at background levels in northern Alberta rivers (usually below 1 ppb), they can be as high as 110 ppm in OSPW.[18] They can enter surface water through groundwater mixing, erosion of riverbank oil deposits, and seepage from tailings ponds.[19, 20] Fig. 2 displays a NASA satellite image of an open-pit mine, tailings pond, and industry surrounding the Athabasca river in northern Alberta, where the proximity of the tailings pond to the river is clearly visible.

Figure 2: A tailings pond and surface mining operation surrounding the Athabasca River in northern Alberta, Canada (NASA)

Environmental concerns regarding these process waters have therefore been at an all-time high as various wildlife encounters, pipeline debates, and reports of leakages provoke public interest in the oil sands.[20-22] In particular, a great deal of attention has been directed towards a better characterization and understanding the primary toxic components of these waters, the naphthenic acids.[13]

1.1.3 Naphthenic Acids, Naphthenic Acid Fraction Components, and Acid Extractable Organics

The classically defined naphthenic acids arise from the acid extractable fraction of OSPW, and represent a complex mixture of largely aliphatic carboxylic acids typically containing one or more rings, with MWs ranging from 200-600 Da, and thousands of individual compounds revealed in high-resolution mass spectrometry data. Mono-carboxylated NAs can be represented by $C_nH_{2n+z}O_2$, where z is a negative integer representing the hydrogen deficiency (resulting from rings and/or double bonds). Fig. 3 shows a variety of classical NA structures, as described by Grewer et al.[23] Recent work has also revealed the presence of aromatic moieties in the classically defined NA structure class.[24, 25]

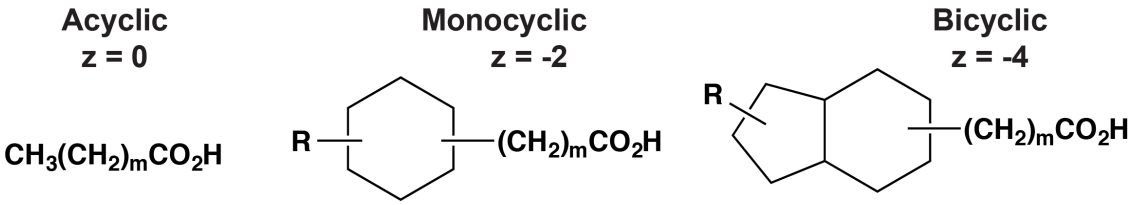

Figure 3: Classical naphthenic acid structures

Since the composition of a particular OSPW sample will be very sensitive to how the sample was handled and processed leading up to analysis, it is important to have an understanding of the operational definitions involved. The acid extractable organic (AEO) fraction of a water sample is typically obtained by lowering the pH of the sample to ~2 and extracting with an organic solvent (such as dichloromethane).[26] As such, AEOs include a collection of organic compounds that are neutral and hence soluble in an organic solvent under acidic conditions. Some AEO protocols also include a solvent wash of the ambient sample to remove neutral, relatively non-polar components (e.g., polyaromatic hydrocarbons) prior to acidification and extraction.[26] Regardless, classical NAs will be a component of AEO, and other compound classes observed will be influenced by how the extraction from OSPW has been performed.

Recently, the term 'naphthenic acid fraction components' (NAFC) has been employed to describe the larger variety of structurally related compounds found in the AEO fraction of process waters, including NAs which incorporate heteroatoms and functionalities other than carboxylic acids.[13, 27] Defining exactly what compounds the NAFCs represent can be complicated, as there is a difference between operationally defined classes or sub-classes of molecules based on solubility differences, and structural definitions based on the presence or absence of particular functional groups or moieties. This is further complicated by the fact that definitions are evolving over time (i.e. aliphatic R-CO_2H versus aromatic R-CO_2H both fit the classical $C_nH_{2n+z}O_2$ definition of NAs). This is in part due to the fact that in early studies characterizing NAs with nominal mass resolution, $z < -6$ were not identified due to the inability to distinguish 12 hydrogens from 1 carbon. Today, with the emergence of high mass resolution data via techniques such as FT-ICR-MS,[4, 13] the molecular formula information to define heteroatom classes (i.e. SO_2, NO_2, etc.) is now available, helping to clear up at least some of these issues. Fig. 4 shows how AEOs, NAFCs, and NAs are related and how they are currently defined.[27]

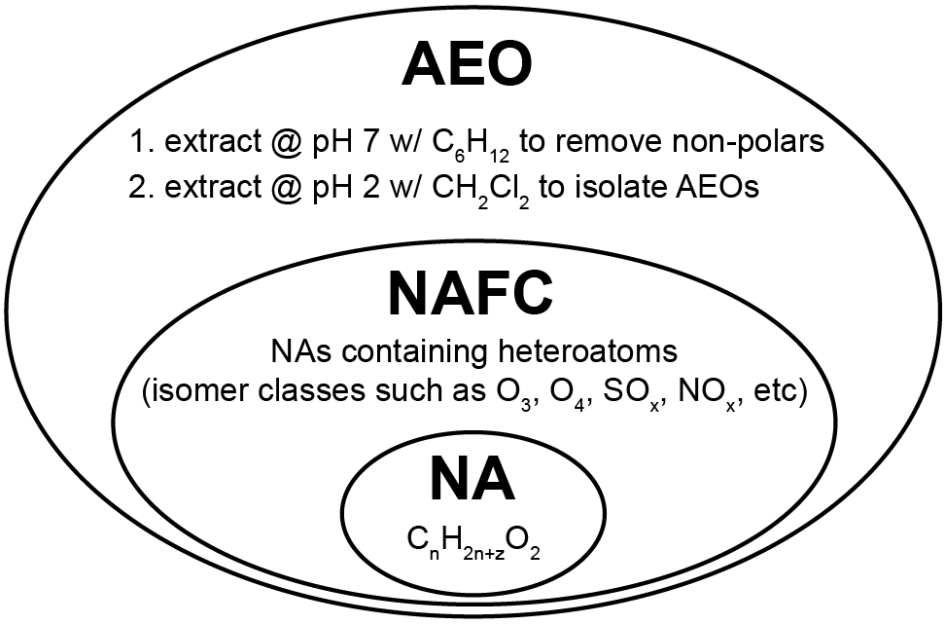

Figure 4: Classification of AEO, NAFC, and NA components

With high-resolution data, NAFCs can be divided into classes, such as those containing O_2 moieties (classical NAs) versus those containing some other number of heteroatoms

(e.g., O_x where x does not equal 2, SO_x, NO_x, etc). Some representative structures of NAFCs in OSPW are shown in Fig. 5, and Table 1 lists some various NAFC compound classes found in an OSPW as revealed by high-resolution Fourier transform ion cyclotron mass spectrometry with four different atmospheric ionization techniques, as performed by Barrow et al.[4] These include positive and negative electrospray ionization (ESI), as well as positive and negative atmospheric pressure photoionization (APPI).

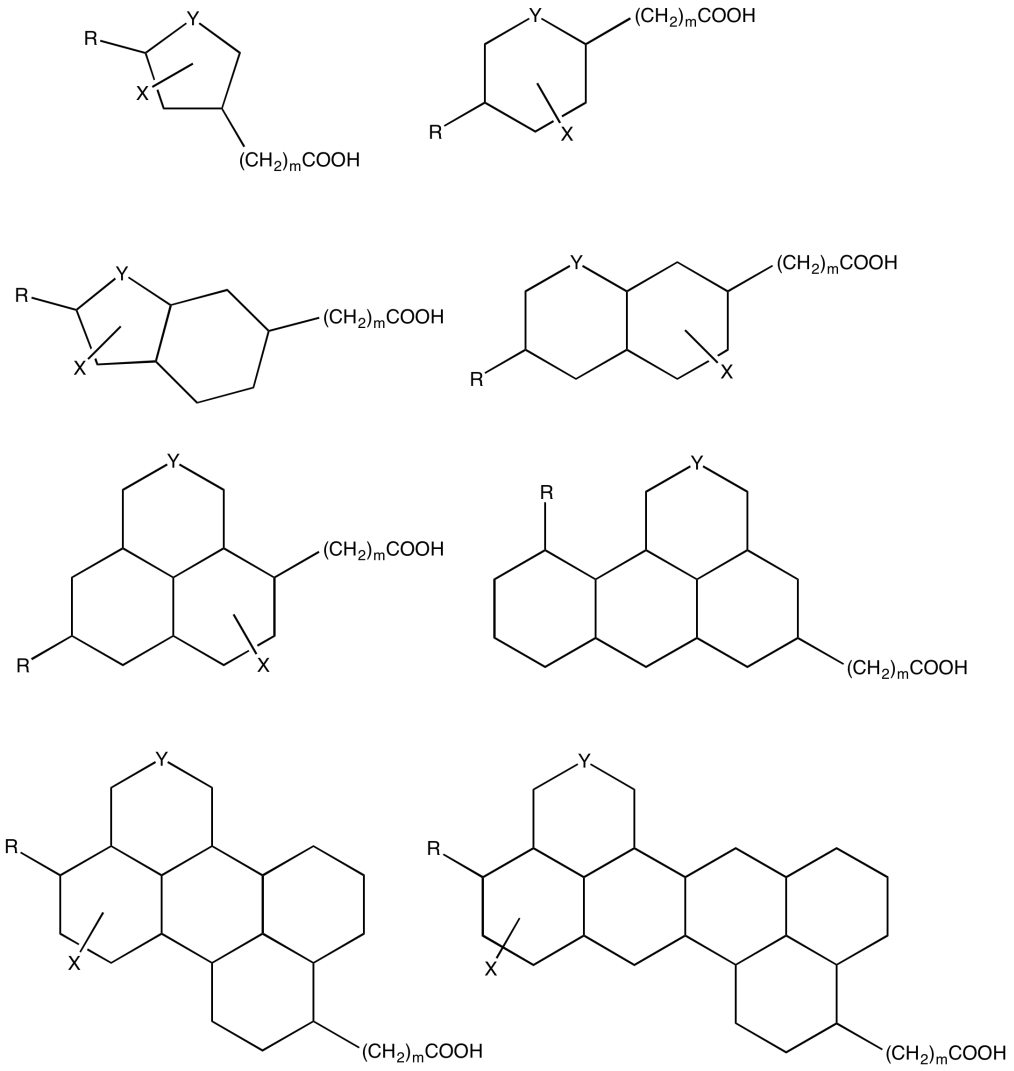

Figure 5: Representative structures of naphthenic acid fraction components (NAFC) in OSPW including the classical naphthenic acids and other acid extractable organics with aromatic functional groups, nitrogen and sulfur atoms, along with unsaturated groups. R = alkyl group, X = COOH, R, OH, SO_x, NO_x, or SH, and Y = C, S, or N. Ring structures may not be fully saturated (figure adapted from Headley et al.[28])

Table 1: High-resolution FT-ICR-MS data from the direct infusion of an AEO mixture isolated from an Athabasca OSPW

Compound class	% of total intensity for 4 ion sources			
	ESI-	ESI+	APPI-	APPI+
CH	0	0	0	12
N	0	<1	1	8
S	<1	0	1	3
O_x	77	58	59	37
O_xS	20	28	30	15
O_xS_2	1	3	3	1
NO_x	<1	10	3	16
NO_xS	0	0	0	<1

All data from Barrow et al.[4]

Table 1 demonstrates the wide variety of structural diversity of compounds in the acid extractable fraction of an Athabasca OSPW sample, and how the compound classes observed are influenced by the ionization technique employed (method bias). For this OSPW, the extraction was performed by the method described by Rogers et al.,[26] including allowing gravity settling of solids, acidifying tailings to pH 2.5, extracting with dichloromethane, collecting the organic phase and reconstituting at pH 13, filtering the insolubles, and isolating the low (< 100 Da) MW acids from the mixture (which were then called 'naphthenic acids'). The choice of ionization technique has a major influence on the compounds identified in the mixture. In particular, APPI is able to reveal some classes of compounds not seen when using ESI (CH, N, S). The majority (77%) of ions seen in negative-ion ESI are observed to belong to the O_x class, which includes the classical NAs as well as NAs with additional oxygen-containing functional groups such as ethers, ketones and/or hydroxyl groups. Considering that the O_2 negative ion class (~classical NAs) is emerging as the primary contributor to NAFC mixture toxicity,[29] a rapid screening or quantitation method based on the direct analysis of sample components that are neutral at acidic pH and readily ionize by negative ion ESI would be relevant and convenient.

1.2 Emerging Analytical Techniques

Scientific interest in naphthenic acids has increased greatly over the last 15 years. A search of the Web of Science database[30] for topic 'naphthenic acids' from the years 2000-2015 shows a clear trend in number of publications addressing this topic (Fig. 6). Nearly a third of the total publications on this topic from 2000-2015 were in research area 'chemistry', with almost half of these published in the last 4 years alone.

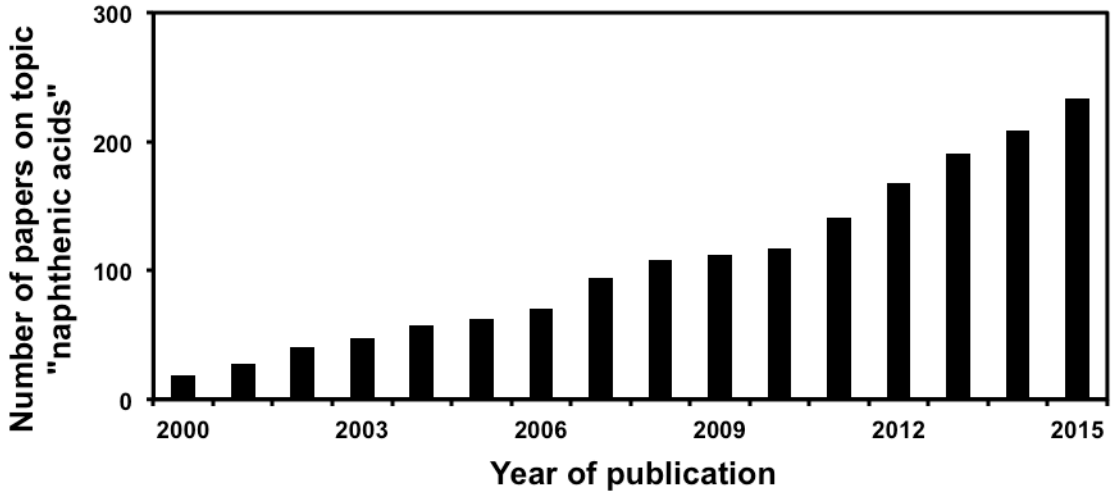

Figure 6: Number of publications in the topic 'naphthenic acids' over the last 15 years, based on a search using the Web of Science database[30]

As a result of this rapidly growing interest, a multitude of both qualitative and quantitative analytical techniques have emerged to better separate, identify, and quantify individual components in NAFC mixtures, as well as assess total NA concentrations. Many incorporate mass spectrometry, taking advantage of the sensitivity and selectivity of this technique, including powerful resolving capabilities and the wealth of information available from high-resolution mass spectra. The Headley group at Environment Canada (Saskatoon, SK) has compiled several excellent reviews of recent advances in mass spectrometric characterization of naphthenic acids.[13, 31] Many of the techniques reviewed pair chromatographic separations with mass spectrometry, including variations of LC-MS used to characterize mostly classical NAs and model NA compounds.[19, 32-38] Two-

dimensional GC-MS (2D-GC-MS) has been useful for examining isolated compounds in complex OSPW mixes, including adamantane and diamondoid components[39] and individual bicyclic aromatic acids.[40] Gas chromatography on chemically derivatized NAs has also been used in combination with Fourier transform ion cyclotron resonance mass spectrometry (GC-FTICR-MS)[41, 42] to give researchers the power of resolving compounds with chromatography, and for co-eluting components, resolution through ultra-high resolution FT-ICR-MS. Capillary electrophoresis (CE) was used by MacLennan et al. to perform efficient separations of NAFCs prior to analysis with TOF-MS, ionized by both positive and negative-ion ESI.[43] Differential mobility spectrometry (DMS), or by another name, field asymmetric ion mobility spectrometry (FAIMS), represents another possible avenue of separating complex mixtures with NAFCs prior to a mass spectrometric analysis.[44] Another emerging ionization technique is APPI,[4, 45] a powerful atmospheric pressure ionization (API) source that allows researchers to observe NAFCs not ionized by the more conventional and common ESI sources (see Table 1 previously). Finally, orbitrap mass spectrometers are relatively new to the field, but can offer resolution on par with FT-ICR-MS, and in one example, were used for the purposes of determining NAFCs in matrices such as plant tissue.[46] In another recent example, ESI-HRMS with an orbitrap was used to measure the solar photocatalytic degradation of naphthenic acids in OSPW, a promising 'green' advanced oxidation process (AOP) for OSPW treatment.[47]

Despite the emergence of a number of eloquent analytical techniques, a number challenges remain. These include 1) the inherent complexity of NAFCs, containing several thousand components ranging in concentration over six orders of magnitude (pptr to ppm) in environmental samples, 2) the inherent biases introduced by different ionization techniques and 3) the lack of discrete analytical standards and agreement on units of expression.[23] The last of these in particular makes it very difficult to compare or validate analytical methods. Refined Merichem naphthenic acids, a popular 'standard' mix of NAs made by the Merichem Company (Houston, TX)[48] has been used by many as a benchmark, but batch-to-batch variability is a concern, in addition to Merichem itself being an immensely complex mix and not necessarily representative of northern Alberta

NAFCs. Fig. 7 shows a high-resolution direct infusion mass spectrum of Merichem,[49] with hundreds of peaks visible when zooming in further on the high-resolution data (not shown). With the use of additional chromatographic methods such as 2D GC (GCxGC) to separate NA isomers, the number of individual NAFC compounds resolvable in a high-resolution spectrum increases from hundreds to thousands.

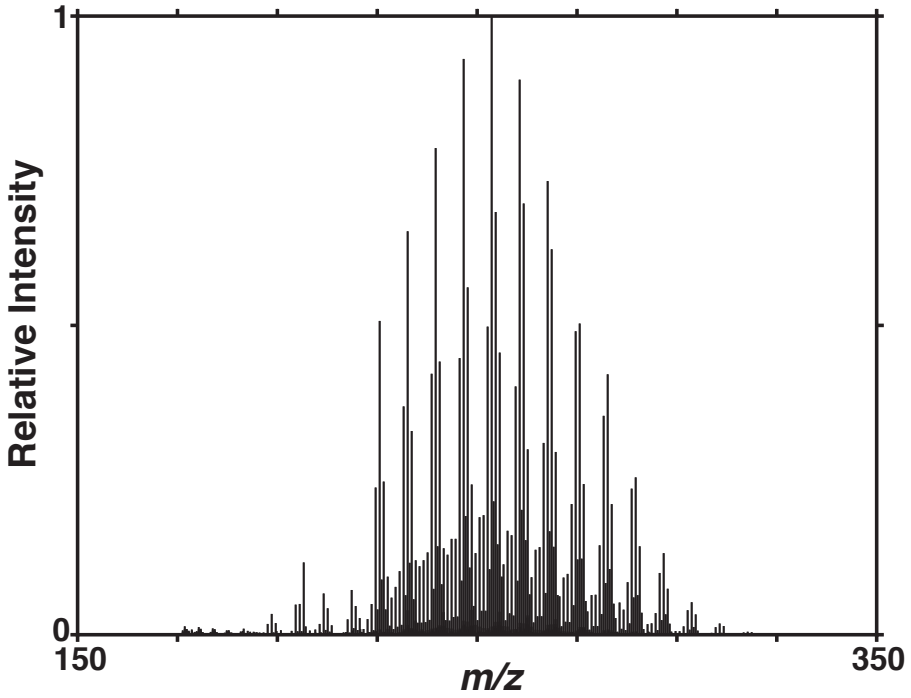

Figure 7: High-resolution direct infusion spectrum of Merichem (reproduced by permission from Duncan et al.[49])

In 2009, Headley et al. stated that "in the absence of availability of authentic standards for the individual components in the naphthenic acid mixtures, to date MS quantification is at best semi-quantitative. Further research is encouraged to develop quantification procedures for congener-specific analyses."[31] Fortunately, since then there have been some developments towards obtaining quantitative data. Woudneh et al.[50] successfully used LC-MS with derivatization of NA mixtures to quantitatively describe NA isomer classes in OSPWs expressed in terms of a surrogate compound 1-pyrenebutyric acid (PyBA). In addition, an inter-lab calibration study conducted by Environment Canada in 2012[51] assessed the capabilities of 15 different methods to detect classical NAs in oil

sands process waters and spiked water samples over a concentration range of environmental relevance (1–50 ppm).[13] More recently, Duncan et al. from our group developed a technique for rapid on-line screening of naphthenic acids directly in complex samples without chromatography, using condensed phase membrane introduction mass spectrometry (CP-MIMS).[49] Bypassing the extensive sample cleanup steps usually encountered in chromatographic methods, Duncan achieved semi-quantitative results for a variety of OSPW, surface, and ground waters from northern Alberta, laying the groundwork for the research presented in this thesis.

1.3 Condensed Phase Membrane Introduction Mass Spectrometry (CP-MIMS)

1.3.1 Membrane Introduction Mass Spectrometry (MIMS)

Membrane introduction (or inlet) mass spectrometry (MIMS) is a direct sampling technique that can be employed as an on-line quantitative analysis method for trace level analytes in complex samples.[52-54] Although MIMS has been around for over 50 years,[55] it has only recently been more fully explored for applications in the bio-analytical and environmental fields,[49, 56-63] and there remain a variety of exciting applications for this technique. MIMS employs a membrane in direct contact with the sample that is permeable to a suite of molecules, which are subsequently transferred to a mass spectrometer as a mixture for resolution based upon their mass to charge ratio (*m/z*) and/or by unique fragmentations [e.g., tandem mass spectrometry (MS/MS)]. The membrane, often constructed of hydrophobic polydimethylsiloxane (PDMS), serves to reject the bulk of the sample matrix, while pre-concentrating analytes from the sample based on their physicochemical properties. A variety of other membrane materials are possible, including materials such as Nafion™.[64, 65] Various ionization techniques and mass analyzers have been employed, providing selective *m/z* measurements with analytical sensitivities in the picogram range (ppt-ppb in solution).[66] In addition, by

continuously operating the mass analyzer, MIMS systems can be used to provide temporally resolved data for multiple analytes in dynamic chemical systems.

The on-line nature of MIMS allows researchers to make rapid, direct measurements in complex samples within minutes, with few or no sample preparation steps. For example, MIMS has been used to directly measure pharmaceuticals and other persistent organic pollutants (POP) in wastewater,[59] dissolved gases and volatile organics in seawater,[57] and a wide variety of organic compounds in aqueous solution.[62, 67-73] Many continuous monitoring applications are possible, including the real-time monitoring of atmospheric contaminants from a moving vehicle,[56, 58] photolysis of organics in water,[74] biogenic volatile organic compound (BVOC) emissions from plants,[75] and chloroform formation and degradation.[76, 77] The excellent kinetic resolution available with MIMS has given rise to studies investigating the photodegradation of halogenated pollutants in waters containing natural organic matter (NOM),[78] the destruction kinetics for aqueous hydrocarbon contaminants at low, environmentally relevant (e.g. nanomolar) concentrations,[79] and the mechanism of benzene derivative degradation with Fenton's reagent.[80] This technique has also been used to screen adsorbents and other binding agents, including the study of small organic guest molecules in cyclodextrin hosts,[81] screening of polyaromatic hydrocarbon (PAH) contaminated sand,[82] and adsorption of organic compounds on activated carbon and in solid-phase extraction (SPE) experiments.[83] MIMS also has a variety of applications in the bio-analytical field, including the measurement of chloroform formation from aqueous algae suspensions,[76] dissolved gases and low molecular weight volatiles resulting from microbiological activity,[84] and catalysis by enzymes.[85]

The overall sensitivity of MIMS depends on the steady-state (S.S.) flux of analyte across the membrane, as well as the efficiency of the chosen ionization source for a particular analyte. According to Fick's first law, for diffusion through a membrane in one dimension, the S.S. flux (J_{ss}) is given by Eqn. 1, where A is the surface area of the membrane in contact with sample, D is the diffusivity of the permeant (analyte) in PDMS, K is the partition co-efficient for the permeant between aqueous sample and

PDMS membrane (approx. K_{ow}[86]), C_s is the concentration of permeant in the sample, and l is the membrane thickness.[87]

Equation 1: $$J_{ss} \propto \frac{ADKC_S}{l}$$

The analyte signal response time in MIMS is limited by the kinetics of mass transport through the membrane (typically seconds to minutes). In general, thinner membrane interfaces increase flux and decrease the analytical response time. Consequently, an analyte's characteristic signal risetime (τ) is a function of its intrinsic properties such as diffusivity (D), which depends largely on size (i.e. molar volume) in addition to extrinsic factors including the membrane thickness (l)[87] as given by Eqn. 2.

Equation 2: $$\tau \propto \frac{l^2}{D}$$

These equations describe diffusion behavior in one dimension, for flat-sheet membrane. In this thesis, a capillary hollow fiber membrane was used, which is three-dimensional and therefore has a different form of the Fick's law equation. The S.S. flux for a hollow fiber membrane is described by Eqn. 3, where L is the length of the hollow fiber; C_1 and C_2 are the concentrations of the substance in the sample and acceptor phase-sides of the membrane, respectively; and r_o and r_i are the outer and inner radii of the hollow fiber, respectively.[87]

Equation 3: $$J_{SS} = 2\pi LD(C_1 - C_2)/\ln\left(\frac{r_o}{r_i}\right)$$

If the acceptor phase side of the membrane experiences a constant flow of sweep gas or solvent, C_2 becomes very small relative to C_1. Since C_1 is the product of the partition co-efficient K and concentration in the sample (C_S) the more generalized form of the S.S. flux equation can be summarized as follows in Eqn. 4:

Equation 4: $$J_{SS} = 2\pi LDKC_S/\ln\left(\frac{r_o}{r_i}\right)$$

Fig. 8 summarizes the processes taking place at the membrane interface (partitioning, diffusion, and desorption) and depicts the time evolution of the concentration gradient that drives mass transport across the membrane. An analyte in the aqueous phase ($X_{(aq)}$) partitions into the PDMS membrane, $X_{(PDMS)}$. Diffusing through the PDMS for distance *l*, it then desorbs off the backside into a sweep gas, now $X_{(g)}$. Towards the bottom of the figure is a visualization of the concentration profile across the membrane from when an analyte is first introduced (t_0) to when it reaches steady-state (t_∞). The time required to pass through this non-steady state region is known as the risetime (τ), and is characteristic for a particular analyte (size) and set of extrinsic conditions (temperature, pressure, membrane viscosity and thickness).

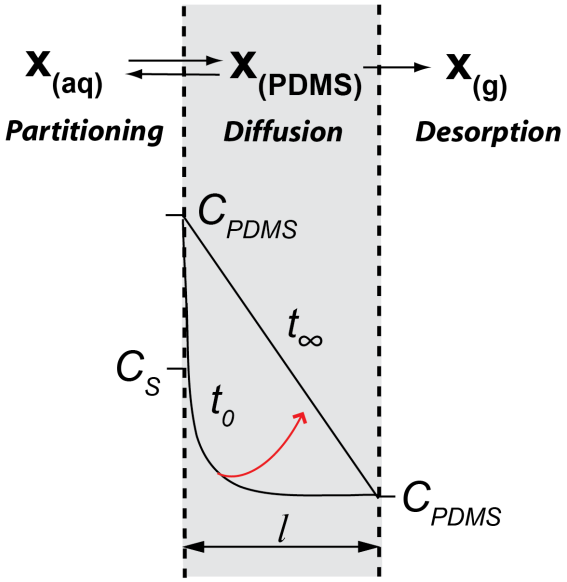

Figure 8: Membrane mass transport schematic

The initial aqueous concentration (C_S) gives rise to an elevated concentration (C_{PDMS}) once the analyte has partitioned into the membrane. This pre-concentration in PDMS is related to the relative solubility of the analyte in PDMS and water. At steady-state, the concentration gradient is maintained by the constant sweeping of analyte off the backside of the membrane. The concentration gradient is a function of the magnitude of the partition coefficient and the membrane thickness. It governs the mass transport of analyte from the sample to the sweep gas (or acceptor solvent, as will be discussed) and then on

to the mass spectrometer. Fig. 9 shows what a typical chronogram signal trace for the rise to steady-state and rinse-out processes looks like. At ~10 min, the membrane is exposed to a 15 ppb aqueous triclosan solution at pH 7. By ~20 min, this signal has risen to steady-state and is left there for ~30 mins before being rinsed out with MeOH at ~47 min.

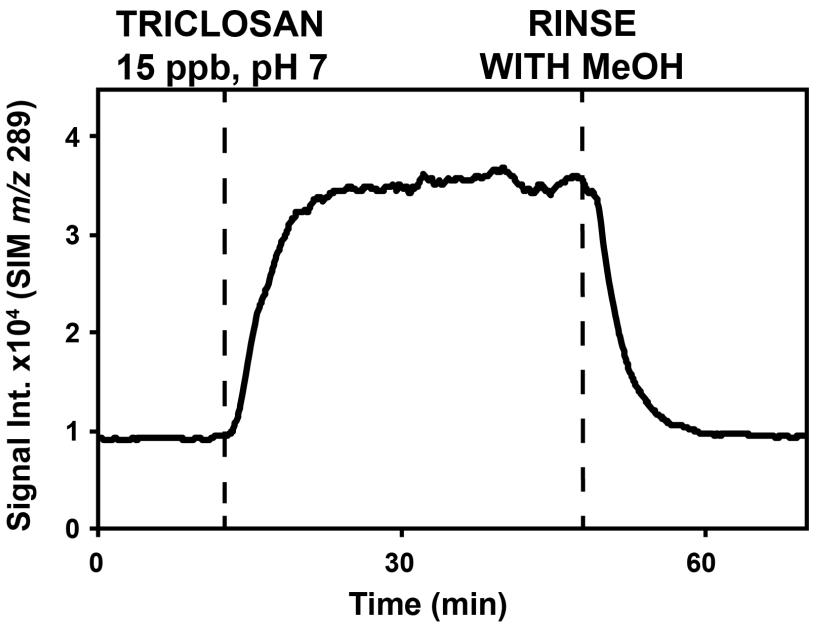

Figure 9: General chronogram showing MS signal rise to steady-state in response to 15 ppb aqueous triclosan solution, monitored by CP-MIMS (Datafile: DLMIMS_007)

1.3.2 Condensed Phase Membrane Introduction Mass Spectrometry (CP-MIMS)

In CP-MIMS, the sweep gas flowing through the lumen of the capillary hollow fiber membrane is replaced with a solvent (or 'condensed phase'), usually methanol. This opens up the MIMS technique to a wider range of analytes, as polar or non-volatile compounds not amenable to transfer to the gas phase in conventional gas-phase MIMS can be easily solvated in a liquid acceptor. Different ionization sources are required to handle a liquid acceptor phase, primarily atmospheric ionization methods such as electrospray ionization (ESI), atmospheric pressure chemical ionization (APCI) and atmospheric pressure photoionization (APPI). This further opens the field of possible MIMS analytes to include molecules that readily fragment in harsher ionization

conditions, as well as those not suited for transfer to the gas phase. Indeed, since its development only a few years ago, CP-MIMS has been used to rapidly quantify a variety of polar and low-volatility analytes, including pharmaceuticals and other contaminants in wastewater down to parts per trillion levels,[59] and has been characterized for use with a variety of membranes, ionization sources and mass spectrometers.[88] Fig. 10 summarizes the components of a CP-MIMS setup, emphasizing the 'tunability' of each stage for a particular matrix and/or analyte.

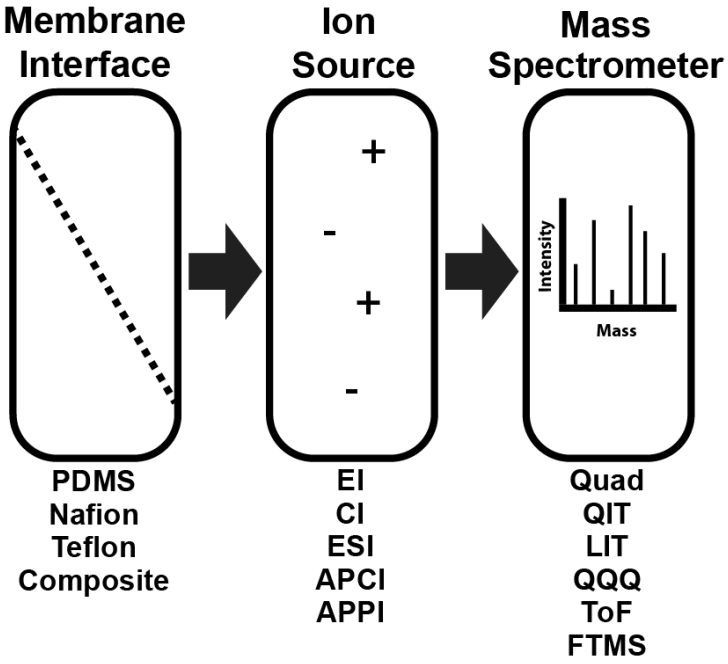

Figure 10: MIMS components (modified from Krogh et al.[66])

Several membrane probe interface configurations were tested, including co-axial flow configurations, before the current 'J-probe' design was developed,[59, 60] schematic displayed in Fig. 11. The J-probe is a simple design involving a small 2 cm piece of hollow PDMS capillary friction mounted on a stainless steel hypodermic tube support, where the liquid acceptor phase flows through the inner lumen of the membrane. The probe is easily rinsed between samples, and is easy to replace in the case of contamination or damage. In addition, the simplicity of a dip-probe design makes it amenable to pairing with an auto-sampler for rapid throughput analysis[59] and *in-situ* reaction monitoring in heterogeneous samples.

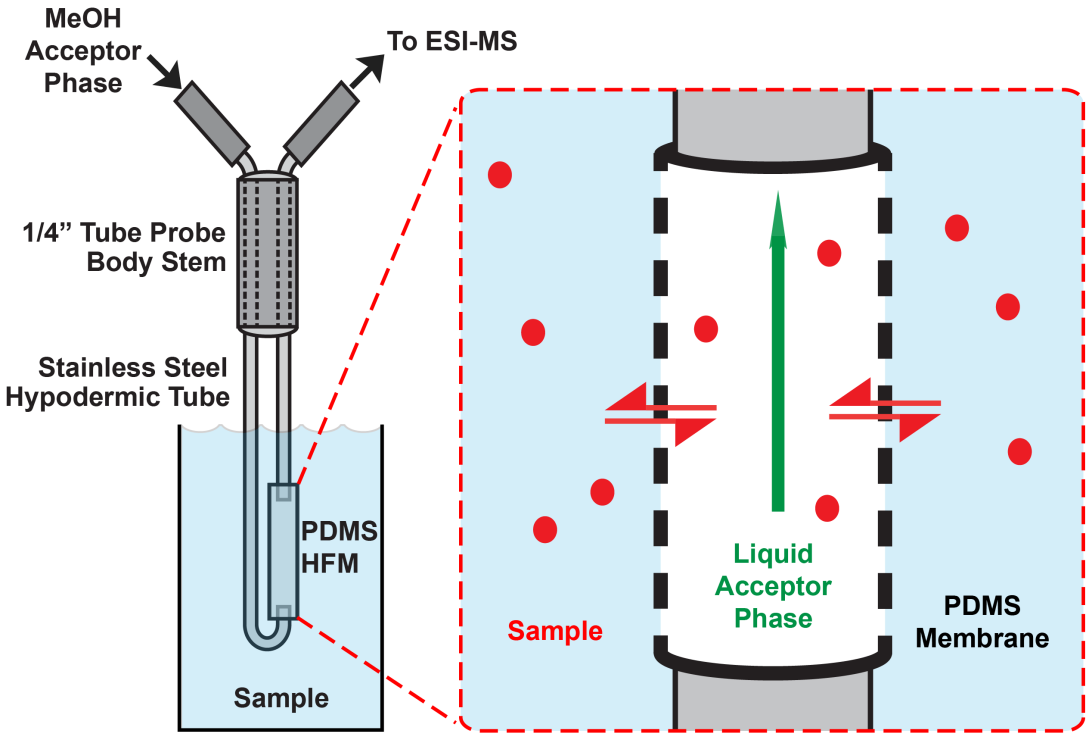

Figure 11: CP-MIMS membrane in the 'J-probe' configuration. Inset shows detail of the sample molecules permeating the membrane and dissolving into the liquid acceptor phase

CP-MIMS has potential to be the basis for a rapid on-line method for direct screening of NA in complex mixtures. NAs are acidic, so protonation should produce neutral species ($pH < pK_a$) that will partition into the PDMS membrane. The PDMS membrane is expected to reject the bulk sample matrix, particularly salts and other components found in OSPW that could otherwise result in significant ion suppression, and can easily be rinsed with MeOH between samples with little to no sample memory. In contrast to other quantitation strategies, such as HPLC-MS, no sample cleanup is required for complex, heterogeneous OSPW samples. In addition, ESI is a well suited ionization source for carboxylated species, which have been demonstrated to readily form $[M-H]^-$ ions in the literature.[89] The selectivity and sensitivity of mass spectrometry should allow for quantitative results to be obtained for complex NA mixtures within minutes. Finally, the vast information contained in the MS fullscan should allow for the observation of NA mass profile changes in real-time to monitor physical or chemical processes such as

degradation or adsorption, and for the rapid screening of possible NA adsorbents for effectiveness with the wealth of high-resolution kinetic data available through MIMS.[78]

Our group recently used CP-MIMS to obtain semi-quantitative results for NAs in complex matrices.[49] In Chapter 3, strategies are explored to improve this technique to attempt quantitative results comparable to other published methods. The primary challenge is the lack of analytical standards or benchmarks for NAs. This challenge was addressed from a variety of perspectives, including exploring and comparing various units of reporting. First, studies were conducted with model NA compounds to investigate the conditions (pH, concentration) under which NAs would cross the PDMS membrane and experience good sensitivity with the CP-MIMS system without suffering significant ion suppression. Attempts were made to correct for the effects of suppression and variations in instrumental sensitivity through the use of an internal standard (I.S.) correction factor. Ionization of carboxylated species was improved with the addition of aqueous base to the acceptor phase. Sensitivity was improved for quantitation in complex samples by targeting specific isomer classes through the use of 30 SIM experiments based on the most common *m/z* in the mass spectrum of a common NA mixture. Calibration curves were constructed to attempt quantitative results with a set of OSPW samples. Several quantitation strategies were developed to report $[NA]_T$ as equivalents of various surrogates, both single compounds and mixtures. These explorations resulted in an improved and optimized CP-MIMS system for NA analysis, and in several alternative quantitation strategies that were compared to other published methods. Some areas of application of CP-MIMS may be able to exploit the ability of the technique to work with complex heterogeneous samples for real-time analysis of dynamic systems, yet not require fully quantitative analysis. Chapter 4 explored one such application (the adsorption of NAs on biochars), and reported screening experiments on sample biochars conducted at the semi-quantitative mass profile level. High-resolution kinetic data allowed decay rate-constants for selected components to be extracted, and experiments conducted with multiple biochar loadings lead to adsorption isotherms for the several biochars evaluated.

Chapter 2: Experimental

This section is intended to discuss general experimental details pertinent to both Chapters 3 and 4, with specific information contained in separate Experimental sections for each chapter, to follow.

2.1 Standard and Sample Preparation

A 25 g aliquot of Merichem NAs (Merichem Company, Houston, TX, USA) was kindly provided by H. Malle at Environment Canada as part of the batch used for the inter-lab calibration study conducted in 2012,[51] and used to make up Merichem standards in both MeOH and aqueous solution. Real-world samples were collected from northern Alberta by our group, and include several industrial oil sands processed waters (OSPW) and natural surface waters. Surface waters (SW) were collected from the Christina river (a natural river several hundred kilometers south of Fort McMurray) and the Athabasca river, both upstream and downstream from the major bitumen surface mining activities. They were well oxygenated, with relatively low total dissolved solids, and dominated by dissolved $CaCO_3$. Oil sands process waters were collected from various locations and include SAGD plant waters, mining tailings waters, mining area surface drainage, and waters from conventional surface mining operations. All water samples were collected in June 2012, filtered through glass micro-fiber filters (GF/C, Whatman, Fisher Scientific) and stored at 4 °C until analyzed by CP-MIMS. Several filtered OSPW samples (OSPW7, 8 and 9) were obtained from an inter-lab calibration study as performed by Environment Canada,[51] but accidentally froze and thawed when a laboratory fridge broke down, and were marked as such. Total organic carbon values were measured as non-purgeable organic carbon (Shimadzu TOC-VCPH, Shimadzu Corporation, Tokyo, Japan) by Zack Yim. Before analysis, all samples were pH adjusted to 7 or < 4 using concentrated base (NaOH) or acid (HCl), added dropwise, or buffered at pH 3.60 ± 0.1

with glycine buffer. Samples known to contain high concentrations of NAs, particularly OSPW1, 2, and 3 and Merichem, were diluted before analysis. Selected water quality parameters for samples where data was available are summarized in Table 2. All data (except TOC values) collected by Erik Krogh.

Table 2: Water quality parameters for real-world water samples studied

Sample[a]	[DOC] (ppm C)	[TOC] (ppm C)	Sp. Cond. (μS cm^{-1})	pH	Turbidity (NTU)	Sample source
OSPW1	434	416	7600	9.5	-	SAGD plant water
OSPW2	2600	2500	100,000	11.3	-	SAGD plant water
OSPW3	218	185	10,300	7.96	-	SAGD plant water
OSPW4	11.5	11.0	750	7.16	82	Mining tailings water
OSPW5	12.2	12.5	907	7.24	19	Mining tailings water
OSPW6	8.2	7.6	795	7.85	0.98	Mining surface area drainage
SW1	10.1	9.7	175	8.15	240	Athabasca river (upstream from mining at Ft McMurray WWT)
SW2	28.5	28.9	229	8.10	10.2	Athabasca river (downstream from mining at Ft MacKay bridge)

[a]All samples collected June 2012

2.2 Condensed Phase Membrane Introduction Mass Spectrometry (CP-MIMS)

2.2.1 Experimental Apparatus

Fig. 12 illustrates the CP-MIMS experimental apparatus used in this thesis. The solvent reservoir contains a MeOH acceptor phase, degassed with a helium sparge line to prevent pumping irregularities. The acceptor phase also contains an added internal standard (typically decanoic acid) used to correct for signal variation due to instrument drift and

ion suppression at the API interface. The acceptor phase is delivered to the lumen of a 'J-probe' design immersion CP-MIMS probe with PEEK™ tubing (0.76 mm ID) using low dead volume PEEK™ unions (VICI Valco, Brockville Ont., Canada). The remainder of the PEEK™ tubing used is 0.25 mm ID to reduce internal dead volume and achieve higher linear velocities in the transfer lines between the membrane interface and the API source. A micropump (Cheminert Model M6, VICI Valco™, Houston, TX, USA) pulls solvent from the probe and passes the flow on to the API source and the triple quadrupole mass spectrometer (Micromass Quattro LC and Micromass Quattro API with an ESCi multi-mode ionization source, Waters-Micromass, Altrincham, UK). A syringe pump (Harvard Apparatus Pump11 Elite equipped with a 25 mL Hamilton Gastight® syringe) is used to deliver 10 μL/min of 2.0% aqueous NH_4OH (Anachemia, environmental grade) into the acceptor phase (final concentration 0.1% after mixing) through a PEEK™ T-junction located after the membrane probe, before the solvent is passed to the API source. A flow divert valve allows solvent to be passed to waste when the mass spectrometer is off. It is also possible to use this valve and a syringe pump to bypass the membrane entirely for a direct infusion experiment, if desired.

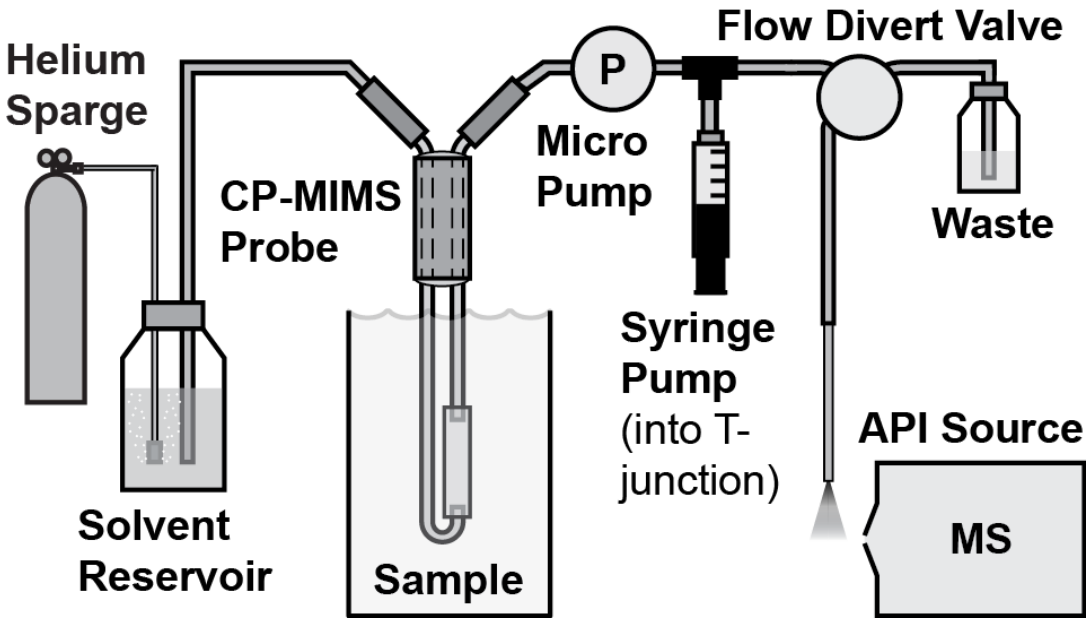

Figure 12: CP-MIMS experimental schematic

2.2.2 Membrane Interface

In-house constructed membrane interfaces were used for this work in the immersion 'J-probe' configuration as outlined in a previous published work.[59] Briefly, hexane (HPLC grade, Fisher Scientific, Ottawa, Ontario, Canada) was used to swell a 2 cm piece of PDMS hollow fiber membrane [Dow Corning Silastic® tubing, outside diameter (OD) = 0.64 mm, inside diameter (ID) = 0.30 mm, 170 μm thickness, Midland, MI, USA], which was subsequently friction mounted on stainless steel hypodermic tubing supports (22 gauge, Vita Needle Co., Needham, MA, USA). A methanol acceptor phase solvent was pulled through the lumen of the PDMS membrane at 200 $\mu L/min^{-1}$ by a low internal volume four piston micropump (Cheminert Model M6, VICI Valco™, Houston, TX, USA).

Sample measurements were made by immersing the membrane probe directly into continuously mixed aqueous samples in 40 mL glass sample vials (Scientific Specialties Inc., Hanover, MD, USA) or 20 mL vials when conserving valuable samples. Sample mixing was accomplished using a magnetic stir plate (Corning PC-420D). Naphthenic acids were analyzed after adjusting the sample pH with either small additions of 6M HCl (Fisher Scientific) to a value below the pK_a of typical organic carboxylic acids (i.e. pH < 4) or diluting into the glycine buffer mentioned previously (pH = 3.60 ± 0.1), protonating carboxylate ions (to yield their neutral form) to facilitate transport across the PDMS membrane. Control experiments to observe neutral compounds present in the sample, conducted at pH ~7, were achieved by raising the sample pH with 6M NaOH (Fisher Scientific) prior to measurement. Sample pH was monitored with a pH meter (Accumet AR25, Fisher Scientific) and/or pH indicator strips (Sigma-Aldrich, Oakville, ON, Canada). All experiments were conducted under ambient conditions (approximately 25 °C, 101 kPa).

2.2.3 Mass Spectrometry

Mass spectrometry experiments (unit mass resolution) were performed using two triple quadrupole mass spectrometers (Micromass Quattro LC and Micromass Quattro API with an ESCi multi-mode ionization source, Waters-Micromass, Altrincham, UK). Negative ion ESI was used for NA analysis with a capillary voltage of 3.2 kV, an entrance cone voltage of 30 V, and a source temperature of 120 °C in conjunction with full scan MS (*m/z* 100–600, 1 s scan time). Selected ion monitoring experiments utilized a 0.5 s dwell time for each *m/z* monitored. Most experiments were conducted with fullscan and SIM experiments incorporated into a single analytical method. Desolvation and cone gas flows (ultra-high-purity grade nitrogen, Praxair, Nanaimo, Canada) were maintained at flows of 750 L/h and 50 L/h respectively, and heated to 300 °C.

2.3 Data Handling

2.3.1 Signal Processing and Mass Spectra

All steady-state MIMS signals were averaged over at least 5 minutes of data (10 minutes preferred) using a 10-point moving boxcar window in Microsoft Excel, and subsequently background subtracted. The location of the 5 minute 'window' used for signal averaging was determined by the time of the event following a steady-state signal in the experimental sequence (i.e. another injection or a rinse) and averaging data for the 5 minutes of signal previous to this. All fullscan data was obtained between *m/z* 100-600, and exported from the MassLynx™ software into Excel after being filtered to eliminate minor peaks under 2% total intensity. Any spectral subtractions (i.e. background subtractions, or pH 4 – pH 7 subtractions for certain OSPW samples) were performed in the MassLynx™ software before exporting. Graphic mass spectra were generated from raw data with the Python programming language using the open-source Matplotlib in the SciPy package[90] and worked up into final figures using Adobe Illustrator (CS5.1).

2.3.2 Internal Standard Correction Factor

Decanoic acid was added to the methanol acceptor phase to correct for variations in signal due to instrument drift and/or ionization suppression. A known volume of MeOH was added to the acceptor phase solvent bottle, and the experiment was started and allowed to baseline on pure solvent. After baseline was achieved, a concentrated spike of decanoic acid stock solution in MeOH was injected into the acceptor bottle and well mixed. The final concentration of decanoic acid (typically 10 ± 1 ppb) was calculated from the known volume of the injected slug and MeOH in the acceptor bottle (less the solvent that had been drawn out pre-injection, calculated based on the known flow rate of the acceptor phase). After the decanoic acid signal had stabilized, the experiment proceeded with the measurement of NA-containing samples. The decanoic acid signal was used to correct all signals, as shown below in Eqn. 5.

Equation 5: $$Corrected\ signal\ (ppb\ DA) = \frac{S.S.\ signal\ of\ OSPW}{S.S.\ signal\ of\ DA} \times [DA]\ (ppb)$$

The averaged steady-state signals for both the OSPW and the DA were taken over the same time window (5-10 minutes of S.S. signal). These internally 'corrected' signals were reported in units of ppb (of DA). Our group has previously observed that co-permeating species can result in significant ionization suppression in the CP-MIMS analysis of concentrated samples.[88] Assuming the ionization suppression effects are similar for all carboxylated species, the decanoic acid added to the acceptor phase reports ionization suppression of the NA analyte signals. It should be noted that significant ionization suppression effects were not typically observed for most of the NA samples reported here (< 5 ppm). More importantly, the corrected signals accounted for variations in instrument sensitivity due to inter/intra-day drift. In addition, this approach also corrected for sensitivity differences between the two mass spectrometers used for this study.

Chapter 3: Quantitative Analysis of Naphthenic Acids by CP-MIMS

3.1 Introduction

One of the primary concerns regarding emerging contaminants such as naphthenic acids are their free and available environmental concentration levels and corresponding toxicity data, as regulatory bodies aim to set limits for the release of these compounds into the environment.[91] In many cases, particularly in industry, a detailed quantitative analysis of a sample is often unnecessary, and decision makers need to know if compounds of concern are present or absent, and if present, if they are above or below current regulatory limits.[91] As introduced in the first two chapters, CP-MIMS is a highly useful tool for these types of semi-quantitative analyses, with the added potential of deploying remotely to achieve rapid screening directly in the field. With the ability to identify high, medium, and low concentration samples with considerable precision, in addition to high data density, low cost, and rapid analysis, CP-MIMS could be used to complement existing analytical methods to screen samples before a costly analysis. However, one of the major goals of this thesis was to try and improve upon the previous semi-quantitative work in our group[49] and further extend the abilities of the CP-MIMS technique to achieve quantitative results for naphthenic acids in complex samples, similar to other mass spectrometry-based methods such as those employed by Woudneh et al.,[50] Ahad et al.,[19] Hindle et al.,[32] Shang et al.[35] and Brunswick et al.[25]

A major challenge in attempting to obtain quantitative information for NA samples lies in the lack of analytical standards to benchmark results against. This is an issue faced by all groups working in this field, as emphasized by Headley et al. in their 2009 and 2015 reviews of NA characterization techniques using mass spectrometry.[13, 31] Naphthenic acids are not a clearly defined set of compounds, and recent advances in characterization of these mixtures reveal thousands of components, including those containing heteroatoms and unsaturations.[13] In addition, these mixtures vary from sample to sample,

location to location, and year to year. A NA sample from northern Alberta may have a very different composition based on when, where, and how it was collected and processed. Biological activity[33] and processes such as oxidation or photodegradation[92] can also affect the composition of these mixtures if appropriate care is not taken to preserve and handle the sample appropriately after collection. Many have chosen to use refined Merichem,[48] a 'standard' NA-mix (as mentioned earlier) as a calibration standard, including an inter-lab calibration study performed by Environment Canada in 2012.[51] However, even Merichem is still an extraordinarily complex mixture, with thousands of compounds identifiable by high-resolution mass spectrometry,[49] and with variations in composition from batch to batch. However, its fairly widespread use and availability made it the primary choice as a standard for quantitation purposes in this thesis. Fig. 13 shows a low-resolution mass spectrum of Merichem at pH 4, obtained via CP-MIMS with a Waters-Micromass QqQ (see section 2.2.3 for instrumental details).

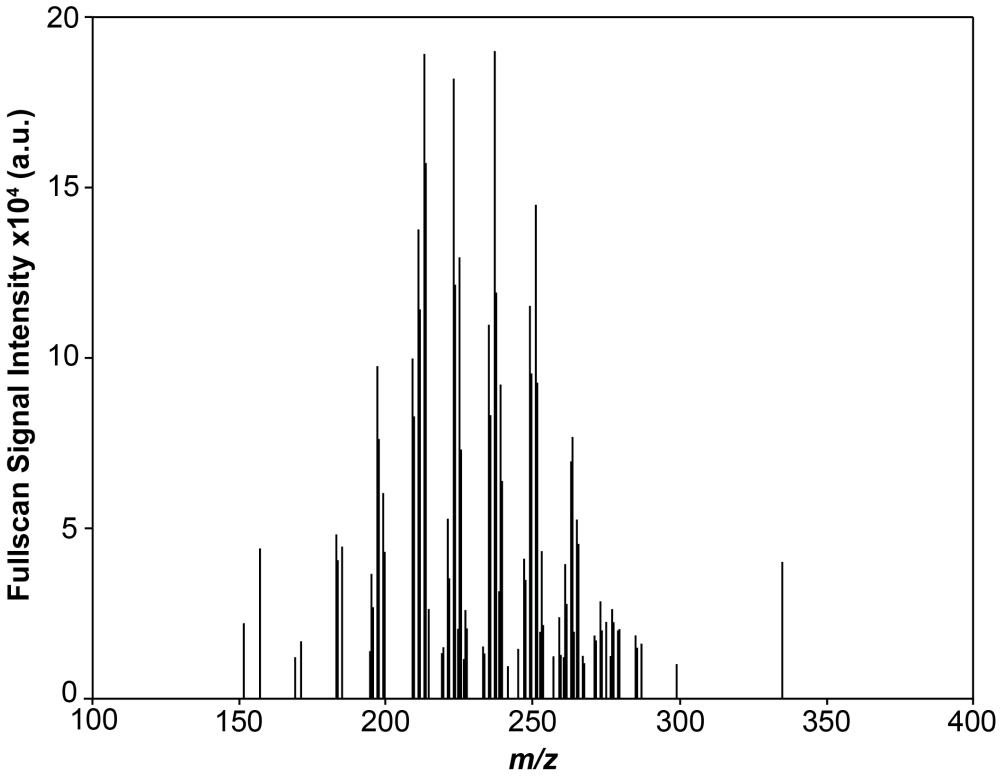

Figure 13: Fullscan low-resolution mass spectrum of Merichem in DI water at pH 4

As an alternative quantitation strategy, AXYS Analytical Services in Sidney, BC chose to use 1-pyrenebutyric acid (PyBA) as a single standard for their SPE-LC-MS/MS method.[50] Although PyBA fits the general formula for a classical naphthenic acid, to date, it has not been widely used as a benchmark among the majority of current quantitative methods.[13] It has the advantage of being a single, well-characterized compound rather than a complex mixture of thousands of compounds (such as Merichem), many of which are unknown. As described in section 3.4.1, all OSPW samples analyzed for this thesis were quantified as equivalents of PyBA (in addition to other quantitation methods), and results were therefore comparable to measurements made by AXYS.[50, 51] Results were also compared to an ESI-HRMS method[47] published by Environment Canada, who generously provided several previously analyzed OSPW samples and extracts used as quantitation standards for their method.[93]

3.2 Experimental

3.2.1 Model Compounds for Method Development

Model compounds were obtained from Sigma-Aldrich (Oakville, Ontario, Canada), including gemfibrozil [5-(2,5-dimethylphenoxy)-2,2-dimethyl-pentanoic acid, ≥ 98.5%], triclosan [5-chloro-2-(2,4-dichlorophenoxy)phenol, 97%], 4-*tert*-butylcyclohexanecarboxylic acid [4-(2-Methyl-2-propanyl)-cyclohexanecarboxylic acid, 99%], 1-pyrenebutyric acid [4-pyren-1-ylbutanoic acid, 97%], decanoic acid (≥ 98.0%), and nonylphenol [4-(2,4-dimethylheptan-3-yl)phenol, ~85%]. Stock solutions of model compounds and Merichem were prepared gravimetrically with HPLC grade methanol (Fisher Scientific, Ottawa, Ontario, Canada), and subsequent standard solutions were diluted in either deionized (DI) water (Model MQ Synthesis A10, Millipore Corp., Billerica, MA, USA) or buffered at pH ~3.5 with glycine/HCl (0.12 M glycine, Fisher Scientific, Ottawa, Ontario, Canada). Care was taken to ensure that there was less than 0.1% methanol in all measured aqueous solutions. Tables 3 and 4 give relevant

physicochemical and mass spectrometry parameters for the six naphthenic acid model compounds chosen for initial quantitation studies.

Table 3: Physicochemical properties of NA model compounds

Compound	IUPAC name	Abbr.	CAS#	M.W.	pK_a[94]
Gemfibrozil	5-(2,5-dimethylphenoxy)-2,2-dimethylpentanoic acid	GF	25812-30-0	250.33	4.5
Decanoic acid	Decanoic acid	DA	334-48-5	172.26	4.9
4-*tert*-butylcyclohexanecarboxylic acid	4-(2-Methyl-2-propanyl)-cyclohexanecarboxylic acid	4tBCHCA	5451-55-8	184.28	5.03
Triclosan	5-chloro-2-(2,4-dichlorophenoxy)-phenol	TC	3380-34-5	289.54	7.9
Nonylphenol	4-(2,4-dimethylheptan-3-yl)phenol	NP	84852-15-3	220.35	10
1-pyrenebutyric acid	4-pyren-1-ylbutanoic acid	PyBA	3443-45-6	288.34	4.9

Table 4: Mass spectrometer parameters for NA model compounds

Compound	SIM (*m/z*)[a]	Cone (V)
Gemfibrozil	249	20
Decanoic acid	171	30
4-*t*-butylcyclohexanecarboxylic acid	183	30
Triclosan	289	30
Nonylphenol	219	40
1-pyrenebutyric acid	287	30

[a] Dwell time = 1 s for all compounds

3.2.2 Standard Solutions and Calibration Curves

Direct Merichem calibration curves were generated by making concentrated injections of Merichem stock solutions in DI water to a pre-weighed 40 mL TOC vial containing ~30 g of 7500 ppm glycine buffer in DI water. Injections were made sequentially in the preweighed vial except for the highest concentration steps (> 1 ppm), where the membrane probe was immersed directly in the more concentrated aqueous Merichem

standards. Data was processed as before (section 2.3.1), with baseline and steady-state signals all averaged over > 5 minutes. Additional OSPW samples were obtained for the purposes of comparing CP-MIMS to another published method, and were kindly provided by Headley and Peru at Environment Canada (Saskatoon, SK)[93] having been previously analyzed using ESI-HRMS (LTQ Orbitrap Elite, ThermoFisher Scientific, San Jose, CA) operating in fullscan and negative-ion mode, with mass resolution set to 240,000 and a *m/z* scan range of 100–600, as per the method published in Leshuk et al.[47] Three OSPWs (OSPW10, 11, 12) were provided along with two large-volume extracts (LVE1 and LVE2), all obtained from different industrial sources. Minimal sample information was provided apart from approximate concentrations of the large-volume extracts (LVE1 ~2700 ppm NAFCs, LVE2 ~8000 ppm NAFCs, both in 0.1N NaOH). Direct calibration curves were constructed for LVE1 and LVE2 in a similar fashion to the Merichem calibration curves described above.

3.2.3 Standard Addition Experiments

Standard addition experiments were performed with a surrogate, model NA compound, 1-pyrenebutyric acid (PyBA). Concentrations of NAs in measured OSPW samples were then reported as equivalents of PyBA, and were therefore comparable to results for the same samples analyzed by AXYS.[50] This was achieved by injecting a concentrated spike of PyBA stock solution (in MeOH) into the NA/OSPW sample contained in a preweighed 40 mL TOC vial, with the final concentration of MeOH below 0.1%. The PyBA signal was monitored with a SIM experiment at *m/z* 287. Once a steady-state signal was achieved for at least 5 minutes, the membrane probe was removed and immersed in MeOH to rinse. The steady-state PyBA signal was averaged and background subtracted, using Eqn. 6 to calculate the concentration of NAs in the OSPW sample as if they were equivalents of PyBA (the average NA signal was also background subtracted):

Equation 6: $$PyBA\ equivalents\ (ppb) = \frac{[PyBA]\ (ppb)}{Avg.\ PyBA\ signal} \times Avg.NA\ signal$$

The average NA signal was either the fullscan TIC for the steady-state signal of the NA sample at pH 4, or the signal resulting from the sum of 30 SIM experiments averaged over at least 5 minutes in the steady-state regions of the NA sample signal at pH 4 (described further in section 3.4.2 of this thesis).

3.3 Studies of Experimental Parameters Affecting the Quantitative Analysis of NAs by CP-MIMS

3.3.1 Sample pH Effect with Model Compounds

Although quantifying naphthenic acids in complex mixtures was the ultimate goal of this work, model compounds were used to optimize experimental conditions before moving on to more complex samples. Six model compounds were chosen as representatives of species that might occur in a typical naphthenic acid mixture: Gemfibrozil [5-(2,5-dimethylphenoxy)-2,2-dimethyl-pentanoic acid], decanoic acid, triclosan [5-chloro-2-(2,4-dichlorophenoxy)phenol], nonylphenol [4-(2,4-dimethylheptan-3-yl)phenol], 1-pyrenebutyric acid [4-pyren-1-ylbutanoic acid] and 4-*tert*-butylcyclohexanecarboxylic acid [4-(2-Methyl-2-propanyl)cyclohexanecarboxylic acid]. The analytical performance of the first five of these compounds was previously characterized using CP-MIMS, and they demonstrated good sensitivity and reasonable signal response times, making them good candidates for this study.[59] Compounds were analyzed in DI water, and in a more complex real-world matrix (Christina river water, northern Alberta).

Fig. 14 shows the chronogram from an experiment performed with four of the six model compounds spiked into a matrix of Christina river water to give final concentrations of 50-70 ppb. The compounds are each monitored by SIM experiments for their corresponding $[M-H]^-$ ions (mass spectrometry conditions detailed in section 3.2.1). At ~40 min, the CP-MIMS probe is introduced to the solution at pH 7, and signal is visible for the hydroxylated species (triclosan and nonylphenol) but not the carboxylated species

(gemfibrozil and decanoic acid). This is because only neutral compounds will pass through the hydrophobic PDMS membrane, leaving behind ionized species. At pH 7, the hydroxylated species are in neutral form and the carboxylated species are ionized, thus only hydroxylated species are observed in the CP-MIMS experiment at this pH. At ~80 min, the probe is rinsed by immersion in methanol, then DI water, and the model compound solution is adjusted to pH 4 offline with concentrated HCl. At ~110 min, the probe is reintroduced to the solution, and all four compounds are visible in the chronogram due to the carboxylated species now being in a neutral form at lower pH. At ~200 min, the probe is rinsed by the same procedure mentioned earlier. As a note, significant variations in signal intensity at steady-state visible in Fig. 14 (after t~140 mins) were a result of experimental/instrumental error and were not a regular observation in most experimental work conducted for this thesis.

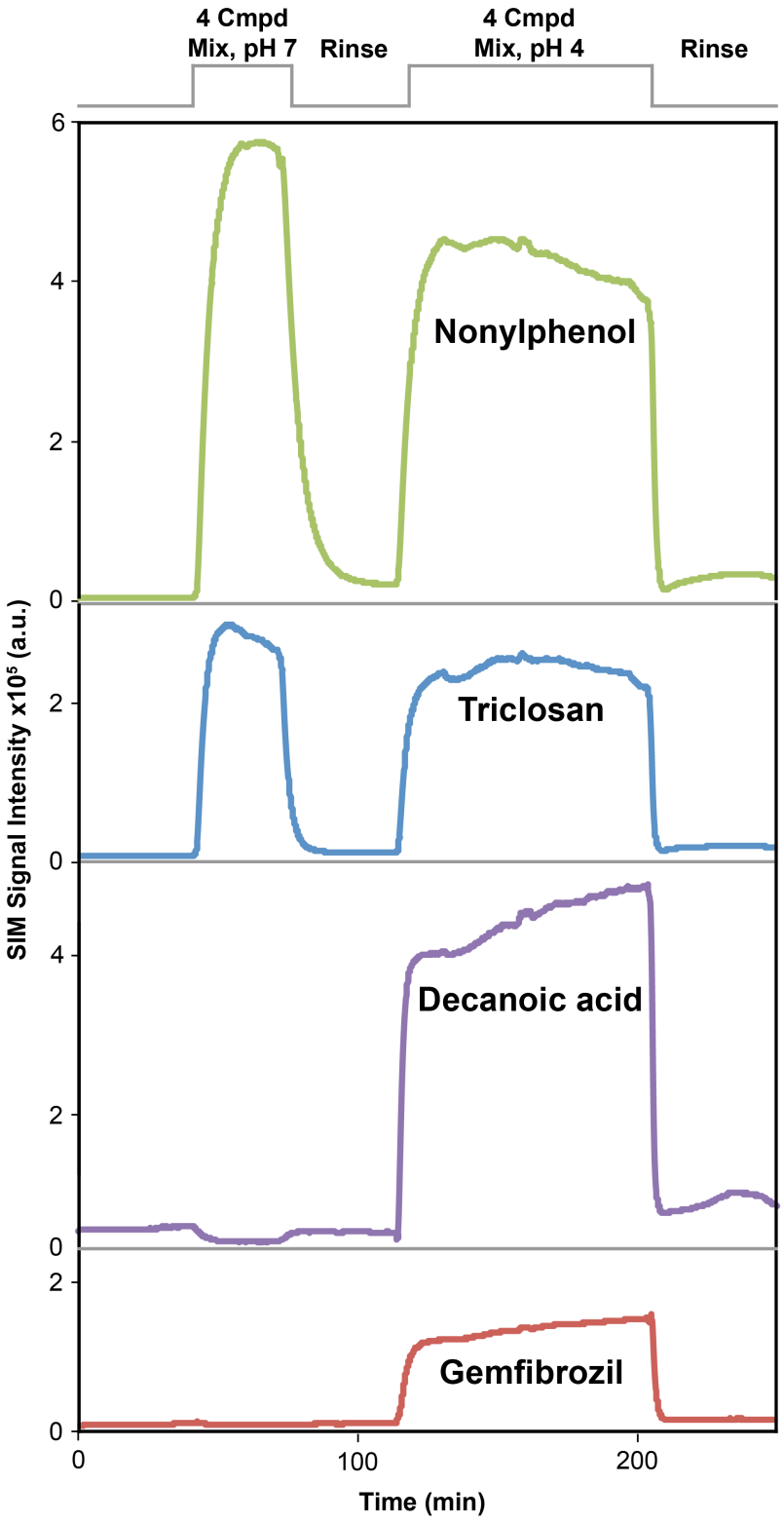

Figure 14: Gemfibrozil, decanoic acid, triclosan, and nonylphenol in Christina River water at pH 7 and 4 (Datafile: DLMIMS_012)

This experiment demonstrates several important features of CP-MIMS. First, only neutral compounds can pass through the membrane, which excludes ionized carboxylated species at pH values > 4. Thus, naphthenic acid samples must be acidified before they can be measured. Second, the presence of both hydroxylated and carboxylated species at pH 4 (and in general, a higher mass load crossing the membrane at lower pH) opens the possibility for ion suppression in the ESI source.[88] To investigate this possibility, a study was conducted to investigate these potential suppression effects, and it was found that carboxylated species suppress both hydroxylated and carboxylated species. Fig. 15 demonstrates this effect in a mixture of four model compounds, each at ~100 ppb, and analyzed at both pH 7 and 4. At pH 7, decanoic acid and gemfibrozil show no signal, as expected (they are ionized in solution and therefore do not cross the membrane), whereas triclosan and nonylphenol experience good sensitivity. At pH 4, however, decanoic acid and gemfibrozil experience good sensitivity while the signals for triclosan and nonylphenol are reduced (suppressed).

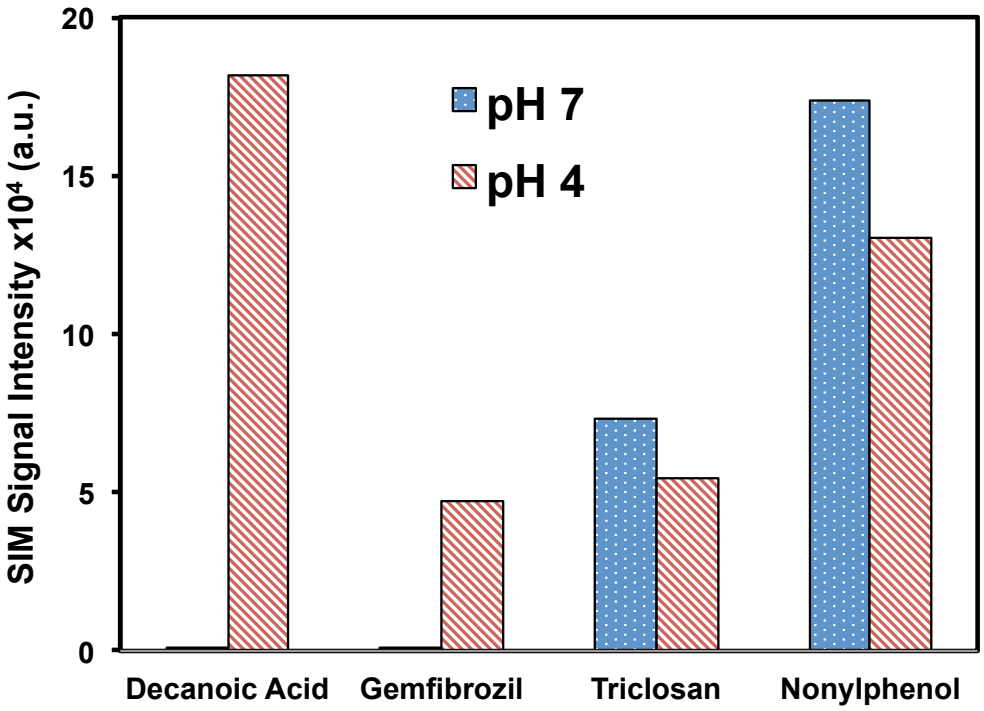

Figure 15: Suppression study with four model compounds at pH 4 and 7 (Datafile: DLMIMS_105)

This experiment was repeated with the concentrations of each component increased to 1 ppm and 3.75 ppm respectively, and similar results were noted. Therefore, it can be concluded that a high concentration of carboxylated species in the ESI source can cause ion suppression for both hydroxylated and carboxylated species, and care must be taken to dilute all concentrated samples before analysis. Additionally, because the decanoic acid internal standard signal is a good indicator of ion suppression, close attention was paid to this signal when measuring samples of unknown concentration for the first time. If significant signal suppression was noted for DA, the sample was diluted and re-analyzed.

Because the pH of a sample can determine what components of a sample mixture cross the PDMS (as discussed previously), it was thought that a pH 4 – pH 7 spectral subtraction would help to isolate and quantify specifically the acidic components (i.e., NAFCs) within a complex OSPW mixture. Fig. 16 demonstrates the effect of changing the sample pH in a complex mixture (5 ppm Merichem made up in DI water), along with a pH 4 – pH 7 spectral subtraction. Three mass spectra are shown: A) Merichem at pH 7, B) Merichem at pH 4, and C) a spectral subtraction of pH 4 – pH 7. Panels A and B clearly show that the components of Merichem appearing at pH 7 (primarily hydroxylated species) are on average higher in mass, but lower in overall intensity, than those appearing at pH 4. This makes sense: At pH 7, carboxylated species are not passing through the membrane, resulting in lower overall signal levels than observed at pH 4, where both hydroxylated and carboxylated species are being detected. Additionally, because of the higher mass load at pH 4, the acids are preferentially suppressing ionization of hydroxylated species, resulting in reduced intensity for the higher masses observed at pH 7. When the pH 4 – pH 7 spectral subtraction is performed (panel C), the result looks like the pH 4 spectrum but reduced in intensity and mass shifted downwards slightly, due to subtraction of the higher-mass hydroxylated components.

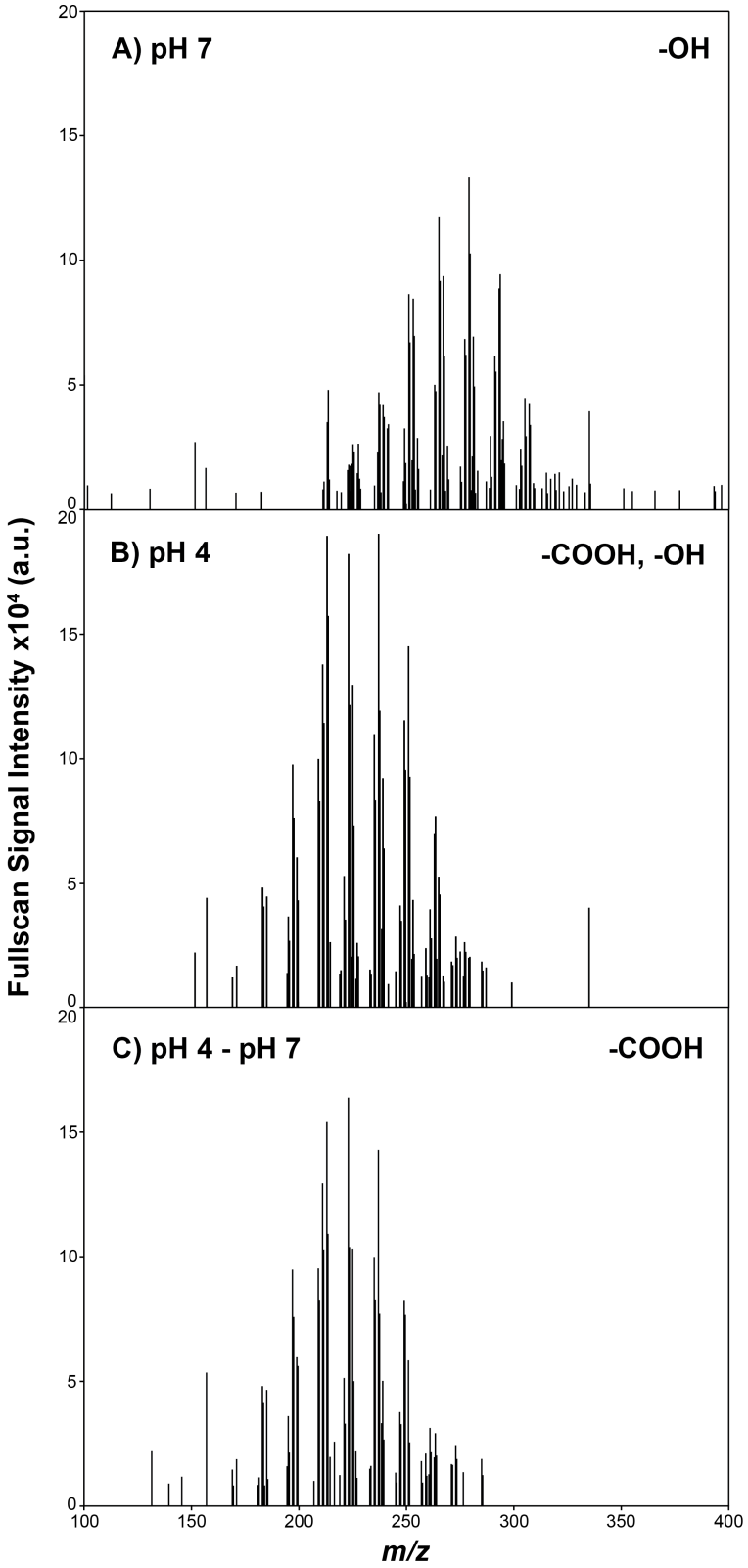

Figure 16: Mass spectra demonstrating the pH correction technique with 5 ppm Merichem in DI water at A) pH 7, B) pH 4, and C) pH 4 – pH 7

Fig. 17 shows chronograms for an experiment involving another complex mixture, this time an OSPW with both high concentrations of non-NA matrix components and NAs. This sample (OSPW2) was diluted 141X before being analyzed, and the pH subtraction technique was attempted in data analysis to try and isolate the NA components from the rest of the complex mixture. The uppermost trace is *m/z* 287, $[M-H]^-$ for the PyBA model compound as well as a common peak in most NA samples. The middle trace is the fullscan TIC, and the bottom is the internal standard (decanoic acid at *m/z* 171). After baseline is established for DA, the CP-MIMS probe is introduced to the OSPW2 sample at pH 7. Signal suppression is noted for all signals (this normally indicated that the sample should be diluted and re-analyzed). The probe is rinsed in MeOH, then DI water, and reintroduced to the OSPW2 sample, now adjusted to pH 4. The fullscan TIC and *m/z* 287 show signal rise after an initial signal drop due to ion suppression, while the DA signal is significantly suppressed, highlighted by the red shaded region of the signal trace (mostly due to the larger amount of material coming across the membrane at pH 4). Following this, a 75 ppb spike of PyBA is added directly to the OSPW2 sample as a standard addition experiment (with no ion suppression noticeable) before the probe was rinsed with MeOH and the measurement duty cycle completed.

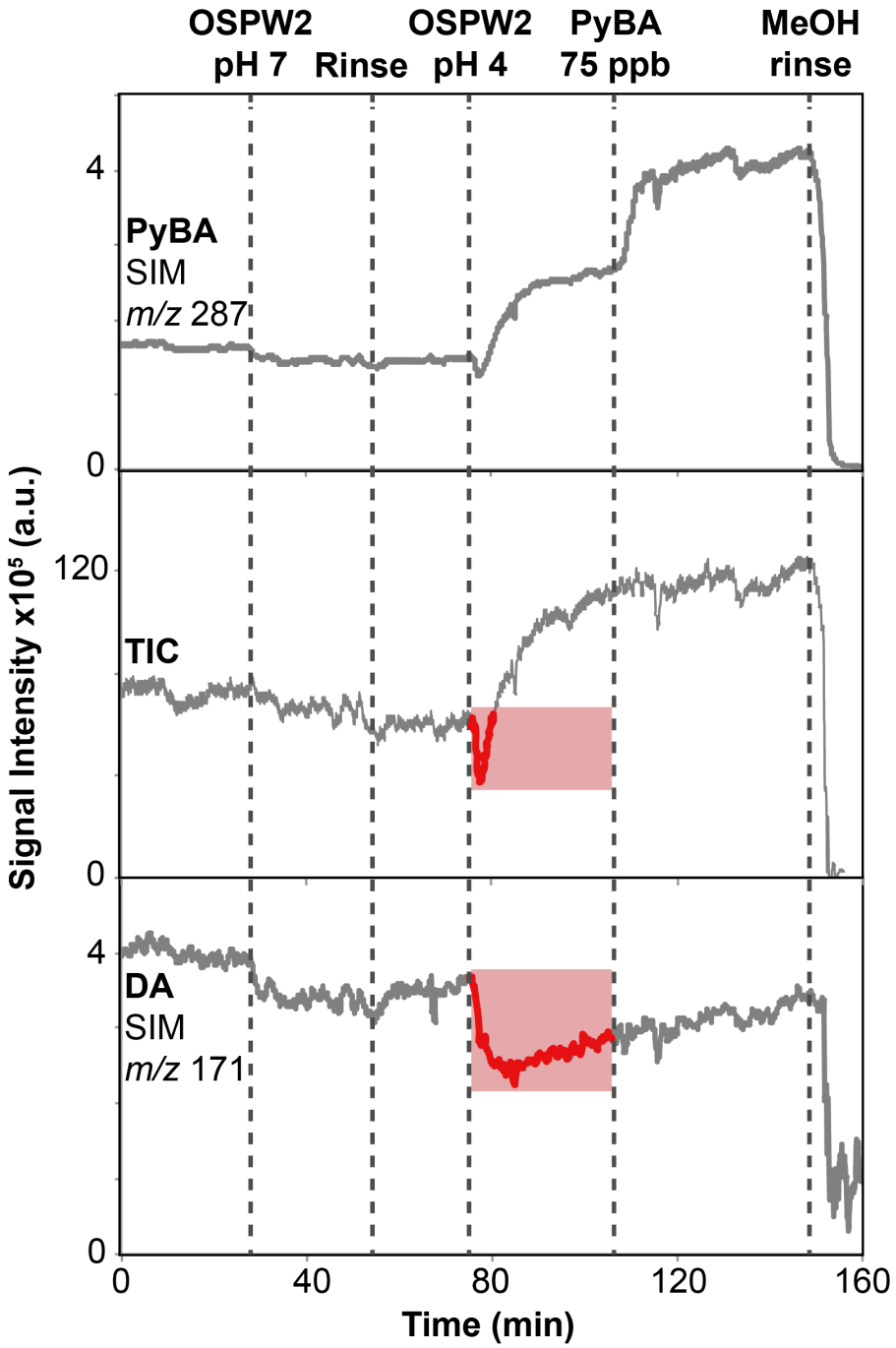

Figure 17: Chronogram for an experiment with OSPW2 141X dilute, at pH 7 and pH 4, with a 75 ppb PyBA standard addition. Upper trace is *m/z* 287 (PyBA, as well as a common *m/z* in the OSPW spectrum). Middle trace is the fullscan TIC, showing signal suppression (red shaded) for OSPW at pH 4. Lower trace is the decanoic internal standard, also showing signal suppression (red shaded) for OSPW2 at pH 4 (Datafile: DLMIMS_054_2)

This experiment reveals several difficulties with the proposed pH subtraction technique. First, in OSPW2, there are neutral species (including hydroxylated species) crossing the membrane at pH 7 that cause ion suppression. Because these species also cross the membrane at pH 4, it would make sense to simply subtract the pH 7 signal from the pH 4 signal to isolate carboxylated species (neutral only at pH 4). However, for certain very concentrated samples such as OSPW2, the mass of compounds permeating the membrane at pH 7 was greater than that at pH 4, presumably due to high levels of non-NA components. The pH subtraction then resulted in a negative signal, which made quantitation impossible. Indeed, differing ionization suppression between pH 7 and 4 was observed for most NA samples analyzed for this thesis that had concentrations greater than ~5 ppm Merichem equivalents. Because the pH subtraction technique was sample dependent, and increased the analysis time and analytical complexity, this approach was not explored further.

3.3.2 Internal Standard Correction

Variations in instrument sensitivity (day-to-day, hour-to-hour, and occasionally variations on the order of minutes) have the potential to introduce significant error into quantitative measurements. This includes inter- or intra-day variation while using one instrument, or variation introduced when using different mass spectrometers. Considering that the experiments completed for this thesis were conducted roughly half-and-half using two different Waters-Micromass ESI-QqQ mass spectrometers (hereafter referred to as QqQ #1 and #2), variation of the second type was expected. Although these were very similar instruments, there were still many variables that had the potential to contribute error in any quantitative results, and thus a solution was required to normalize measurements between these machines. Another significant form of instrumental variation common to all users of ESI-MS is ionization suppression,[95] as demonstrated in section 3.3.1. Direct measurements in complex matrices with high salt loads and other chemical species can result in suppression of ion formation in the ESI spray. As OSPW samples can have high concentrations of acids, alcohols and other co-permeating neutral species that may pass through the PDMS membrane, the potential for ionization suppression is high, although

the membrane does prevent many matrix components (such as salts) from permeating.[88] Fluctuations in this suppression effect with varying concentrations of matrix species can make achieving reproducible quantitative results very difficult.

A solution to both of these issues was to introduce an internal standard correction to account for both the temporal variation in instrument sensitivity and potential ion suppression issues. This idea was previously explored in our group,[88] but will be expanded upon in this thesis for the purposes of quantitation. The internal standard correction differs from the mode in which a traditional internal standard is used. First, it is not present in the sample, but rather in the solvent acceptor phase that passes through the inner lumen of the membrane, and is therefore directly infused into the mass spectrometer. Second, the internal standard is not directly used to quantitate, but rather to correct signals to improve quantitation and reduce signal variation due to ion suppression and variability in instrument sensitivity. Decanoic acid was chosen for this purpose, as it fits the definition of a classical naphthenic acid ($z=0$). The primary assumption made with regards to this surrogate compound is that the suppression experienced by DA is the same as experienced by NAs, which is reasonable given their structural similarity. Thus, after establishing baseline in a given experiment, DA was injected into the methanol acceptor phase to give a final concentration of 10 ± 1 ppb. The exact concentration depended on the DA standard used and the volume of the MeOH acceptor phase, and was taken into account in data processing as mentioned in section 2.3.2. The DA signal was allowed to stabilize before any NA samples were analyzed. Fig. 18 shows a chronogram for an OSPW quantitation experiment with the SIM signal intensities for *m/z* 287 (both a common NA peak and the molecular ion for PyBA) and *m/z* 171 (the molecular ion peak for the DA internal standard) shown. At 0 min, baseline is established. At ~60 min, the CP-MIMS probe is immersed in the OSPW sample at pH 4, which has a sufficient concentration of NAs to cause ionization suppression in the ESI source. This is reflected in the reduction of the DA signal below baseline value. At 100 min, the standard addition of ~30 ppb PyBA does not seem to have any effect on the DA signal. At 175 min, the probe is rinsed with MeOH.

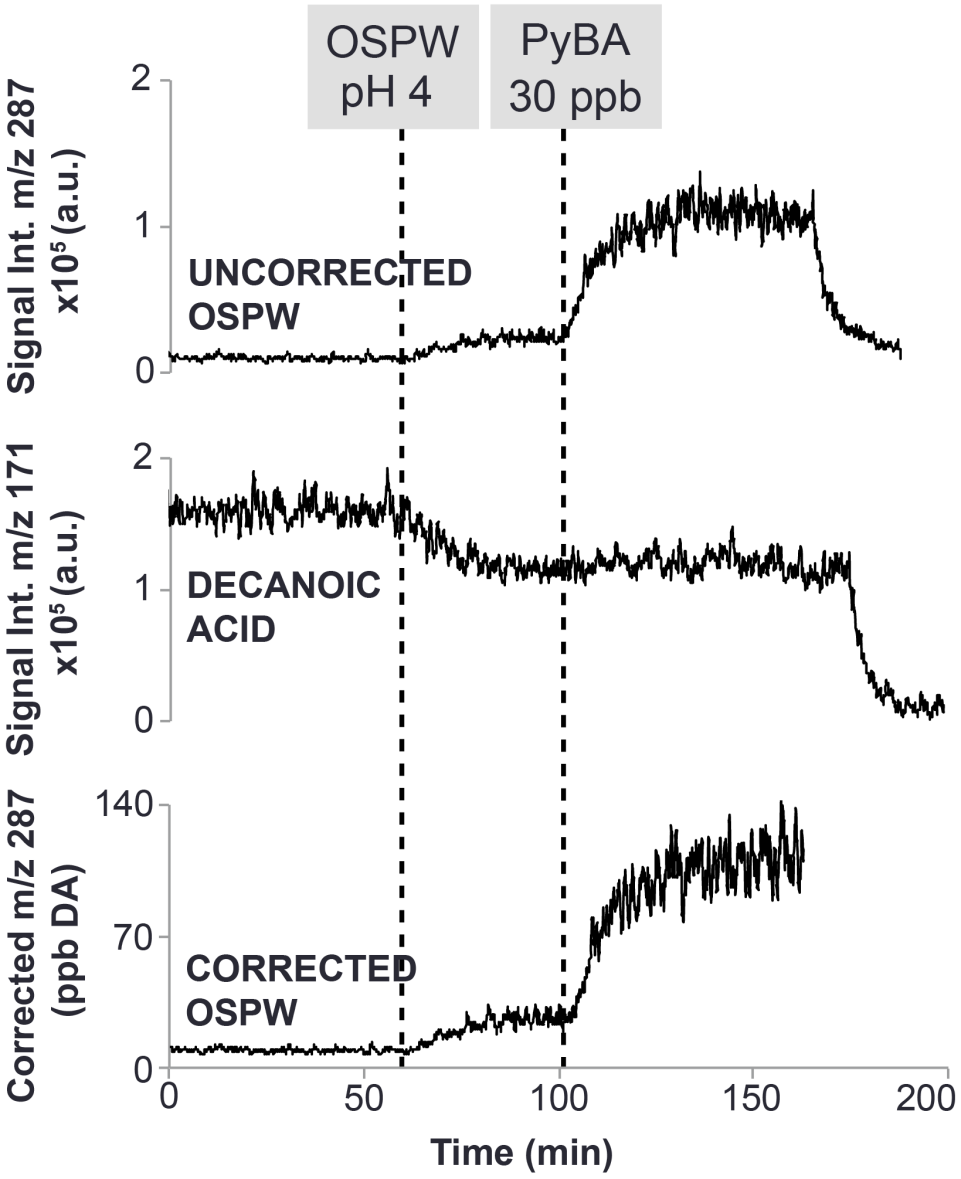

Figure 18: Correction for signal loss/ion suppression with a decanoic acid internal standard. The top trace shows the uncorrected OSPW signal at fullscan *m/z* 287. The middle trace shows the DA internal standard experiencing signal suppression when the probe is immersed in the OSPW at pH 4. The bottom trace shows the OSPW signal after correction with the DA signal and DA concentration, in units of ppb DA (Datafile: DLMIMS_077)

As described in section 2.3.2, the signal depression of DA can be used to correct all other NA-related signals (such as *m/z* 287) to mitigate the effects of ion suppression on the quantitation experiment. This is done by dividing the average S.S. signal (or signals) for the OSPW by the averaged S.S. signal of DA over the same timeframe (Eqn. 3),

essentially functioning to add the percent DA signal lost because of suppression back to all OSPW signals. Further, as the concentration of DA varies slightly in every experiment (due to variations in the concentration of the DA standard used and volume of methanol present in the acceptor phase during a given experiment), these 'corrected' signals can then multiplied by the concentration of DA present in the acceptor phase (in ppb). This gives a final corrected signal with units of ppb DA, shown as the bottom trace in Fig. 18.

3.3.3 Evaluation of pH Subtraction and Internal Standard Correction Methods on Quantitative Results

Quantitation experiments were conducted to assess the effectiveness of the pH subtraction and internal standard (I.S.) correction techniques for a variety of OSPW and surface waters. For any given sample, concentrations of total NAs ($[NA]_T$, based on the fullscan TIC) were expressed as equivalents of Merichem (ppm) through the use of direct Merichem calibration curves. These calibrations were performed in separate experiments, some days to weeks beforehand. Four Merichem calibration curves are shown in Fig. 19. Although all from the same dataset, they represent different treatment of the data with either A) I.S. correction but no pH subtraction, B) I.S. correction with pH subtraction, C) no I.S. correction and no pH subtraction, or D) no I.S. correction with pH subtraction. As such, the units of the y-axis in Fig. 19 vary for each scenario A-D, depending on the correction methods used, as demonstrated below in Eqns. 7-10 (S denotes 'signal' from the fullscan TIC, or for decanoic acid, signal from a SIM at m/z=171).

Equation 7: A) $y = \frac{S_{pH\ 4}}{S_{DA\ (pH\ 4)} / [DA]}\ (ppb\ DA)$

Equation 8: B) $y = \frac{S_{pH\ 4} - S_{pH\ 7}}{S_{DA\ (pH\ 4)} / [DA]}\ (ppb\ DA)$

Equation 9: C) $y = S_{pH\ 4}\ (\times 10^6)$

Equation 10: D) $y = S_{pH\ 4} - S_{pH\ 7}\ (\times 10^6)$

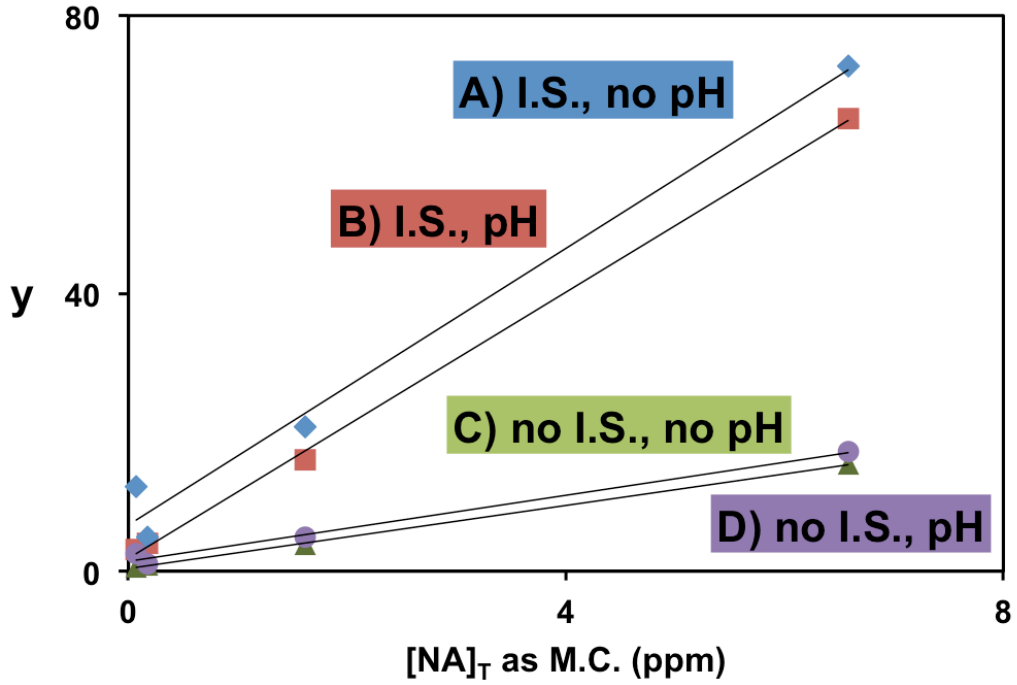

Figure 19: Calibration curves, 0.1-7 ppm $[NA]_T$ as Merichem. Four scenarios are presented: A) I.S. but no pH subtraction, B) I.S. with pH subtraction, C) no I.S. and no pH subtraction, and D) no I.S. with pH subtraction, with units of the vertical axis depending on the scenario but all derived from the fullscan TIC (Datafiles: DLMIMS_063-066)

Table 5 collects data from these four calibration curves. As above, the units for the equation of the lines varies whether the I.S. correction is performed or not – without, the units are signal intensities from the fullscan TIC, and with, they are a ratio of fullscan TIC counts normalized to the DA signal and concentration, in units of ppb DA.

Table 5: Calibration curve data (0.1-7 ppm $[NA]_T$ as Merichem) for four scenarios A-D conducted with and without the internal standard correction and pH subtraction techniques

Scenario	A	B	C	D
pH adjustment	pH 4 only	pH 4 – pH 7	pH 4 only	pH 4 – pH 7
Internal std?	Yes	Yes	No	No
Equation of line	y = 10.537x + 3.4236	y = 9.5837x + 1.8326	y = 2,495,129x + 760,993	y = 2,271,443x + 377,959
R^2 value	0.9999	0.9991	0.9998	0.9993

Datafiles: DLMIMS_063-66

Each of these direct Merichem calibrations was used to attempt quantitation with a variety of OSPW and surface waters. Table 19 in Appendix A collects the full results, while Figs. 20 and 21 display results for select samples with significant concentrations of NAs (> 0.5 ppm $[NA]_T$ as Merichem).

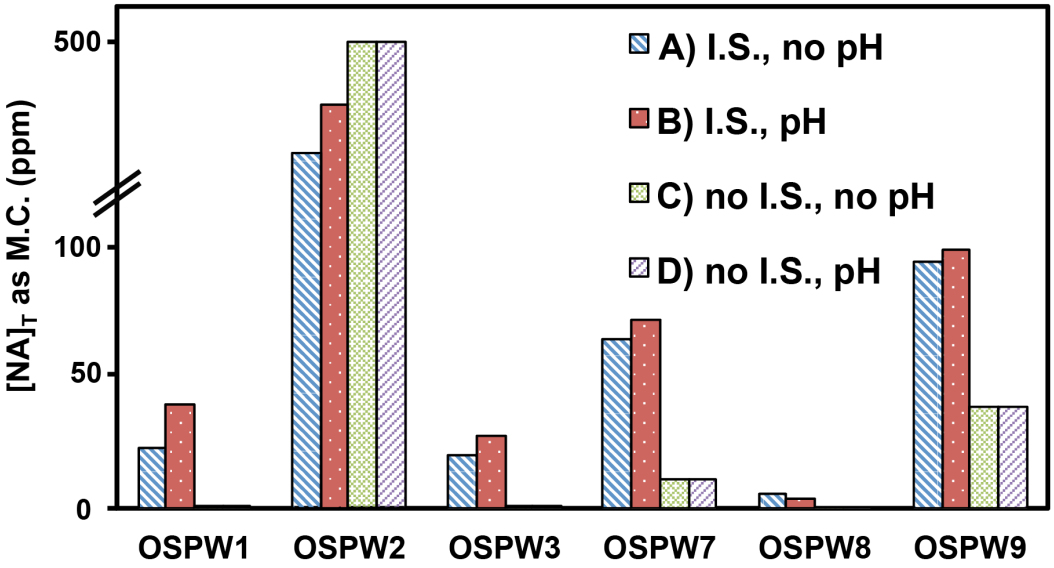

Figure 20: Quantitation of several OSPWs as Merichem equivalents, evaluating the effectiveness of the internal standard correction and pH subtraction techniques (Datafile: Initial Comparison of OSPWs by CP-MIMS)

Table 5 and the above figures demonstrate that the pH subtraction technique did not significantly affect results, and since it involved twice the time as simply measuring samples at pH 4, it was abandoned, effectively halving the measurement duty cycle as described previously. However, the use of the internal standard correction did result in

significant quantitative improvements. Data was obtained for several samples that previously gave zero or negative results due to ion suppression and/or pH subtraction (see OSPWs 4, 5 and 6 in Table 19 in Appendix A), and reproducibility was significantly improved. Table 6 collects data from replicate quantitation experiments for OSPW2, performed on a single mass spectrometer (QqQ #1) and a larger set of experiments performed on both mass spectrometers (QqQ #1 and #2). For the 3 experiments performed on QqQ #1, the use of the I.S. resulted in a reproducibility improvement of 45 %RSD to 19 %RSD. For the 7 experiments performed between QqQ #1 and QqQ #2, the use of the I.S. resulted in an improvement of 41 %RSD to 36 %RSD. The success of the I.S. in these studies meant it was implemented in all quantitation work conducted for this thesis. In summary, thus far CP-MIMS quantitative work requires samples to be adjusted to pH 4 only, with the addition of the I.S. in the acceptor phase.

Table 6: Reproducibility improvements for OSPW2 using the internal standard correction

	NO I.S.		***WITH I.S.***	
	Avg. $[NA]_T$ as M.C. (ppm)	**%RSD**	**Avg. $[NA]_T$ as M.C. (ppm)**	**%RSD**
QqQ #1 *(n=3)*	333	45	230	19
QqQ #1+#2 *(n=7)*	392	41	245	36

Datafiles: DLMIMS_051, 052, 054_2, 055, 061 and GV_14_26_2, 27, 29 and 30

3.3.4 Acceptor Phase pH Control

The bulk of literature reporting on analysis of carboxylic acids (including naphthenic acids) via ESI-MS utilizes the addition of aqueous base to improve ionization and therefore sensitivity for these compounds.[13] Most HPLC/ESI-MS studies use 0.1% aqueous ammonium hydroxide or ammonium acetate in a methanol/water mobile phase, prompting the addition of a similar concentration of base to the CP-MIMS acceptor phase. Logistically, initial attempts at doing this made it clear that order-of-operations in the experimental setup was crucial. Attempting to add base to the acceptor phase before the solvent passed through the inner lumen of the membrane was ineffective, as the base interfered with membrane transport processes. After learning this, base was added post-

membrane via a syringe pump feeding into a T-junction, and was found to be most effective and least disruptive to solvent flow when injected into the acceptor at 90º (see the experimental schematic shown previously in Fig. 12). A parametric study was performed with both ammonium hydroxide and ammonium acetate added to the CP-MIMS acceptor phase at various concentrations, with the results summarized in Table 20 in Appendix A and visualized in Figs. 21-23 below. These studies were performed on a NA model compound mix consisting of two representative carboxylated species (4-*t*-butylcyclohexanecarboxylic acid and lauric acid) and two hydroxylated species (nonylphenol and triclosan) at low concentration (8-11 ppb) in buffered solution at pH < 4. First, an initial experiment was performed to infuse the two bases dissolved in MeOH at two different concentrations. Final solvent composition in the CP-MIMS acceptor phase was therefore MeOH with either 0.1 or 0.2% base. However, no improvements in sensitivity were observed, as visualized in Fig. 21. All four compounds experienced significantly reduced sensitivity (50-100% reduction) compared to a control experiment performed with no base added (indicated by dotted line in the figure).

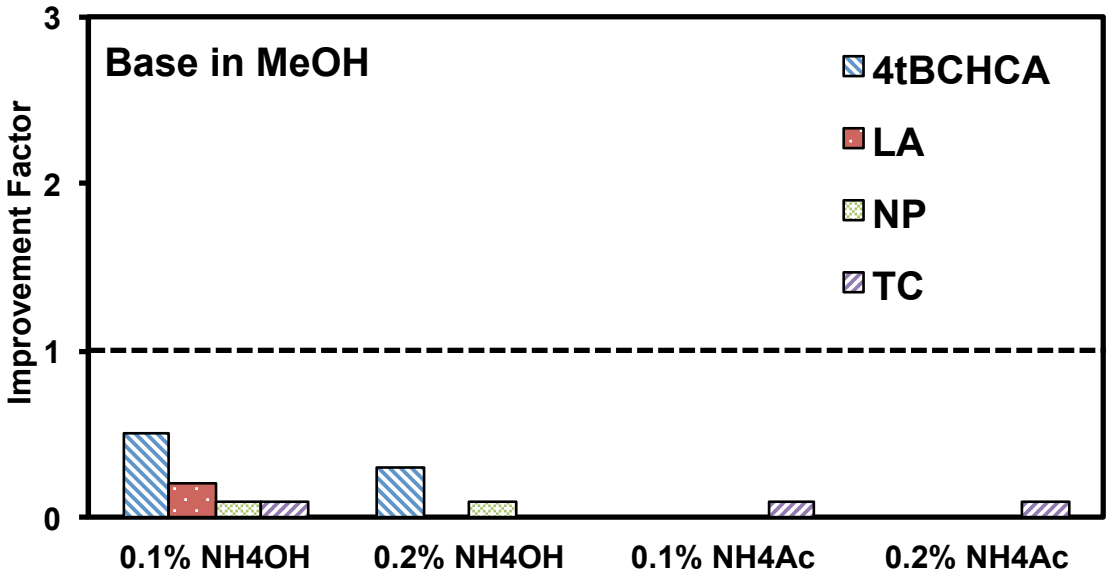

Figure 21: Improvement factors for four model compounds after base addition in MeOH to acceptor phase. Vertical axis is an improvement factor calculated from [sensitivity with base added / sensitivity with no base added]. A dotted line represents no improvement (the same sensitivity as with no base added) (Datafiles: DLMIMS_146-155)

Following this, the effectiveness of dissolving and infusing the two bases in aqueous solution (instead of MeOH) was evaluated. First, an experiment was attempted where water with no added base was injected into the acceptor phase to see whether there would be any affect on ionization for the four target compounds. The final composition of the acceptor phase was MeOH with 5-20% water. As seen in Fig. 22, this affected sensitivity for some test compounds (NP, LA) more than others (4tBCHCA, TC), although overall resulted in decreased sensitivity for all compounds except in one case (4tBCHCA with an acceptor phase composition of 90% MeOH/10% water).

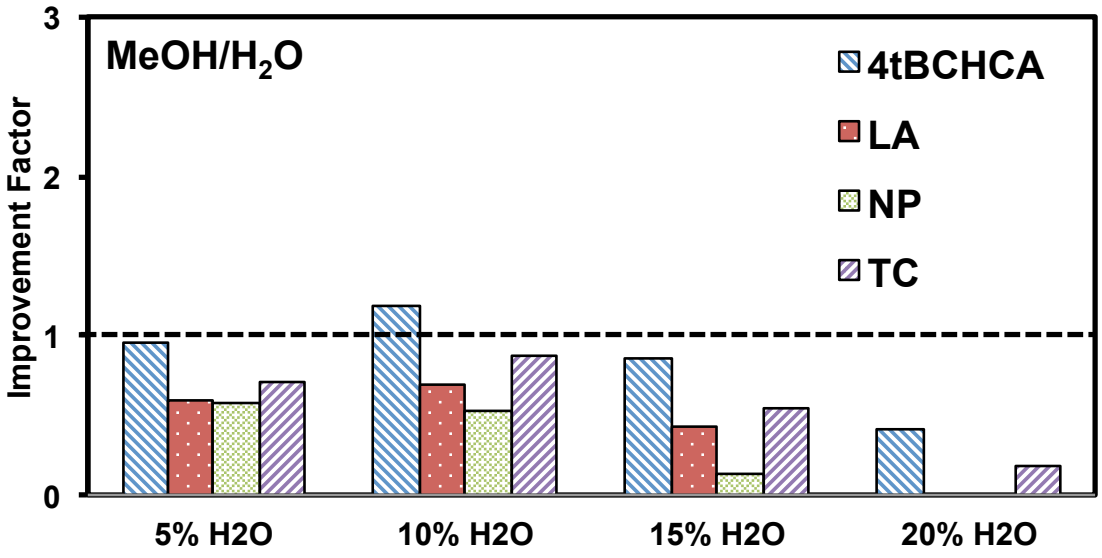

Figure 22: Improvement factors for four model compounds after water addition to MeOH acceptor phase, with no base added (Datafiles: DLMIMS_146-155)

Finally, an experiment was performed to test the effectiveness of the addition of these two bases in aqueous solution, the same conditions reported in the bulk of literature studies surveyed. The acceptor phase was now composed of MeOH, water, and 0.1 or 0.2% base. Finally, positive results were achieved, although primarily for one base (NH_4OH) at one particular concentration (0.1%), where a 2-3X improvement in sensitivity was observed for all four model compounds. For the other scenarios, it was assumed that the benefit of the base addition was overwhelmed by the negative effect of the water addition. This is likely a result of the increased aqueous content of the acceptor affecting ionization efficiency. Fig. 23 displays the results.

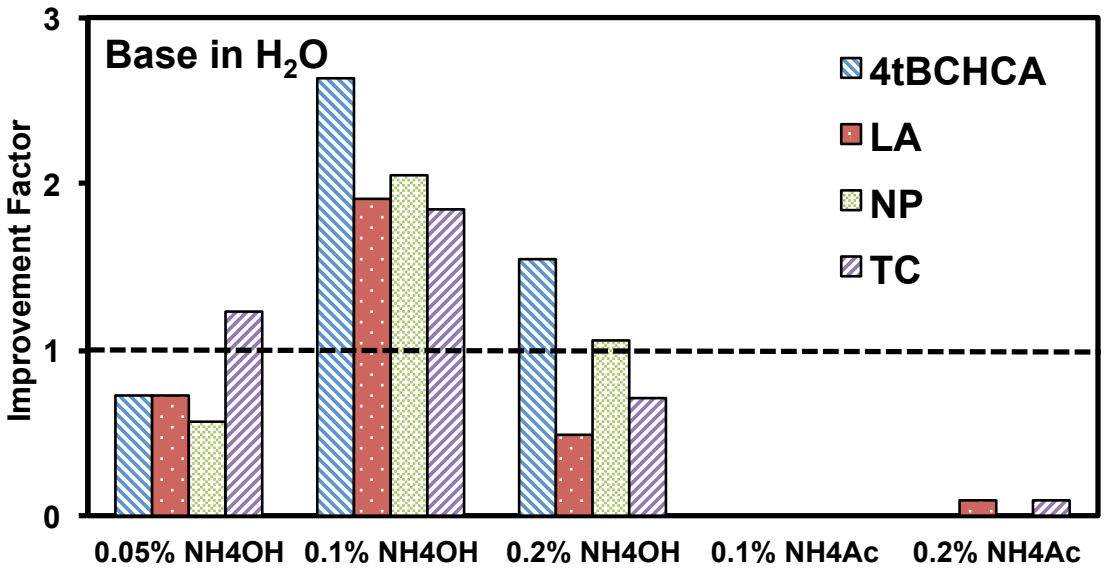

Figure 23: Improvement factors for four model compounds after aqueous base addition to acceptor phase (Datafiles: DLMIMS_146-155)

Results from these base addition studies overwhelmingly supported a final acceptor phase composition of 95% MeOH/5% water with 0.1% NH_4OH for improvement of carboxylic acid ionization, consistent with the literature.[1, 31] This technique was therefore applied across all quantitation experiments as a standard part of the experimental setup shown previously in Fig. 12.

3.3.5 Targeted Selected Ion Monitoring

The experiments shown in previous sections were quantified using the fullscan TIC, with all masses between *m/z* 100-600 measured for each scan. Fullscan mode provides a full characteristic mass profile for every sample, which is highly useful in qualitative studies when attempting to distinguish complex mixtures. However, this can come at cost to analytical sensitivity, particularly when attempting to quantify NAs in more complex OSPW samples with hundreds to thousands of peaks in a fullscan mass spectrum. Mass spectrometric modes such as selected ion monitoring (SIM) and tandem MS (MS/MS) allow for much more sensitive and selective information to be obtained, and are therefore highly desirable for quantitative work. For a SIM experiment, analytical sensitivity is

increased because of the longer dwell time on a single *m/z* (1000 msec), allowing for a more accurate count of the ions of that mass than in a fullscan, where only 500 msec of scan time is allotted to cover a range of 500 *m/z* values (in a typical fullscan from *m/z* 100-600), yielding ~1 msec measurement time at each *m/z*.

The difficulty with complex samples such as OSPWs is selecting which peaks in the mass spectrum to include in these types of experiments. Given the diversity of composition of NA-containing samples, the lack of analytical standards, and the potential for batch-to-batch variation in calibrants such as Merichem, this is not a trivial task. A proposed solution was to select a number of common masses in the Merichem fullscan spectrum and set up selected ion monitoring (SIM) experiments at these *m/z*, in addition to collecting fullscan spectra. The SIM experiments should in theory provide greater analytical sensitivity at the representative masses, while the fullscan would still be available for unique mass spectral information. A method was developed, establishing SIM experiments at the 30 most abundant masses in the Merichem spectrum at pH < 4 (see Table 21 in Appendix A). This method was termed 'targeted selected ion monitoring'. Fig. 24 shows A) a partial ion chronogram for several concentration steps in a Merichem calibration curve, with six SIM signals displayed, including the internal standard at *m/z* 171, and B) an inset fullscan mass spectrum of Merichem showing the *m/z* selected for the SIM experiments. The resulting calibration curve (1-2300 ppb $[NA]_T$ as Merichem) for one SIM (*m/z* 223) is shown in panel C.

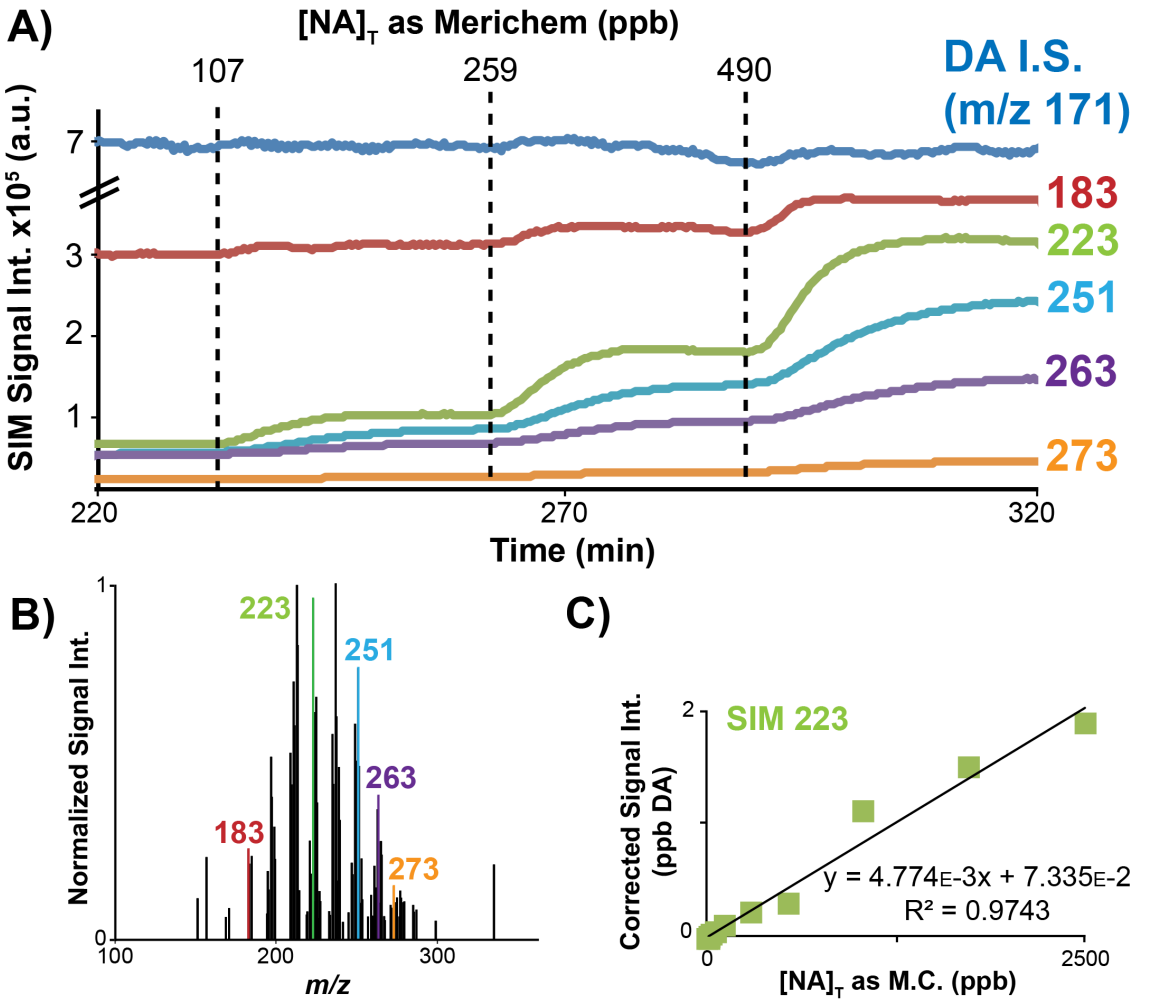

Figure 24: Merichem calibration curve using targeted selected ion monitoring method. A) Partial chronogram showing three steps in a 1-2300 ppb Merichem calibration curve with 5 SIM channels, B) fullscan mass spectrum shown for Merichem at pH < 4 highlighting the masses chosen for SIM experiments, C) full worked-up calibration curve for SIM *m/z* 223 (Datafile: DLMIMS_159)

The primary disadvantage to this method is that the 30 most abundant Merichem peaks may not represent the most abundant masses in every NA-containing sample, and key information may be lost for unique samples. Although the 30 SIM *m/z* chosen capture 87% of the fullscan Merichem spectrum (see Fig. 25), they may capture a much lower percentage of the NAs present in other samples.

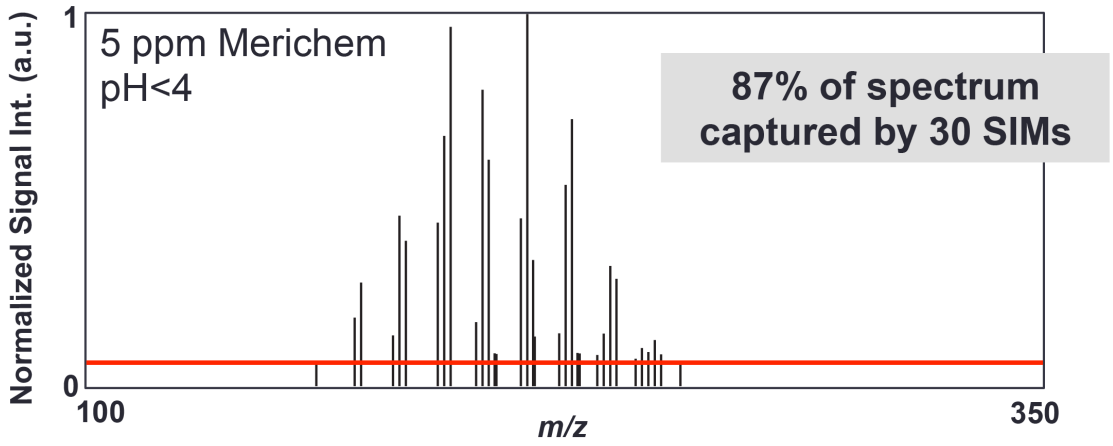

Figure 25: Percentage of Merichem spectrum captured by 30 SIMs selected from the top 30 most abundant fullscan *m/z* at pH < 4 (red line indicates subtraction of peaks less than 13% relative intensity)

To illustrate this point, fullscan data was collected for a variety of northern Alberta OSPW samples, and the percentage of each sample's mass spectrum that was represented by the targeted SIM *m/z* was calculated, with results collected in Table 7 (full data available for all fullscan mass spectra in Appendix B). Values are reported in two ways – the first being the percent of the fullscan TIC represented by the sum of fullscan counts from the 30 targeted *m/z*, and the second being the number of targeted *m/z* in each sample's top 30 masses as observed in the fullscan. This analysis was repeated for the top 30 *m/z* from the fullscan of the LVE2 sample provided by Environment Canada. Because the LVE samples were obtained towards the end of experiments conducted for this thesis, these *m/z* were not selected for creation of unique SIM experiments and were therefore not incorporated into a method that was used when analyzing samples. However, because fullscan data was also collected for every sample analyzed, it was possible to reprocess this data after the fact to observe how well the 30 *m/z* from LVE2 represented each sample. It was hypothesized that because LVE2 is an extract of northern Alberta waters, its top 30 *m/z* would better represent samples also obtained from northern Alberta. Table 7 summarizes the results.

Table 7: Percentage of various OSPW spectra represented by 30 targeted *m/z* for both Merichem and LVE2

	TOP 30 MERICHEM		TOP 30 LVE2	
Sample	**% of fullscan spectrum represented by 30 *m/z***	**# of targeted *m/z* in sample's top 30 *m/z***	**% of fullscan spectrum represented by 30 *m/z***	**# of targeted *m/z* in sample's top 30 *m/z***
Merichem	**87**	**30/30**	68	17/30
LVE1	60	17/30	68	24/30
LVE2	74	19/30	**88**	**30/30**
OSPW1	75	22/30	80	26/30
OSPW2	68	21/30	79	26/30
OSPW3	67	21/30	68	22/30
OSPW7	77	19/30	89	26/30
OSPW8	33	13/30	20	10/30
OSPW9	75	15/30	91	26/30
OSPW10	68	17/30	81	24/30
OSPW11	58	15/30	75	24/30
OSPW12	52	15/30	72	23/30
AVG.	**66**	**19/30**	**73**	**23/30**

Datafiles: DLMIMS_156, 160, 165, 170, 174, 183, 184, 186

It is clear from Table 7 that the 30 *m/z* chosen from the Merichem fullscan do not fully represent the spectra of many of the samples studied here. This makes the collection of a fullscan a necessary addition to SIM experiments to ensure full unique sample data is available. The top 30 *m/z* from LVE2, however, capture on average 7% more sample information for the samples studied (and 17-20% more for certain samples such as OSPW11 and 12). An average of 23 out of the top 30 LVE *m/z* are found in all OSPW samples studied, compared to the 19/30 for the top 30 Merichem *m/z*. This supports the earlier hypothesis that the northern Alberta extract better represented northern Alberta samples than Merichem, which is processed and produced in Texas, USA.

3.4 Three CP-MIMS Quantitation Strategies

3.4.1 Quantitation of OSPWs with Standard Addition of PyBA

One possible method of assigning a quantitative value to a NA sample is to quantify the signal for every peak in the sample's mass spectrum using a surrogate, model compound as a standard. This has the advantage of simplicity and reproducibility, as comparison is made with only one, defined compound as opposed to a complex mixture such as Merichem. However, deciding which compound to pick for comparison is a more difficult task. Naphthenic acids represent a diverse mixture of compounds, and no one structure properly represents the full variety present in a real sample. In addition, there is no agreement in the literature about a possible representative model compound as a quantitative standard. One example of a single calibrant used for quantitation is PyBA, as used by AXYS in their SPE-LC-MS/MS method (vide supra). Samples analyzed using this method from a previous collaboration[50] were still available, and therefore this thesis attempted to employ the same single-compound calibration technique in CP-MIMS experiments to compare results to AXYS.

Quantitation as PyBA by CP-MIMS was typically performed as a standard addition experiment at the end of a sample's duty cycle, although several techniques were attempted, including a 3 point direct calibration curve (performed in a separate experiment days to weeks beforehand) in addition to 1 and 2 point standard addition techniques (performed directly in the sample being analyzed). Fig. 26 shows a typical duty cycle for an OSPW quantitation experiment incorporating a 3 point internal PyBA calibration curve and the sample pH adjustment technique. At ~15 min, the CP-MIMS probe is immersed in the OSPW at pH 7. At ~70 min, the probe is immersed in the same sample at pH < 4. At ~100-160 min, three injections of ~30 ppb PyBA each are added on top of the sample to create the 3 point internal calibration curve. PyBA is monitored using SIM at *m/z* 287.

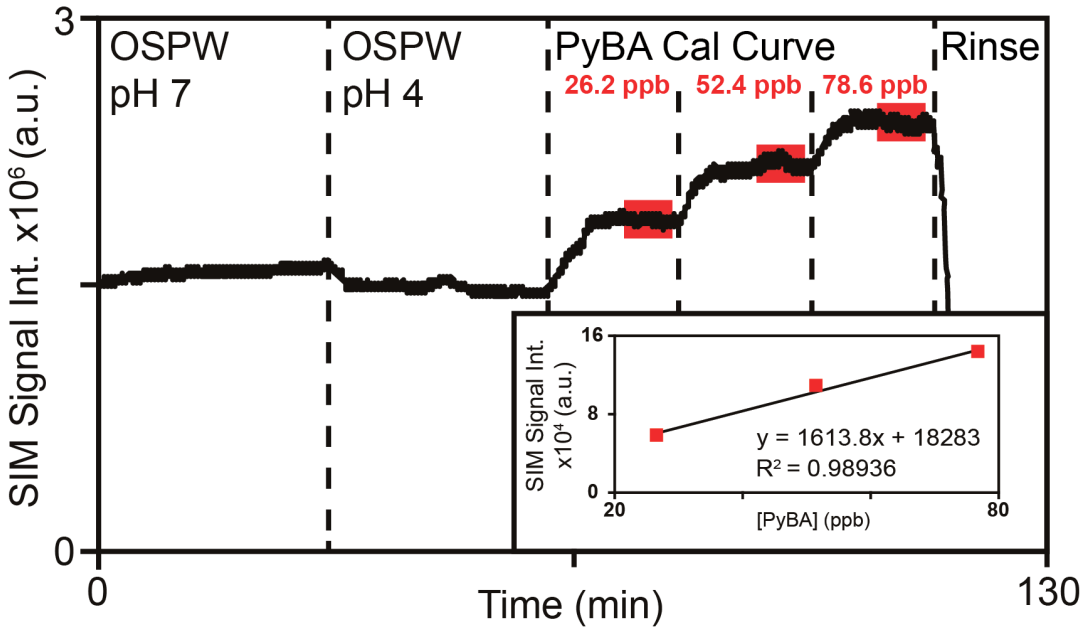

Figure 26: Ion chronogram for an OSPW quantitation experiment with a 3 point PyBA calibration curve created through standard addition directly in the sample. Regions highlighted in red show the 5 min windows used to average data in processing. Inset shows the calibration curve generated from the above data (Datafile: DLMIMS_055)

Fig. 27 shows an ion chronogram outlining the typical duty cycle for quantitation of an OSPW sample using the 1 point PyBA standard addition technique. First, baseline is established after injection of the internal standard earlier (not shown). At ~30 mins, the membrane probe is exposed to an OSPW sample diluted in buffer at pH < 4. At ~60 mins, after the resulting signal has achieved steady-state, a 30 ppb PyBA spike is injected directly into the sample, resulting in a rise and steady-state region used to quantitate as per the standard addition method described in section 3.2.3. An exact concentration of PyBA to one decimal place was calculated from the known injection volume of the spike and the known mass of the sample vial containing sample (as per Equation 6 in section 3.2.3). Windows encompassing the 5 minute regions over which all signals were averaged are shown highlighted in red.

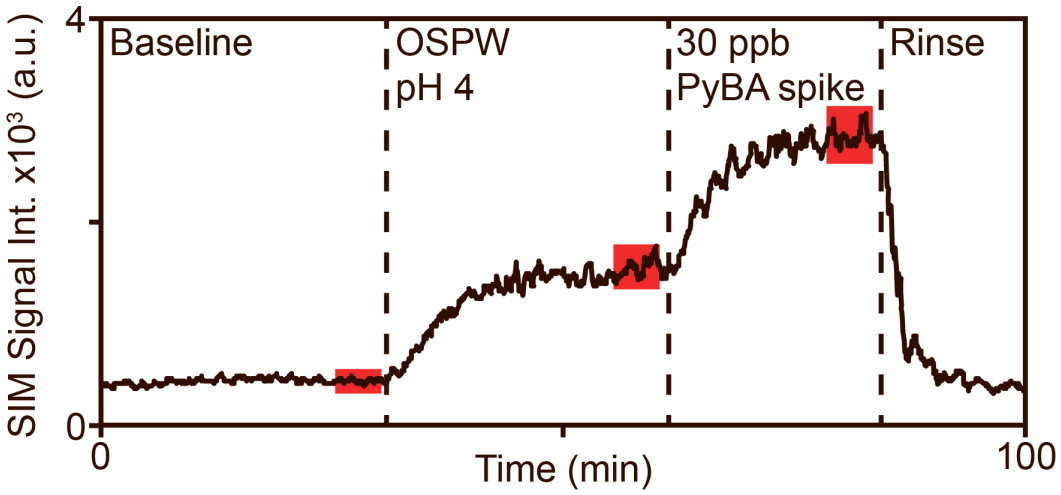

Figure 27: Quantitation of an OSPW at pH 4 as PyBA equivalents using the standard addition method. Signal trace is a SIM at *m/z* 287 (channel also used to monitor PyBA). Regions highlighted in red show the 5 min windows used to average data in processing (Datafile: DLMIMS_061)

A dataset of OSPW2 quantitation experiments (sample replicates) was used to compare the reproducibility of the PyBA standard addition techniques to direct PyBA calibration curves. Table 8 gives the results of this study, performed across both mass spectrometers used in this thesis. Individual results are shown for each mass spectrometer (QqQ #1 and #2) as well as results from experiments performed across both systems. A 1 point standard addition is performed on 7 samples, and a 2 point standard addition is attempted on 2 samples. Finally, a 3 point direct calibration for PyBA conducted in a separate experiment is applied to all 7 samples. Worked examples of all calculations are shown in Appendix C.

Table 8: Reproducibility studies for quantitation of OSPW2 as equivalents of PyBA

STANDARD ADDITION	Avg. $[NA]_T$ as PyBA (ppm)
1 point PyBA standard addition	
Avg. from QqQ #1 *(n=3)*	220
%RSD	13
Avg. from QqQ #2 *(n=4)*	170
%RSD	12
Avg. from both *(n=7)*	190
%RSD	17
2 point PyBA standard addition	
Avg. from QqQ #1 *(n=2)*	190
DIRECT CALIBRATION	
3 point PyBA cal curve	
Avg. from both *(n=7)*	230
%RSD	33

Datafiles: DLMIMS_051, 052, 054_2, 055, 061 and GV_14_26_2, 27, 29 and 30

17 %RSD was achieved across 7 sample replicates conducted on two different mass spectrometers with the use of the internal standard correction factor and the 1 point PyBA calibration. The direct calibration performed poorly (33 %RSD) when compared to the standard additions, likely due to the fact that the direct calibration curve was performed once, days before the OSPW sample was analyzed, whereas both standard additions occurred directly in the sample within the same experiment. In general, it was noted that the closer in time a calibration was to the sample being calibrated, the better the result. Standard additions occur as close in time to analysis as possible – the calibration is performed right in the sample. Ultimately, the 1 point PyBA standard addition was preferred over the others, as it compared well to the 2 point standard addition but was much faster (only one injection of PyBA was required, significantly reducing the analysis time for each sample), as well as being much more reproducible than the direct PyBA calibrations. A 1 point PyBA standard addition was therefore performed for every OSPW sample analyzed in addition to any another quantitation methods employed (i.e., direct calibration with Merichem). This allowed for comparison of results to the published AXYS method, regardless of the success of any other quantitation strategies.

3.4.2 Direct Calibrations with Merichem

Another possible method of NA quantitation is to quantify every peak in a sample spectrum as if it were a peak in the spectrum of some standard NA mixture. While this deviates from traditional analytical methodology, a mixture may more accurately represent the complexity of a real-world NA sample than a single model compound, if batch-to-batch composition is consistent. Unfortunately, there is no one 'standard' NA mixture represented in the body of NA literature. Many have used Merichem,[11, 51] and a lot of work has been to done to characterize this mixture,[96] but little has been attempted in the way of making this a benchmark standard to which researchers in this field can compare to, and the literature is long overdue for a review article encouraging standardization of NA quantitation practices. Experimentation proceeded with the available batch of Merichem to construct several calibration curves, which were used to quantify NAs in unknown samples. Section 3.3.3 presented several M.C. calibrations without the addition of aqueous base and targeted selected ion monitoring improvements, which suffered poor detection limits and narrow linear dynamic ranges. Calibration curves were redone using targeted SIM acquisition, and in the presence of added base in the CP-MIMS acceptor phase, resulting in 100X lower detection limits (from 100 ppb to 1 ppb), and increased LDR from < 2 orders of magnitude to almost 4. Four replicate calibration curves were performed to probe the reproducibility of these experiments. Table 9 summarizes the data from these four experiments.

Table 9: Data from direct Merichem calibration curves with addition of base and targeted SIM techniques, 1-1600 ppb $[NA]_T$ as Merichem

Calibration Curve #	Experiment Date	Slope (ppb DA/$[NA]_T$ as ppb M.C.)	Intercept (ppb DA)	R^2
1	Oct. 27, 2015	0.077	0.32	0.9909
2	Nov. 2, 2015	0.064	1.6	0.9524
3	Nov. 4, 2015	0.072	1.1	0.9710
4	Jan. 12, 2016	0.12	3.9	0.8473
	AVG.	0.084	1.7	
	%RSD	27	-	

Datafile: Improved Merichem Cal Curves Overview (DLMIMS_157, 158, 159, 178)

In particular, it can be observed that the first three calibration curves (which were performed within days of each other) agree well with regards to calibration slope, whereas the fourth curve (performed months later) has a significantly different slope from the first three (71% difference from the average of curves 1-3). This illustrates a key point in achieving reproducible quantitation, namely that calibrations must be performed in close proximity to quantitation experiments. Even with the use of an internal standard correction factor, variations in instrument sensitivity over time had a significant influence on the reproducibility of quantitative results. Fig. 28 illustrates direct calibration curves performed with only a fullscan and no base added to the acceptor phase (red), with a very limited LDR (just under 2 orders of magnitude) and detection limit of ~100 ppb $[NA]_T$ as Merichem as well as one incorporating the base addition and targeted SIM techniques (black), with an improved LDR of 1-2300 ppb and detection limit of 1 ppb $[NA]_T$ as Merichem.

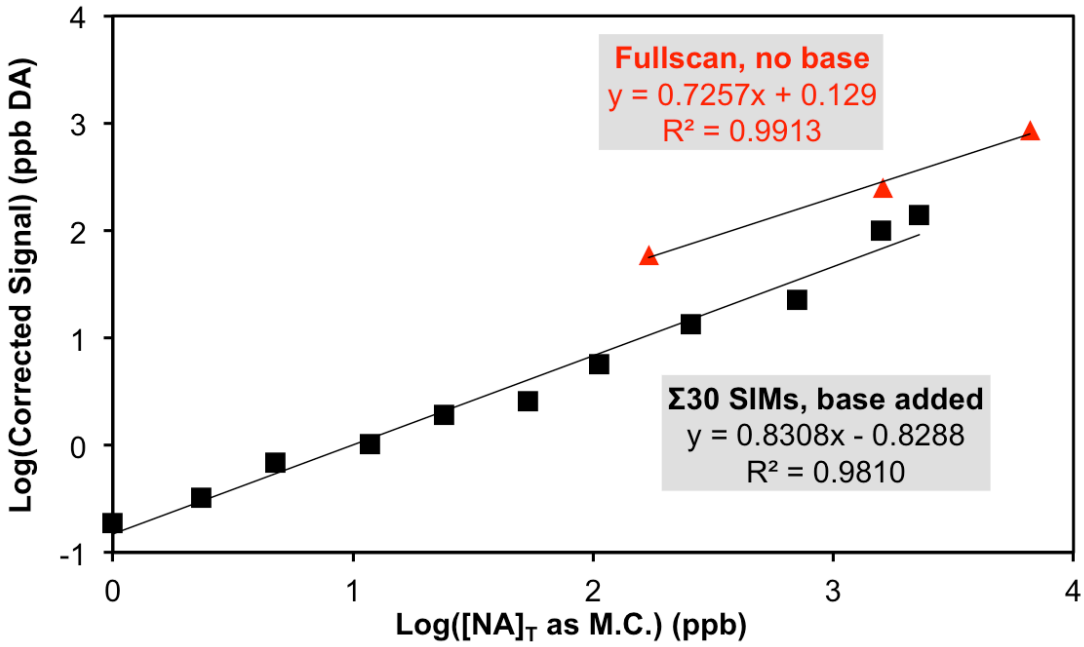

Figure 28: Direct Merichem calibration curves performed with and without addition of base to acceptor phase and Σ30 SIMs. The curve performed with fullscan and no base addition (red) has a LDR of < 2 orders of magnitude (170-6600 ppb). In comparison, the calibration curve implementing the Σ30 SIMs and base addition techniques (black) has a LDR of almost 4 orders of magnitude (1-2300 ppb) (Datafile: DLMIMS_158)

An alternative method of quantifying $[NA]_T$ as Merichem equivalents is to consider each of the 30 SIM *m/z* as individual calibration curves, which can then be used to quantify individual peaks in any given NA-containing sample as if they were the corresponding peak in the Merichem spectrum. Targeting specific compound classes within a NA mass spectrum allows for congener-specific quantitation, and could be especially effective when paired with high-resolution mass spectrometry. For the same direct Merichem calibration experiment performed above (with addition of base and Σ30 SIMs), the data was extracted and processed as 30 individual calibration curves for each SIM *m/z*, with equations of the best-fit lines listed in Table 21 in Appendix A. Fig. 29 displays four such calibration curves from 1-2300 ppb $[NA]_T$ as Merichem.

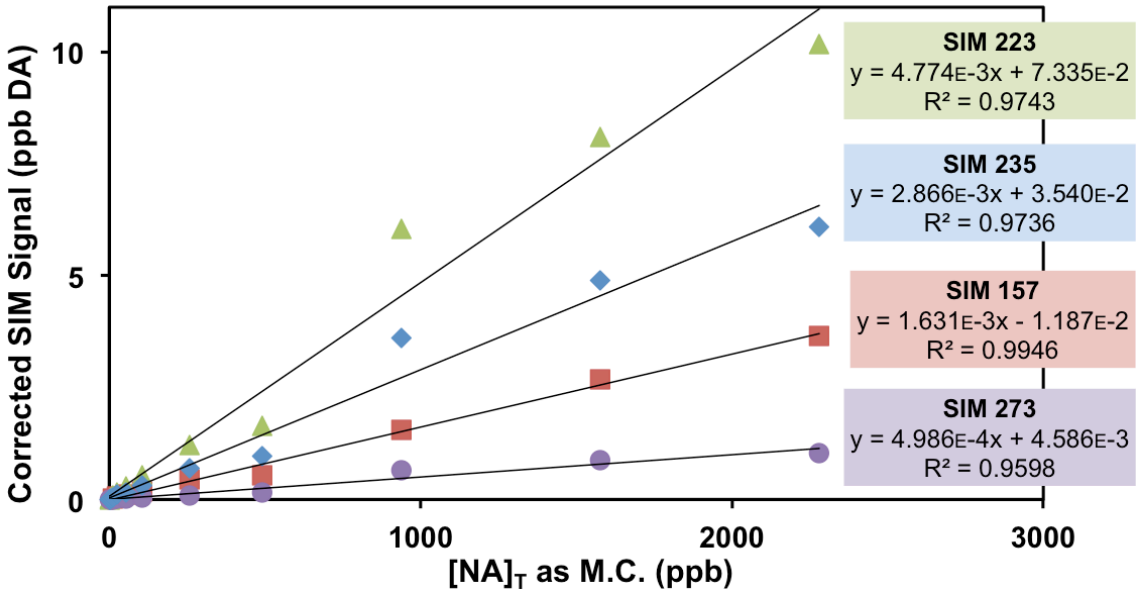

Figure 29: Four individual SIM calibration curves for Merichem with base addition to acceptor phase, 1-2300 ppb (Datafile: DLMIMS_159)

With this method, the power of mass spectrometry is fully utilized to attempt the best possible quantitation with this complex mixture. Selectivity and sensitivity are achieved through SIM experiments, and specific classes of compounds in the complex mix can be targeted for quantitation, if desired.

3.4.3 Direct Calibrations with N. Alberta Large Volume Extracts

When looking for quantitative results from other published methods to compare to the results obtained in this thesis, an obvious choice was to contact John Headley and Kerry Peru (Environment Canada, Saskatoon, SK), leaders in the field of quantitative NA analysis using mass spectrometry.[13, 31] They kindly provided a variety of OSPW samples they had quantified using their ESI/HRMS method,[47] as well as their calibration standard used to assign units to the results. These included OSPW samples from three separate, 'unknown' industries (OSPW10, 11, and 12 in this thesis), and two large volume extracts (LVE1 and LVE2) used as standards to establish calibration curves and units of quantitation. The LVE extracts were given with approximate concentrations of NAFCs (LVE1 ~2700 mg/L NAFCs, and LVE2 ~8000 mg/L NAFCs). Fullscan mass spectra of OSPW samples and LVE standards are displayed in Fig. 30.

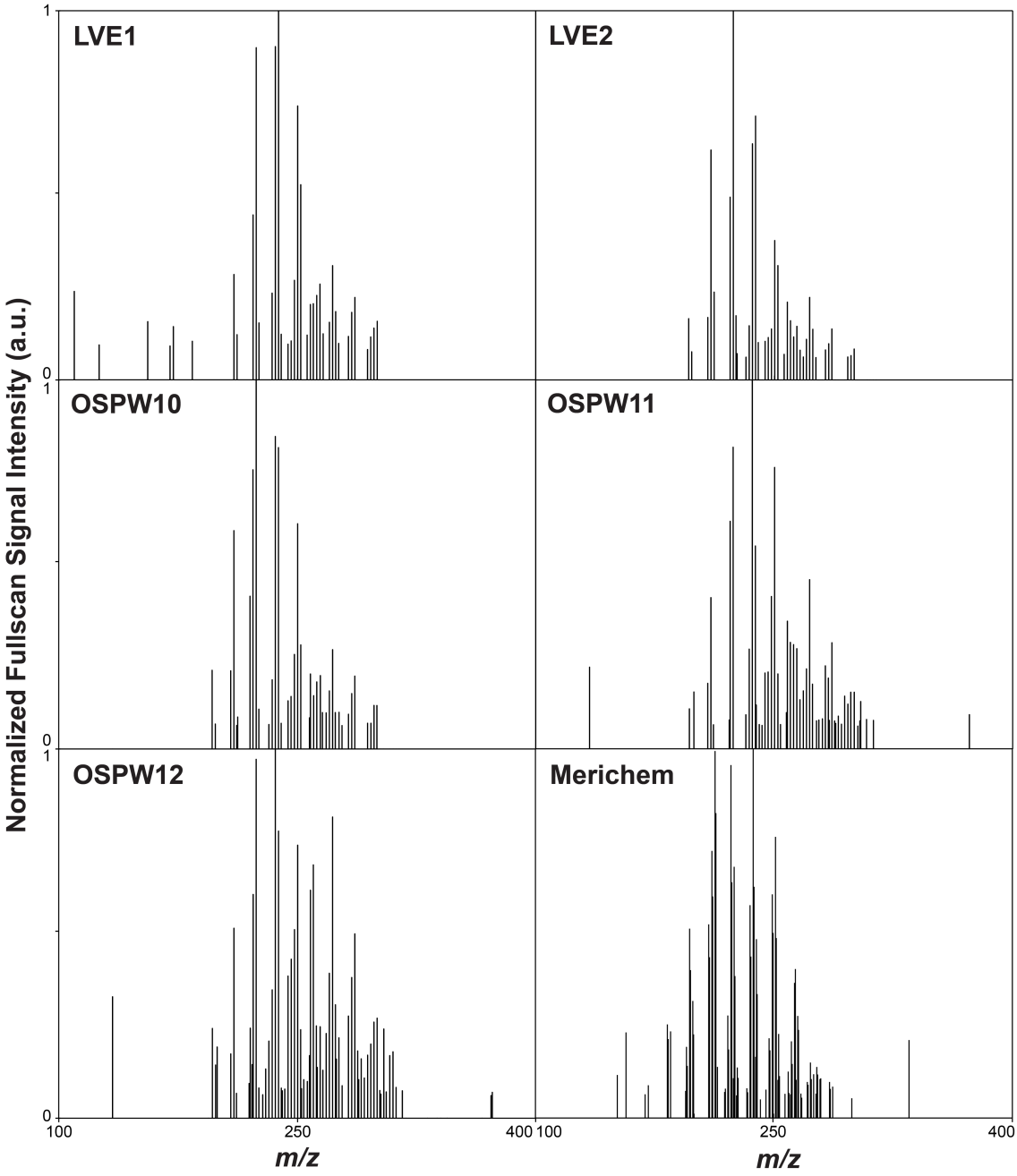

Figure 30: Environment Canada OSPW and LVE spectra overview, with Merichem for reference. All spectra taken at pH < 4, made up to 1-10 ppm in buffered solution, and background subtracted (Datafiles: DLMIMS_183-187)

The similarities between the various OSPW, LVE, and Merichem spectra shown in Fig. 30 are apparent, with all spectra sharing a common envelope of NA peaks between *m/z* 200-300. However, peak abundances and distributions vary (see Appendix B), and as

seen previously in Table 7, the 30 SIM *m/z* chosen from the most abundant peaks in the Merichem spectrum do not fully represent the Environment Canada LVE and OSPW samples. In particular, LVE1 and LVE2 have strong contributions from *m/z* 271, 257, 233, 285, and 269, five major peaks contributing ~10% of the overall spectral intensity for these samples, but not appearing in the top 30 *m/z* chosen from the Merichem spectrum. Although existing methods should be modified to incorporate the unique spectral characteristics of the LVE samples, successful quantitation using the LVE extracts was still carried out using the current targeted SIM method with 30 *m/z* chosen from Merichem. Calibration curves were performed for both LVE samples from 1-7000 ppb $[NA]_T$ as LVE1 or LVE2 NAFC equivalents (based on concentrations of NAFCs in the LVE samples as provided by Environment Canada, discussed in section 3.2.2), and are displayed in Fig. 31. Quantitative data resulting from applying these direct calibrations to various OSPW samples is presented below in section 3.5.

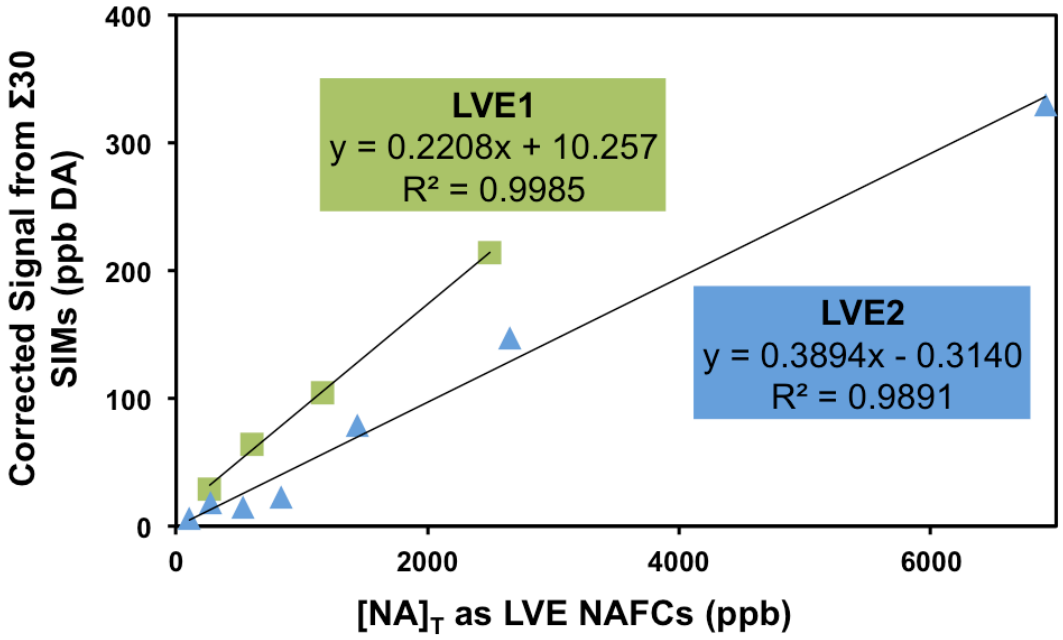

Figure 31: Large volume extract calibration curves (Environment Canada samples LVE1 and 2), 1-7000 ppb $[NA]_T$ as LVE1 or LVE2 NAFCs (Datafile: DLMIMS_183)

3.5 Comparison of Quantitative Analysis of NAs by CP-MIMS

The ultimate goal of these quantitative studies was to analyze a variety of OSPW samples using CP-MIMS and compare results to data from a third party method to validate. In attempting to get the most quantitative data possible, replicate experiments were performed for most OSPW samples, and quantified via both direct calibrations with Merichem and by standard additions with PyBA. All results presented incorporate the aqueous base addition (to the methanol acceptor phase between membrane interface and the ESI ion source) and Σ30 targeted SIM techniques. This data is collected below in Table 10, exhibiting reproducibility generally in the ~20% RSD range for both quantitative methods. Given the complexity of the samples, the large number of different NAs present and inherent limitations of the calibrants, the precision of these results is remarkably good and in the range exhibited by other methods.[50, 51]

Table 10: Results from OSPW analyses using two different quantitative methods, both incorporating aqueous base in the acceptor phase, Σ30 SIMs, and the I.S. correction

	DIRECT CALIBRATION			STANDARD ADDITION		
Sample	Avg. $[NA]_T$ as M.C. (ppm)	n	%RSD	Avg. $[NA]_T$ as PyBA (ppm)	n	%RSD
OSPW1	15	5	22	16	4	9
OSPW2	74	7	20	113	4	23
OSPW3	15	2	-	9.2	2	-
OSPW7	42	2	-	24	2	-
OSPW8	7.4	2	-	4.8	2	-
OSPW9	18	1	-	17	1	-
		AVG:	21		**AVG:**	16

[a] % difference = [(PyBA – M.C.) / M.C.] *100
Datafile: OSPW Improved Quantitation Summary

In general, variance in the quantitative CP-MIMS results is strongly influenced by fluctuations in instrument sensitivity, even with improvements resulting from the use of the internal standard correction. Instrumental variation as well as various aspects of the experimental setup can affect sensitivity on timescales of hours, days, weeks, and months. These variations are most noticeable for direct calibrations performed distant in time to the analysis of the samples being calibrated. Standard additions do not suffer

these issues to the same degree as they are performed directly in the sample at the time of analysis. This is reflected in the average %RSD for each method: 21% for the direct calibrations versus 16% for the standard additions. Aspects of the experimental setup can also affect sensitivity. Fouling of the PDMS membrane was usually not a major issue, but did occur on a timescales of weeks to months if very dirty heterogeneous samples were regularly analyzed. Therefore, the membrane was usually changed out every 2-3 weeks. Clogging of the ESI capillary was also a common issue, especially with the use of aqueous base in the acceptor phase (contributing salts that may have caused clogging of the very narrow diameter capillary). As a result, for weeks where experiments were performed continually, the capillary was usually changed out every ~2 days depending on instrument performance. On a longer timescale (~months), the fouling of the ESI cones became an issue, and needed occasional cleaning (usually by placing in an ultrasonic bath in MeOH). However, within the context of other methodologies, CP-MIMS still fares well: Variation in quantitative results for replicates of a single OSPW as reported by the previously mentioned 15-lab calibration study[51] varied from 1.0 to 23.7 %RSD, depending on the lab/analytical method. This still places CP-MIMS in good standing with existing methodologies with regards to reproducibility.

Given that CP-MIMS is a relatively new method for NA quantitation,[49] it is useful to put this work into context and compare with other published results. As mentioned previously, all CP-MIMS experiments conducted for this thesis incorporated a standard addition of PyBA to make results comparable to the SPE-LC-MS/MS method developed by AXYS.[50] Unfortunately, only a limited number of samples were available that had also been analyzed by AXYS, and some were quantified in units of $[NA]_T$ as PyBA equivalents, while others were quantified in units of $[NA]_T$ as Merichem equivalents from a previous inter-lab calibration study.[51] Fortunately, this thesis also quantified samples using both calibrants, and results were therefore comparable for a total of five samples (data collected in Table 11).

Table 11: Comparison studies with AXYS using Merichem and PyBA calibrations

	CP-MIMS[a]		AXYS Analytical		
Sample	**Avg. $[NA]_T$ as M.C. (ppm)**	**Avg. $[NA]_T$ as PyBA (ppm)**	**$[NA]_T$ as M.C. (ppm)[c]**	**$[NA]_T$ as PyBA (ppm)**	**% diff.**
OSPW1	15	16	-	25.9	-38[b]
OSPW2	74	113	-	150.5	-25[b]
OSPW7	42	24	56.0	-	-25[c]
OSPW8	7.4	4.8	56.9	-	-87[c]
OSPW9	18	17	57.1	-	-68[c]

[a] Data from Table 10
[b] % difference = [(CP-MIMS-PyBA – AXYS-PyBA) / AXYS-PyBA] *100
[c] % difference = [(CP-MIMS-M.C. – AXYS-M.C.) / AXYS-M.C.] *100
[d] Data from Environment Canada inter-lab calibration study[51]
Datafile: OSPW Improved Quantitation Summary

A comparison of results shows that the CP-MIMS derived concentrations are lower than those reported by AXYS. This may in part be the result of the time elapsed between analysis (CP-MIMS analysis was carried out 2-3 years earlier) and the fact that some OSPW samples froze during the storage time. OSPW1 and 2 displayed relatively good agreement in comparison with AXYS (< 40% difference). The large differences between results for OSPW8 and 9, in particular, may be partially explained by the fact that these samples froze and thawed when a lab fridge malfunctioned, and that the time between analyses was even longer than for the other OSPWs (~4 years since the Environment Canada inter-lab calibration study where data from AXYS was collected).[51] Over this time frame, processes such as biodegradation may have affected the composition of these unpreserved samples. However, even within the inter-lab calibration study itself, results for different methods varied widely. Final %RSD values for $[NA]_T$ as Merichem for OSPW7, 8 and 9 from 15 labs were 82, 74, and 75% respectively, demonstrating the inherent difficulties in the quantitation of NAs in enormously complex samples such as OSPWs.

Further comparisons for the CP-MIMS method was also achieved by comparing to results obtained by Environment Canada for three provided samples (OSPW10, 11, and 12) that had been recently analyzed by the group using LC-HRMS (orbitrap[47]). All OSPWs were quantified in units of $[NA]_T$ as equivalents of LVE2 NAFCs by first performing direct LVE2 calibration curves using the existing methodology developed in this thesis,

including addition of aqueous base and targeted SIMs based on the top 30 *m/z* in the fullscan Merichem spectrum. Agreement was good for these samples (~30 %RSD, n=3), although more replicates of both samples and LVE2 calibration curves are desired for future studies. Results are collected in Table 12.

Table 12: Comparison studies with Environment Canada using LVE2 direct calibration

	CP-MIMS[a]		Env. Canada[93]	
Sample	**$[NA]_T$ as LVE2 NAFC (ppm)**	**%RSD**	**$[NAFC]_T$ (ppm)**	**% diff.[b]**
OSPW10	45	23	45.0	0
OSPW11	29	34	43.6	-33
OSPW12	40	-	57.1	-30

[a] n=3 for all samples except OSPW12 (n=2)
[b] % difference = [(CP-MIMS - Env. Canada) / Env. Canada] *100
Datafile: Headley OSPW Sample Overview

3.6 Conclusions and Future Directions

3.6.1 Conclusions

Quantitative results for the rapid determination of total naphthenic acids in a variety of OSPWs were obtained with good reproducibility (~20% RSD) and sensitivity (detection limit ~1 ppb as $[NA]_T$). Given that analysis can be carried out directly in complex samples after a simple pH adjustment (pH < 4), the complete analytical duty cycle using CP-MIMS is limited only by the permeation kinetics at the membrane and is on the order of minutes. Quantitation was achieved by three methods: A standard addition of PyBA directly in the OSPW samples, direct Merichem calibrations (1-2300 ppb LDR), and direct LVE2 calibrations (1-7000 ppb LDR) using extracts obtained from Environment Canada. In all cases, the signals were normalized against decanoic acid added to the acceptor phase to correct for ion suppression and drift. Quantitative results were reported as total naphthenic acids ($[NA]_T$) in units of equivalents of a surrogate compound (i.e. PyBA) or a mixture (i.e. Merichem or LVE2 NAFCs) depending on the calibrant employed. Parameters that controlled quantitative analysis were explored, including

sample pH adjustment, the use of a DA internal standard to correct for some variation in instrument sensitivity, adding aqueous base to the acceptor phase to improve ionization for carboxylated species, and performing a sum of 30 SIM experiments rather than a fullscan to improve sensitivity of quantitation for complex mixtures. The base addition and targeted SIM techniques resulted in up to 30X improvement in sensitivity for some samples, 100X lower detection limits for Merichem, and almost 2 orders of magnitude improvement in LDR for Merichem calibration curves. While the subtraction of the signal at pH 7 from that at pH 4 did not in general lead to an improvement in the accuracy or precision of the method (and was thus abandoned), it did demonstrate that the presence of high concentrations of organic acids can suppress the ionization of both carboxylated and hydroxylated compounds in the ESI- spray. In particular, it was observed that carboxylated model compounds were more effective at suppressing hydroxylated ones under the conditions employed here. Although the membrane is permeable to a variety of relatively non-polar contaminants (e.g. PAHs, ethers, and ketones), they are not readily ionized and do not easily hold a charge in the ESI- source. Consequently, the primary AEOs observed in these CP-MIMS experiments at pH 4 are in fact carboxylic acids. Our group and others have previously shown that the O_2 negative ion class (classical NAs) represents a significant portion of ESI- compounds in OSPWs.[41, 49]

Quantitative results for a variety of OSPW samples compared well (around 30% difference for most samples) to published methods from Woudneh et al.[50] and Leshuk et al.[47] Considering the on-going challenges inherent in this work including the complexity of the samples and analyte sub-classes, lack of analytical standards, and methodological protocols for sample handling, the work presented here makes an important contribution to analysis of naphthenic acids. As a reference, a single OSPW sample analyzed by 15 different labs for an Environment Canada interlab calibration study[51] returned results with intra-method variances of up to 23.7 %RSD and inter-method variances of up to 81.7 %RSD. In summary, NA quantitation via CP-MIMS is best achieved with 1) samples buffered at pH < 4, diluted to a concentration where ionization suppression is not significant (ideally < 20% signal suppression, typically $[NA]_T$ < 5 ppm), 2) addition of

aqueous base to the acceptor phase to improve R-CO_2H ionization, 3) correction for instrumental sensitivity variations with a DA internal standard in the acceptor phase, and 4) calibration with a geographically relevant extract performed close in time (± 1 day) to the samples being analyzed, or ideally, directly in the sample as with the 1 point standard addition method with PyBA (or some other desired calibrant).

CP-MIMS as a rapid-screening tool for NAs is expected to be of high value for decision makers in the Canadian oil sands, as the storage, treatment and release of OSPW is a multi-billion dollar concern.[20] The method as currently described with nominal mass resolution can be used to pre-screen samples so that only those with significant concentrations of NAs can be collected for a more intensive, thorough analysis employing chromatographic separation. Furthermore, the adaptation of condensed phase membrane introduction methods to high resolution mass spectrometry and multiple ionization modes will provide greater characterization of multiple contaminant sub-classes in OSPWs. Ultimately, this method is expected to be mobilized and operated in the field to make rapid measurements of naphthenic acid-containing samples directly at contaminated sites in the oil sands. With a low-cost, rapid, mobile measurement tool such as CP-MIMS, researchers can obtain higher data density, allowing them to make on-the-fly decisions and adapt their sampling techniques to reflect where the compounds of concern are located. This research will therefore assist industry and policy-makers support the protection of human and environmental health through an improved understanding of the concentrations and whereabouts of naphthenic acids in contaminated waters present at oil sands extraction and processing sites, as well as improved environmental monitoring downstream from transportation and refining processes.

3.6.2 Improving Duty Cycle

One of the strengths of CP-MIMS is the ability to rapidly screen samples to obtain quantitative and qualitative information within minutes.[49] In this thesis, a duty cycle of ~50 minutes was achieved for NA quantitation, which included obtaining baseline, analyzing the OSPW sample at pH 4, performing a PyBA standard addition, and finally rinsing the membrane with MeOH. This stands to be improved, and reducing the time of analysis can be achieved in several ways. Eqn. 2 (section 1.3.1) shows that risetime is proportional to the square of the membrane thickness. Therefore, thinner membranes have the potential to improve risetimes and significantly speed up analysis. Previous work with such membranes (such as the 0.5 μm and 35 μm membranes used by Duncan et al.[49]) has shown them to be very fragile, with careful handling required to avoid compromising their integrity. Despite this, their use could allow the quantitation duty cycle to easily be halved to just over 20 minutes per sample. Preliminary experiments were conducted with a 35 μm membrane and dilute Merichem, and it was found that risetimes were significantly reduced (up to 50%), and steady-state could be achieved for the complex mixture in under 5 minutes. This would mean that a quantitation experiment involving achieving baseline, analyzing an OSPW sample at pH 4, performing a 1 point PyBA standard addition, and rinsing the membrane back to baseline signal would be achievable in ~20 minutes. Risetime is also inversely proportional to the diffusivity of the analyte in the membrane, which increases with temperature. Therefore, another possible method of improving the analytical duty cycle would be to employ a heated membrane, as in previous work from other members of our group.[97]

It is also possible to add a nonpolar cosolvent to the CP-MIMS acceptor phase to potentially decrease risetimes and assist the transport of other classes of molecules, including PAHs, across the membrane. In addition to swelling the membrane and therefore making the membrane more permeable, the cosolvent may also assist ionization in the ESI source. An organic solvent can increase the organic character of the ESI droplets, meaning compounds with lower K_{ow} (smaller degrees of organic partitioning) will have increased sensitivity, as they prefer to partition out of the highly organic droplet

and into the gas phase. This was hypothesized to hold true for components of OSPW, and a preliminary experiment was conducted employing 12% v/v heptane as an acceptor phase dopant. Results showed reduced risetimes (~54% reduction) and increased sensitivity (~30%) for a solution of 5 ppm Merichem in DI (Table 13).

Table 13: Cosolvent study with 5 ppm Merichem in DI in the donor phase and 12% v/v heptane/MeOH in the acceptor phase

Acceptor phase	Signal Intensity (ΣSIM *m/z* 213, 223, 237)	t_{10-90} (min)	% Signal increase
MeOH	1,383,204	6.14	-
MeOH + heptane	1,961,666	3.31	29.5

Datafile: DFMIMS_030

With an improved duty cycle, CP-MIMS dip-probe experiments could be automated to achieve rapid screening of larger numbers of samples. For example, pairing the 'J-probe' design with an autosampler is a simple task, and can make automated, rapid analysis of multiple OSPW samples very simple.[59] In addition, preliminary work from our group has shown that it is possible to reproducibly quantify samples in complex matrices using the non-steady state region of the CP-MIMS signal.[59] This would significantly reduce analysis times, particularly for compounds with longer risetimes (such as many components of Merichem NAs), and further enable rapid analysis of multiple samples. Samples with significant concentrations of NAs could then be selected for more a thorough analysis, for example, with high-resolution mass spectrometry paired with chromatography.

3.6.3 Improving Quantitation

Quantitation improvements should begin with a detailed analysis of inter- and intra-day precision, particularly with regards to instrument sensitivity fluctuations, as these seem to be the largest source of error in experiments conducted for this thesis. The quantitation strategy that experienced the least of this error was the PyBA standard addition, likely because it occurred directly in the sample at the time of analysis, and therefore left the least amount of time for the introduction of instrument sensitivity fluctuations to affect

results. Experiments where quantitation is achieved via a direct calibration run several days-weeks earlier could also incorporate a 1-2 point calibration 'check' on the day of the experiment to assess if the calibration slope has changed due to sensitivity variations. However, a possible future avenue of research is to try to perform standard additions of complex mixtures (such as Merichem or one of the large volume extracts) directly in a sample rather than performing direct calibration curves. This would minimize the time/sensitivity issues and still allow calibration with a more representative mixture. With these existing methodologies, future work should certainly involve analyzing replicates of both the Merichem and LVE calibration curves, in addition to pushing the high end of these curves to more clearly understand when ion suppression becomes an issue.

In general, there are many aspects of CP-MIMS that can be further 'tuned' to optimize quantitation. This thesis only managed to explore a few out of many available options for optimizations at the sample, membrane, acceptor phase, ion source, and mass spectrometer levels. Some ideas are outlined in Table 14, indicating options that have been explained to date by our group.

Table 14: Future studies 'optimizations' for various aspects of CP-MIMS

SAMPLE		MEMBRANE		ACCEPTOR PHASE		ION SOURCE		MASS SPEC.	
pH ±	✓	170µm PDMS	✓	I.S.	✓	ESI-	✓	QqQ	✓
Buffer	✓	35µm PDMS	×	Cosolvent	✓	ESI+	×	FT-ICR	×
PyBA	✓	0.5µm PDMS	×	Base addition	✓	APPI-	×	Orbitrap	×
pKa	×	Nafion™	×	Acid addition	×	APPI+	×	Single Q	×

✓=attempted in this thesis, ×=not attempted in this thesis or attempted elsewhere

For this thesis, sample pH adjustments, buffers, and standard additions of PyBA were attempted, but there remains interesting work to be done with regards to pH studies. CP-MIMS has shown potential to rapidly determine pKa values for specific NAFC isomer classes. pKa values are important parameters in beginning to better describe components of OSPW mixtures, and can offer insight into the behavior of NAFCs during remediation processes. By monitoring the CP-MIMS signal for an isomer class within a NA sample (i.e. all NAFCs present at nominal mass *m/z* 237) as the pH is changed over time, it is

possible to elucidate a pKa value for that class. If this is repeated for all major nominal masses in the NA spectrum, it can provide a wealth of information useful for those interested in remediation as well as researchers interested in better characterizing these complex samples. A 170μm PDMS membrane was used for all the work presented in this thesis, but there are many other options including thinner membranes as described in section 3.7.2, and other membrane materials such as Nafion™ that can be chosen depending on the characteristics of the analyte being studied.[64] An internal standard and addition of aqueous base in the acceptor phase were both used to optimize quantitation, and the possibility of using a cosolvent to improve risetimes and potentially ionization was briefly explained in section 3.7.2. Negative-ion ESI was the only ion mode used in work presented by this thesis, but others have been used with CP-MIMS with great success.[88] A simple modification of the existing setup would allow for several experiments to be re-analyzed in ESI+ mode, with aqueous acid added to the acceptor phase instead of base to assist ionization of carboxylic acids. Positive ion mode could reveal a greater variety of species present in complex mixtures such as Merichem, and perhaps in tandem with negative ion mode, improve the reproducibility and accuracy of CP-MIMS quantitation considerably. Finally, although only one 'type' of mass spectrometer was used in this thesis (a low resolution triple quadrupole MS), there are many others that remain to be explored. Preliminary qualitative work with CP-MIMS and a high-resolution FT-ICR instrument was published by our group,[49] but there remains work to be done with this configuration to achieve quantitative results. Other high-resolution instruments (such as orbitraps) have been shown to be effective in tandem with ESI for quantifying NAs,[47] and CP-MIMS could easily be applied to this configuration. Finally, single-quadrupole instruments have the distinct advantage of portability, and could be paired with CP-MIMS to mobilize this technique for rapid screening of NA samples directly in the field.

3.6.4 Analytical Standards

Looking more broadly, future goals for any project looking at quantitation of NAs in complex samples should include finding a better standard against which to validate

quantitative results. This is a problem affecting the whole field of NA analysis, and one that will continue to provide challenges in attempting to quantify real-world naphthenic acid mixtures. With the existing Merichem and LVE extracts, a good deal more could be done to differentiate the two mixtures and improve quantitation based on the specifics of each. For example, a different 30 SIM experiments could be developed based on the top 30 *m/z* peaks in the LVE1 or LVE2 spectra. Based on data from Table 7 previously, these would very likely better represent compounds present in northern Alberta process waters, and would certainly capture more information for the set of samples analyzed for this thesis than the top 30 *m/z* chosen from Merichem that were used. Techniques such as chemometrics might allow greater differentiation of these two calibration standards and optimization of how they are used to quantitate. In general, the field of NA quantitation needs to adopt the standardization of quantitation practices and calibration standards for NA mixtures. Ongoing work in this area continues to evolve the field and enable improved inter-laboratory comparisons. Until then, comparable quantitative analytical data for naphthenic acids will be hard to obtain, despite significant advances in instrumentation and our qualitative understanding of these complex mixtures.

Chapter 4: Qualitative Applications of Naphthenic Acid Analysis with CP-MIMS

4.1 Introduction

There is considerable interest in understanding more about the factors affecting the relative abundance of NAFCs in complex mixtures such as OSPWs and impacted natural waters, from industrial, government and academic perspectives. Industrially, decision makers need to know what components of their process to monitor, and to develop appropriate responses for emission mitigation and/or remediation.[91] Academically, these complex mixtures provide a welcome challenge for the ever-expanding world of high-resolution mass spectrometry, as described by researchers such as Barrow[98] and Headley.[12] Mass spectrometry is very well suited to both qualitative and quantitative studies aimed at teasing apart the many components constituting these mixtures, especially when combined with emerging separation techniques such as 2D gas chromatography[27] and capillary electrophoresis.[43] Selective and sensitive quantitative information is available alongside a wealth of unique qualitative fullscan sample data, and when using a high mass accuracy instrument, determination of molecular formulae becomes possible. This has allowed for the identification of hundreds of compound classes and thousands of individual compounds within OSPW samples, including NAFCs containing heteroatoms such as nitrogen and sulfur.[4]

However, high-resolution instruments and chromatographic techniques are generally expensive and time consuming, requiring specialized technical personnel, extensive sample handling and cleanup, and are far from portable. Because samples can be directly measured by CP-MIMS within minutes to obtain nominal mass resolution using a single quadrupole mass spectrometer, the technique offers a useful intermediate between quick presence/absence tests (i.e. FTIR)[99] and more thorough analyses[13] with the potential to portabilize and deploy directly in the field. Since the bulk of the complex matrix is excluded while neutral hydrophobic analytes diffuse through the membrane, the

technique allows for the direct *in-situ* monitoring of processes in complex, even heterogeneous samples as shown in Fig. 32. The mass spectrometer provides nominal mass selectivity and is sensitive to sub-ppb levels for individual isomer classes using targeted SIM experiments. In addition, fullscan data provides mass profiles that can be employed to rapidly screen and identify samples as well as observe qualitative changes in real-time during dynamic processes such as adsorption[49] or photochemical degradation.[78] It should be noted that CP-MIMS measures the free concentration of analyte in solution. If the total amount of analyte added to a heterogeneous system is known, then the amount adsorbed can be determined by mass balance.

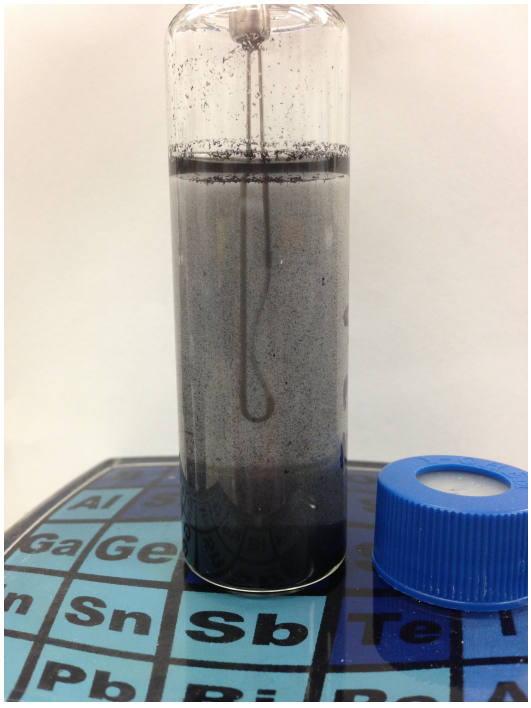

Figure 32: Direct screening of adsorption processes in a complex heterogeneous sample using the CP-MIMS 'J-probe'

The relevance of this work to activities in the Athabasca oil sands is manifold. With naphthenic acids being a major contaminant of concern in tailings ponds, there is great interest in possible methods of cleanup or removal for these compounds.[47, 91] CP-MIMS is potentially a very powerful tool for direct real-time monitoring of processes designed to remove naphthenic acids. In the laboratory, the continuous on-line nature of CP-MIMS

allows researchers to probe the kinetics of NA removal for effectiveness in test systems, and to rapidly screen possible adsorbents for their adsorption capacity.[100] CP-MIMS can be used to obtain kinetic data not accessible to other methods, including *in-situ* measurements of 1) qualitative changes in the mass profiles of naphthenic acid mixtures during adsorption, 2) the sorptive capacity of different materials using steady-state signals before and after adsorbent addition, and 3) the adsorption kinetics of various naphthenic acid isomer classes. If needed, all of this data can be obtained with a single CP-MIMS experiment. The motivation of this work is to develop rapid screening methods to assess the performance of a variety of adsorbents for NA removal, potentially providing invaluable information to developers of sorbent-based clean-up methods for NAs. These applications of CP-MIMS are explored in this chapter.

4.2 Experimental

4.2.1 Solutions and Buffers

Merichem NA solutions were made up gravimetrically to 5 ± 1 ppm $[NA]_T$ as Merichem by adding concentrated Merichem stock to both buffered and unbuffered aqueous solution. Units of ppm refer to mass ratios (e.g., mg of analyte or biochar / kg solution), and all solutions were prepared gravimetrically. Solutions were either made up in 40 mL TOC vials or 250 mL beakers, depending on the sample volume desired (higher sample volumes allowed for greater dilution of the biochars, which could only be weighed out to a minimum of ~1 mg). During initial studies, the pH of these solutions were adjusted to pH ~4 with concentrated HCl added dropwise. After it was observed that the some adsorbents were alkaline and thus changed the solution pH at high loadings, a citrate buffer (68.3 ppm, pH 4.5) was employed to prevent pH shifts. However, this buffer proved ineffective at the desired sample pH range (3-4) because citrate in acidic form is neutral and crosses the PDMS membrane, interfering with analytical sensitivity, and potentially introducing signal suppression in the ESI source. In addition, a higher buffer

capacity was desired to counteract the highly alkaline adsorbents. An improved glycine/HCl buffer was then employed,[101] using 7500 ppm glycine (Fisher Scientific) made up in DI water with addition of concentrated HCl to adjust the pH to 3.60 ± 0.1. Because glycine is zwitterionic at pH values 3-4, it does not cross the PDMS membrane, and is therefore ideal for this application.

4.2.2 Adsorption Studies

Adsorption studies were carried out by continuously monitoring NAs directly in aqueous solutions with fullscan and SIM experiments (mass spectrometry conditions described in section 2.2.3). Activated biochar samples were added to buffered NA samples to achieve final concentrations ranging from ~20-2000 ppm, with constant stirring. Two distinct biochar samples were used for comparison purposes. Sample A was prepared by pyrolysis of Aspen wood under nitrogen at 600°C. Sample B was commercially available (ColorSorb G5®, Jacobi, Kalmar, Sweden). These biochars were chosen for their availability and observed differences in adsorptive properties.[102] After achieving stable baseline signals in DI water, the CP-MIMS membrane probe was immersed in an aqueous solution containing ~4-5 ppm of Merichem. After obtaining at least 5 min of steady-state NA signal, a dose of solid biochar was added to the Merichem/buffer solution. Upon initial addition, the sample vessel and newly added adsorbent were well shaken to ensure wetting. Signal decay resulting from NA adsorption was monitored via the fullscan TIC as well as targeted SIM values (e.g. *m/z* 185, 223, 231, 237, and 263).

4.2.3 Multi-Loading Experiments

Multi-loading experiments were carried out either by adding successive loadings of solid biochar to a prepared glycine-buffered NA solution (1-2 mg per loading, final conc. 8-10 ppm in sample vial), or starting with a heterogeneous solution of glycine-buffered biochar and successively loading NA via volumetric injections of a stock solution (~0.2 mL of ~30 ppm stock, final conc. ~20 ppb in sample vial per loading). Multi-loading

experiments were performed at constant temperature (34 ± 1°C) using a hotplate and a glass thermometer to monitor temperature readback. All solutions were rapidly stirred via a magnetic stir plate set to 400 rpm. To eliminate any potential interference between experiments from biochar adhering to the membrane surface, the membranes were either replaced or washed thoroughly by immersing in methanol between samples.

4.2.4 Data Processing and Mass Spectra

Final fullscan mass spectra were background-subtracted and filtered to eliminate minor peaks under 2% total intensity using MassLynx™ software. Some experiments were performed at both pH 7 and pH 4 and subtracted (pH 4 - pH 7) in an attempt to remove non-acid components (i.e. hydroxylated species) in the sample from the spectrum. Other experiments simply analyzed the sample at pH 4, once it was established that the subtraction technique tended to over-correct the mass spectra (vide supra). To ensure that that observed changes in the mass spectra were not a result of any undesired pH changes in the sample induced by biochar dosing exhausting the buffer capacity, the sample pH was continuously monitored during adsorption experiments using a pH meter (Accumet AR25, Fisher Scientific) immersed in the sample.

4.3 Adsorption with Engineered Biochars

4.3.1 Preliminary Adsorption Study

An exploratory experiment was conducted by adding 1700 ppm of 'off-the-shelf' activated charcoal to an aqueous solution containing 6.2 ppm $[NA]_T$ as Merichem. The concentration of solution phase NAs was continuously monitored via CP-MIMS, as shown in Fig. 33. The upper panel shows the Merichem spectrum before addition of adsorbent, and the lower panel shows the spectrum ~1 hour after activated charcoal was added and the signal had reached steady-state. The capability of CP-MIMS as a dynamic

process monitor is demonstrated by the inset chronogram, which shows the fullscan TIC signal. After the addition of Merichem NAs, the TIC rises to steady-state within ~10 mins. When 1700 ppm of adsorbent is added, the signal decays to baseline over the course of the next ~60 mins, showing nearly 100% removal of all NA isomer classes. Given measurement frequency of 0.2 Hz, this corresponds to thousands of data points with excellent temporal resolution.

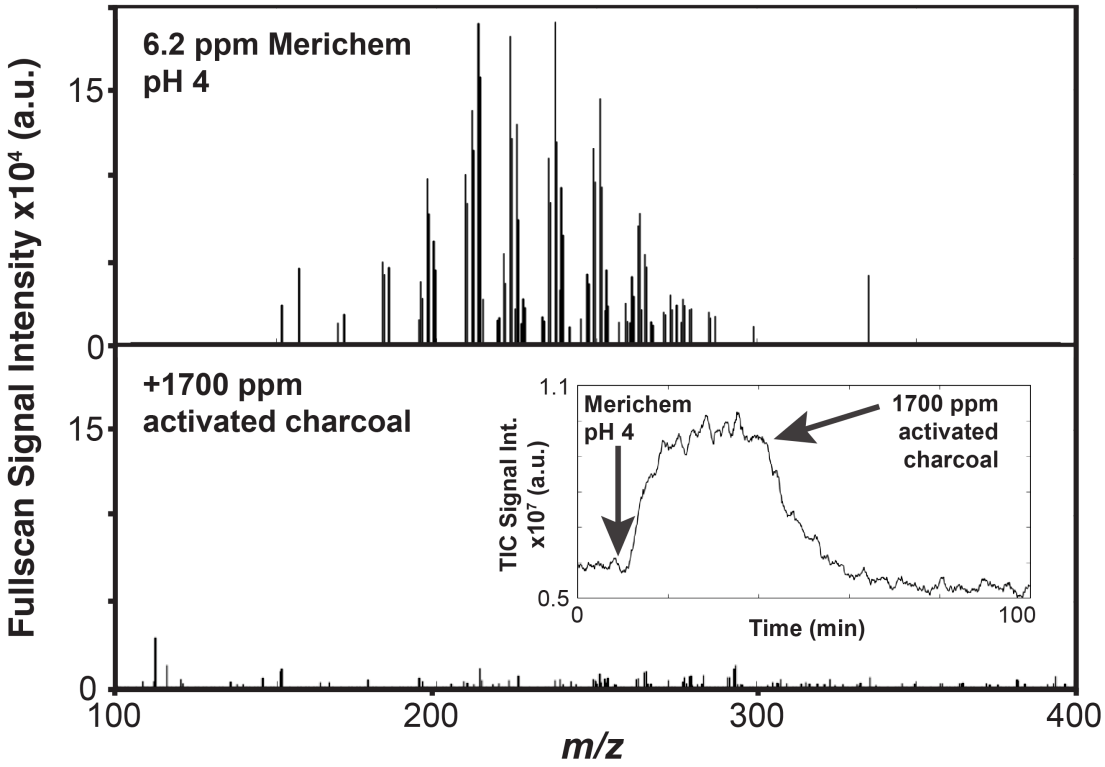

Figure 33: Merichem adsorption on activated charcoal. Upper panel shows the 'before' spectrum (0 min) for an aqueous solution of 6.2 ppm Merichem at pH 4. Lower panel shows the spectrum after it has experienced a full decay (100 min) after the addition of 1700 ppm activated charcoal at roughly 40 min (Datafile: DLMIMS_034)

The mass spectra displayed in Fig. 33 represent a snapshot of the 'before' and 'after' conditions with regards to addition of adsorbent, and every one of the hundreds of data points contained between represents a full mass spectrum available for any particular point in time during the decay. This demonstrates the capability of CP-MIMS to directly probe what is occurring during a dynamic process at any point in real-time, versus

traditional analytical methods where discrete samples are collected every few minutes, which can be laborious, giving far fewer data points with poorer kinetic resolution.

4.3.2 Sample pH and Buffering

Several engineered biochars (Layzell, University of Calgary) were screened for their ability to adsorb naphthenic acids. The Layzell group kindly provided two biochar samples with differing sorptive properties towards NAs, given without prior knowledge of their identity and simply labeled 'A' and 'B'.[102] This thesis set out to characterize the effectiveness of both materials in terms of their capacity and rate of NA removal using *in-situ* measurements enabled by CP-MIMS. Initial experiments revealed that biochar B was significantly more effective at removing naphthenic acids, and indeed most components in the Merichem mass spectrum. It was also observed that in addition to being fairly ineffective at adsorbing naphthenic materials, biochar A seemed to effect an upwards mass profile shift. Fig. 34 demonstrates this behavior with a 5 ppm Merichem solution and 'high' loading of biochar A (2300 ppm). The upper panel shows the 5 ppm Merichem solution, brought to pH < 4 using concentrated HCl before biochar A is added. The lower panel shows an inverted spectrum after the biochar is added and decay is complete (~55 mins). The inset ion chronogram shows the decay of three SIM *m/z* upon addition of biochar A.

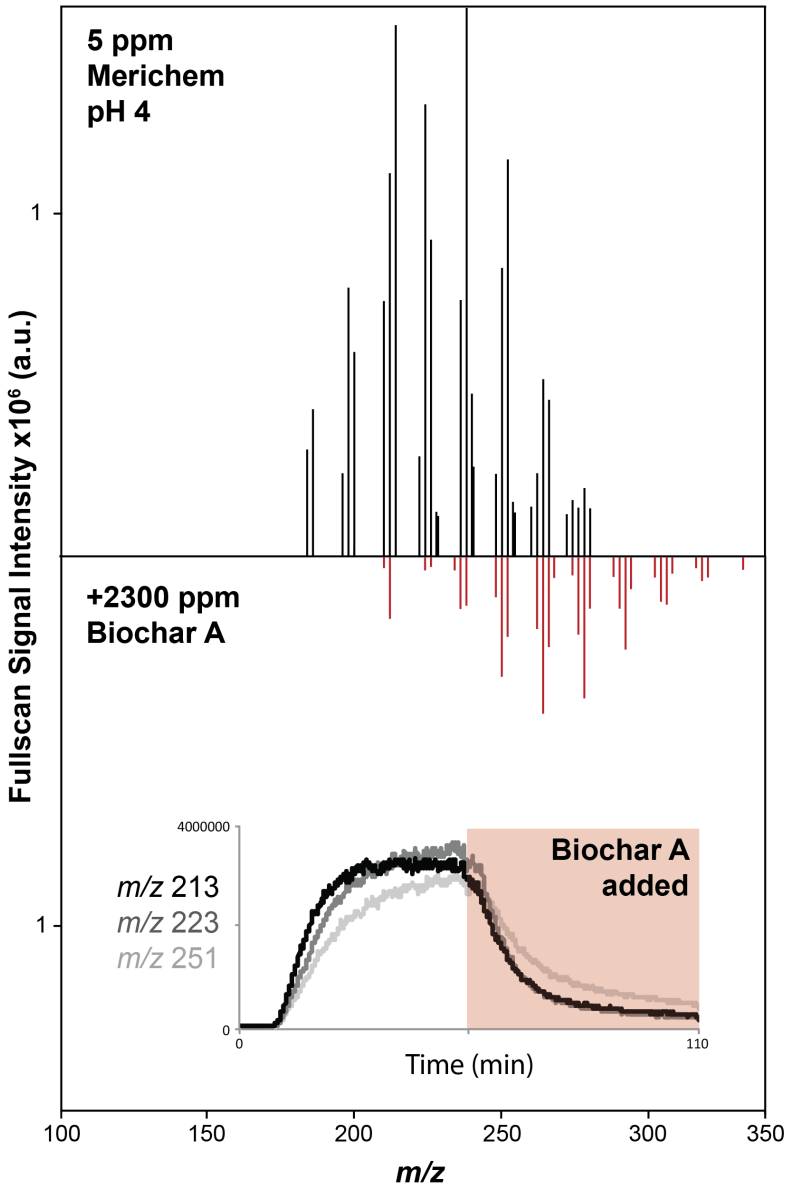

Figure 34: Spectral shifting and loss of intensity due to pH changes in solution after addition of biochar A adsorbent to a 5 ppm Merichem solution (Datafile: DLMIMS_108)

When the pH of the Merichem and biochar solution was checked after adsorption decay was complete, it was found to have shifted from pH 4 to 6.5. This was assumed to have resulted from the addition of biochar A, which was shown to have a high alkalinity. It was therefore suspected that the behavior observed in Fig. 34 was due to pH change (affecting membrane transport) and not adsorption activity. To probe whether biochar A had been at all effective as an adsorbent (i.e. how much of the decay/spectral shift was

due to the pH change), another experiment was performed where 5 ppm Merichem at pH 4 was monitored after the addition of a high loading of biochar A (3200 ppm). After the signal had decayed to a baseline, the pH was taken, and the sample filtered to remove the adsorbent (presumably with adsorbed NAs). Finally, the pH was adjusted back down to 4 with concentrated HCl added dropwise. Fig. 35 shows the resulting spectra. Panel A displays Merichem before addition of adsorbent. Panel B displays a spectrum taken after signal decay had reached baseline, showing reduced intensity and an upwards mass shift. Panel C shows the spectrum after the sample was filtered and adjusted back to pH 4 – essentially identical to panel A, the initial Merichem spectrum before addition of adsorbent. Finally, panel D shows the spectrum in panel C after a concentrated Merichem spike (final concentration 5 ppm) was added on top of the filtered sample.

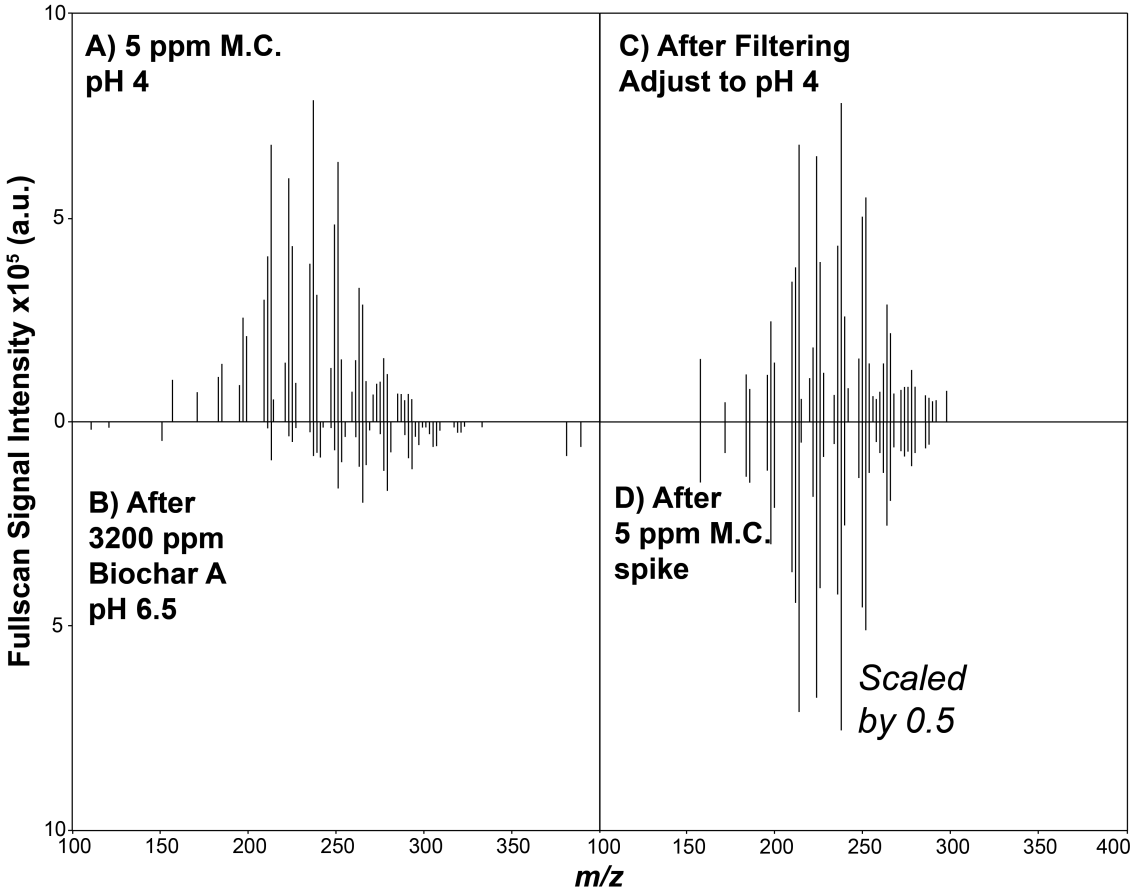

Figure 35: 5 ppm Merichem A) at pH 4, B) after 3200 ppm of biochar A added, C) after filtering the biochar from this solution and adjusting the pH back to 4, and D) after 5 ppm of Merichem is spiked on top of the filtered sample (Datafile: DLMIMS_108)

The addition of the final concentrated Merichem spike in panel D resulted in essentially a doubling of the intensity of the spectrum in C, confirming that C also represented ~5 ppm Merichem, the same amount started with in panel A. This experiment therefore confirmed that the perceived decay and mass shifting upon addition of a high loading of biochar A were due entirely to pH change upon addition of adsorbent, and not due to adsorption activity by biochar A. To further elucidate this, several experiments were performed where the pH meter probe was continuously immersed in the NA solution as the adsorption process occurred. Results confirmed that the addition of biochar did change the pH of the solution by up to 2.5 pH units. However, given the high loading of this biochar in Fig. 35 (and other results obtained where adsorption behavior due to addition of this biochar was confirmed), it seems unlikely that biochar A was unable to adsorb any components of the Merichem solution over the ~60 minute 'decay' experiment. It was hypothesized that the initial pH change (upwards by 2.5 pH units) upon addition of the biochar ionized the acids in the sample and made their adsorption on biochar A unfavorable. Thus, it seems that in this case, carboxylic acids ($R\text{-}CO_2H$) adsorb to biochar, whereas carboxylates ($R\text{-}CO_2^-$) do not.

Because of this, it was determined that all NA samples should be buffered prior to addition of adsorbent. Unfortunately, at pH < 4 the protonated form many buffers will pass through the PDMS membrane and compromise ionization in the ESI source or show up in the mass spectrum. A citrate buffer was tried but was ineffective at the concentration levels and pH required to perform these experiments. Finally, a 7500 ppm glycine buffer at pH 3.6 was employed, which effectively held the pH constant to within ± 0.1 pH units at even the highest loadings (2300 ppm) of biochar. The success of this buffer is attributed to both acidic and basic forms of glycine being ionized at pH values < 3, therefore it did not pass through the membrane even at very high concentrations in the sample. Experiments were redone at stable pH with various loadings of biochar. These experiments revealed no major mass profile shifts, only spectral decay presumably due to adsorption behavior. Fig. 36 shows a buffered adsorption experiment with a high loading of biochar A.

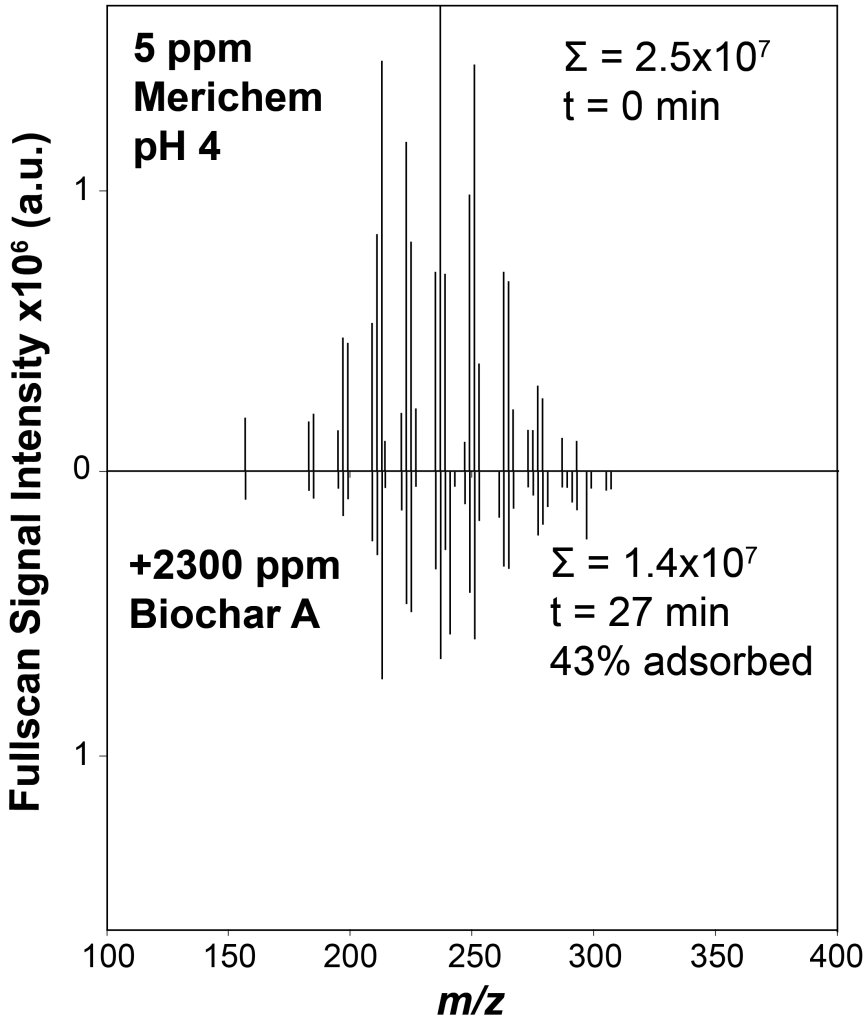

Figure 36: Biochar A high loading with buffer. Upper panel: 5 ppm Merichem spectrum at pH 4 (in buffer). Lower panel: Inverted spectrum after high loading (2300 ppm) of biochar added, effecting a 43% decay of the original Merichem spectrum (Datafile: DLMIMS_111)

In this case, the addition of biochar had no mass-shifting effect on the Merichem spectrum. The only spectral change was a reduction in overall intensity, presumably because of adsorption onto biochar A, although possible sources of error in the high-loading experiments include improper stirring (high loadings of biochar adhered to the surface of the sample solution, the surface of the CP-MIMS probe, and membrane and never fully mixed into the solution), and also the possibility of membrane fouling.

4.3.3 Screening of Engineered Biochars

After a buffer had been chosen and experimental procedure established, a control experiment was performed with biochars A and B added to a sample vessel containing buffer, with no naphthenic acids, to see if any components of the two biochars crossed the membrane and showed up in the range of typical NA masses (*m/z* 100-400). Fig. 37 shows the results from the background-corrected spectra, which mostly consist of noise. All extracted spectra for these adsorption studies were background subtracted using the background for pure glycine buffer.

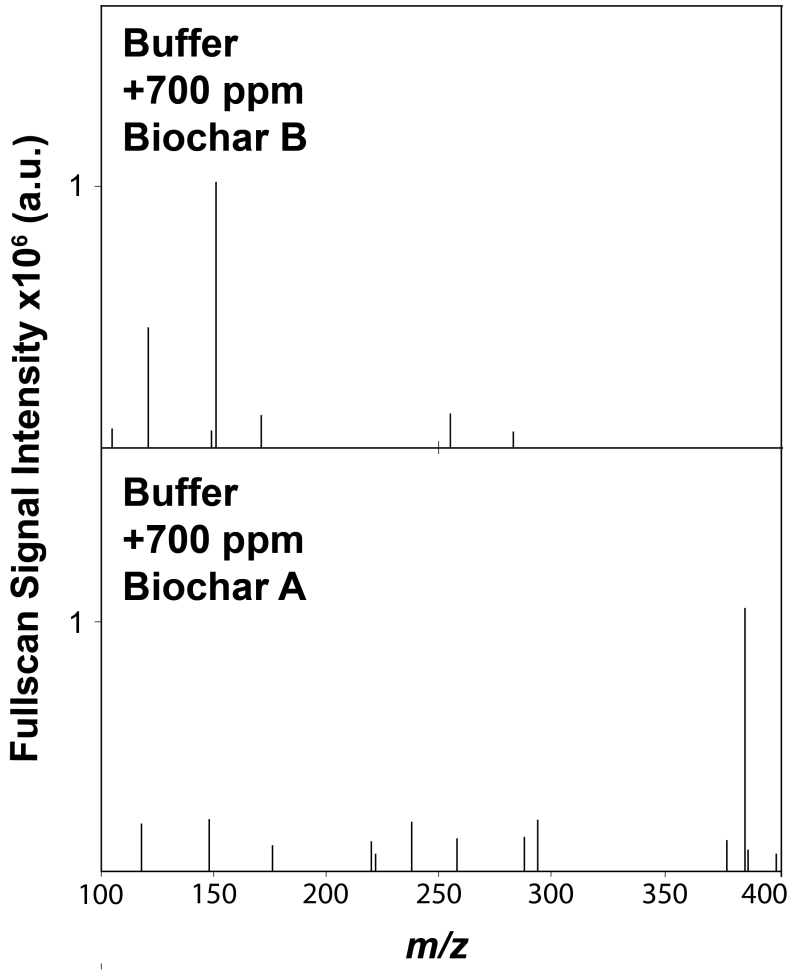

Figure 37: Sample A and B background spectra (Datafiles: DLMIMS_101-102)

The next experiments attempted with a buffered Merichem solution involved both biochars added at a medium loading (~700 ppm). Fig. 38 gives a visual reference for the quantity of biochar required to achieve this loading in the 40 mL TOC sample vial, with a one dollar Canadian coin (26.5 mm diameter) for reference.

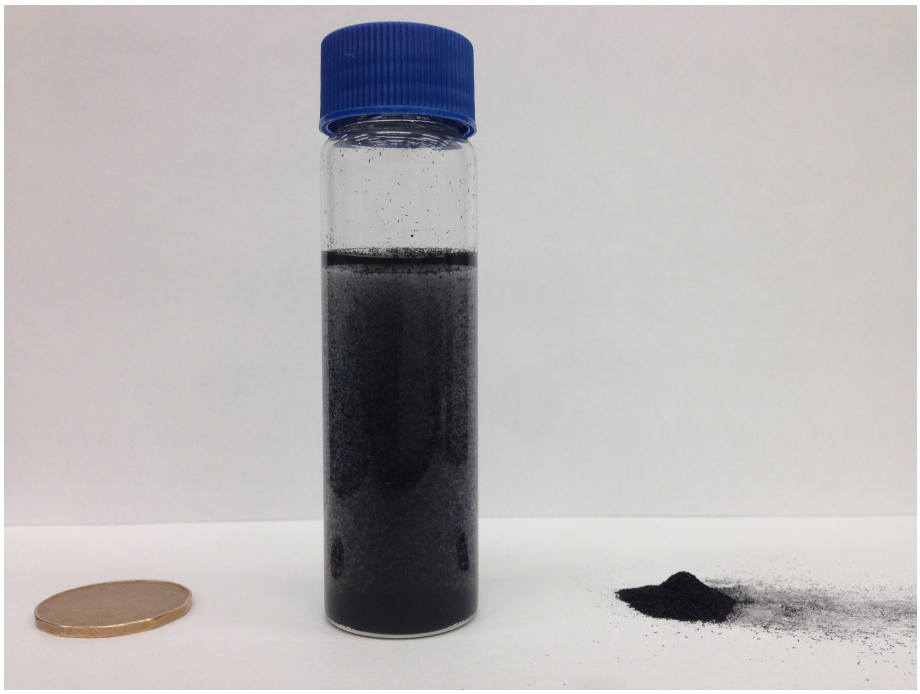

Figure 38: Biochar A medium loading by itself and in solution (700 ppm), with a 1 dollar Canadian coin (26.5 mm diameter) for reference

Fig. 39 displays results from the medium loading experiments. The figure shows spectral changes for loadings of both biochar A and B, presented as spectra before addition of biochar (upper panels) and after addition of biochar (lower panels). From the figure, it is evident that biochar B has nearly caused a complete decay (99%) of the spectrum to baseline, almost completely removing all major components of Merichem between *m/z* 100 and 400 (presumably due to adsorption behavior). Biochar A at the same loading has affected only a partial (40%) spectral decay.

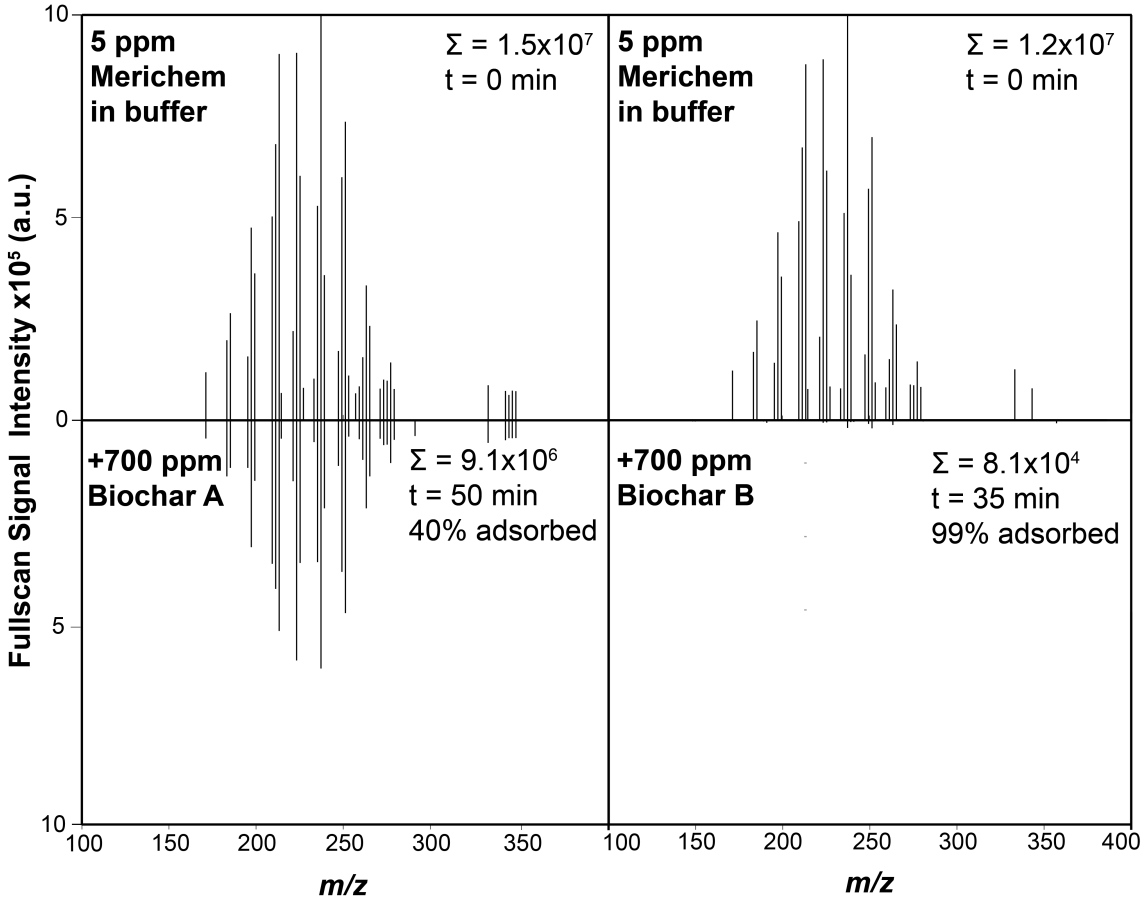

Figure 39: Biochar adsorption study with Merichem. Upper left: 4 ppm M.C. at pH 4, lower left: Same M.C. solution with biochar A medium loading. Upper right: 4 ppm M.C. at pH 4, lower right: Same M.C. solution with biochar B medium loading (Datafiles: DLMIMS_131-132)

These experiments confirmed that biochar B is indeed more effective than biochar A at removing most components in the Merichem solution. These results were relayed to the Layzell group, who confirmed that biochar B was indeed the biochar engineered to adsorb naphthenic acids. At this stage, the Layzell group provided full information on both samples (described previously in section 4.2.2). Various loadings of the biochars were attempted to better characterize their behavior. Low loadings (~25 ppm) were determined based on the smallest mass of biochar that was convenient to weigh out and deliver into the 40 mL reaction vessels. High loadings (~3200 ppm) were determined based on the maximum amount of biochar material that would easily stir into the reaction vessels. Fig. 40 shows results from a low loading of biochar A and a low loading (25

ppm) of biochar B. The upper panels show the mass spectrum of 5 ppm Merichem solution before biochar is added. The lower panels display the final mass spectrum after decay has ceased (35 min).

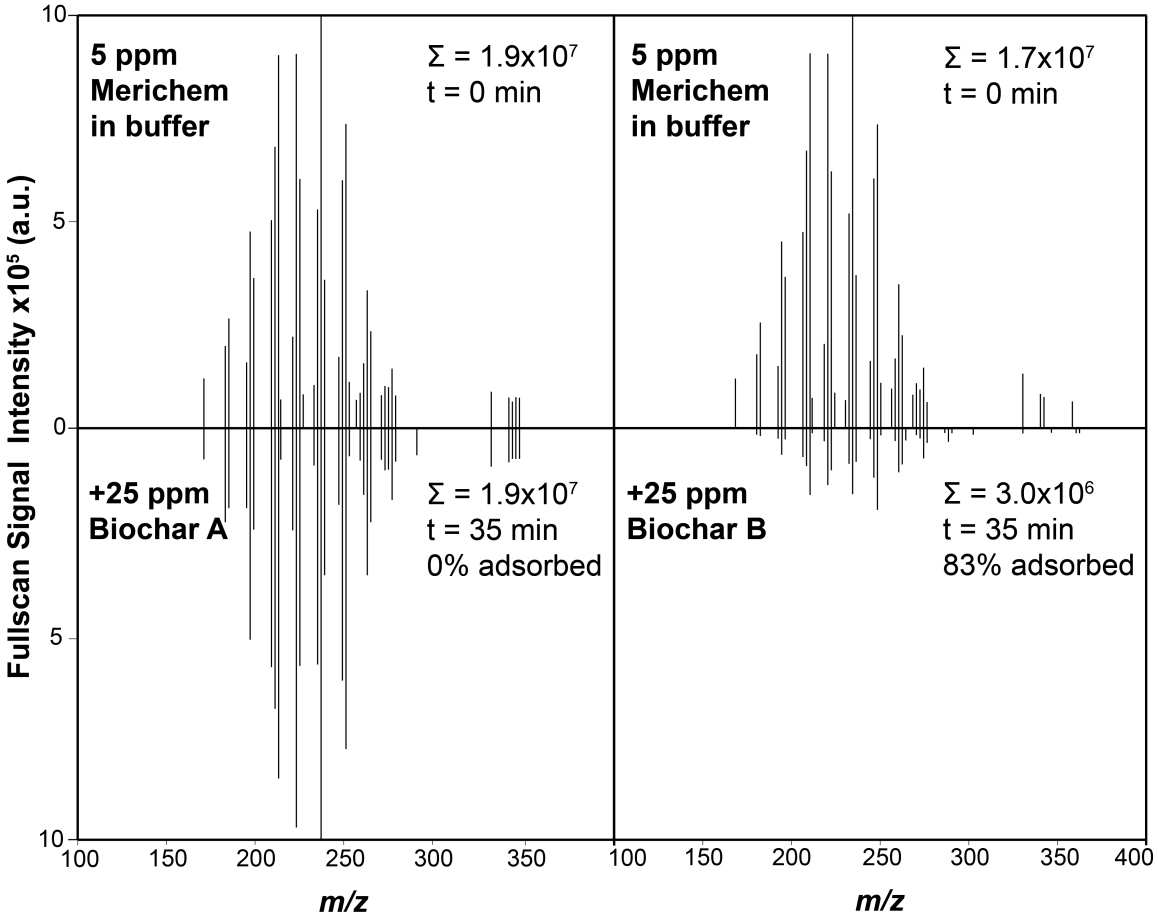

Figure 40: Biochar adsorption study with Merichem. Upper left: 4 ppm M.C. at pH 4, lower left: Same M.C. solution with biochar A low loading. Upper right: 4 ppm M.C. at pH 4, lower right: Same M.C. solution with biochar B low loading (Datafile: DLMIMS_131)

The low loading of biochar B has resulted in an incomplete spectral decay, allowing for some interpretation of the resulting final spectrum (unlike in the medium loading, where biochar B left an essentially 'blank' spectrum at the end). This biochar has appeared to select certain peaks in the spectrum over others, preferring to remove lower masses and therefore leaving the resulting final NA spectrum shifted to higher *m/z*. Recalling from the quantitative work that hydroxylated species in Merichem samples generally show up

at higher *m/z*, this strongly indicates the preference of biochar B to adsorb the carboxylated over the hydroxylated components present in the mix, and therefore its effectiveness at removing naphthenic acids from solution. These results are consistent with the description provided by the Layzell group, and demonstrate the ability of CP-MIMS to rapidly screen adsorbents for their effectiveness in removing NA components from solution. Table 15 collects the final results for the two biochars that were screened. Percent removals are presented after decay signals have reached steady-state, although for the 2300 ppm loading of biochar A, data is inconclusive as the experiment should have been allowed to continue to at least 50 minutes after biochar addition before the % removal was calculated. In addition, high loadings of biochar caused significant fouling of the membrane interface, especially when stir rates were insufficient to ensure proper mixing. Therefore experimental error must be taken into account when interpreting these results.

Table 15: Adsorption of 5 ppm Merichem with various loadings of biochars A and B

	BIOCHAR A		BIOCHAR B	
Loading (ppm)	**% removal**	**After time (min)**	**% removal**	**After time (min)**
25	0	35	83	35
700	40	50	99	35
2300	28	27	100	-

Datafiles: DLMIMS_111, 131, 132

4.3.4 Kinetics of NA Adsorption

The decay chronograms for these adsorption experiments reveal another layer of information, this time in the kinetic regime. As mentioned previously, a strength of MIMS is its excellent temporal resolution, provided by its continuous on-line monitoring capabilities. This gives rise to a wealth of interpretable kinetic data, as previously described by the author[78] and others.[79] Decays can easily be fit to first- or second-order (or higher) exponential functions, and risetimes can be exploited to characterize individual compound behavior within the PDMS membrane.[86] Figs. 41 and 42 show typical chronograms of raw and worked up data for an adsorption experiment with 5 ppm Merichem and a medium loading of biochar B. Three SIM *m/z* are selected, and shown

first as raw signals (Fig. 41), exhibiting a rise to steady-state beginning at ~11 min and experiencing decay due to addition of biochar B at ~50 min. Next, the same three SIMs are shown as first order kinetic plots (Fig. 42) for a 10-minute decay region where signals drop from 90% to 10% intensity due to adsorption.

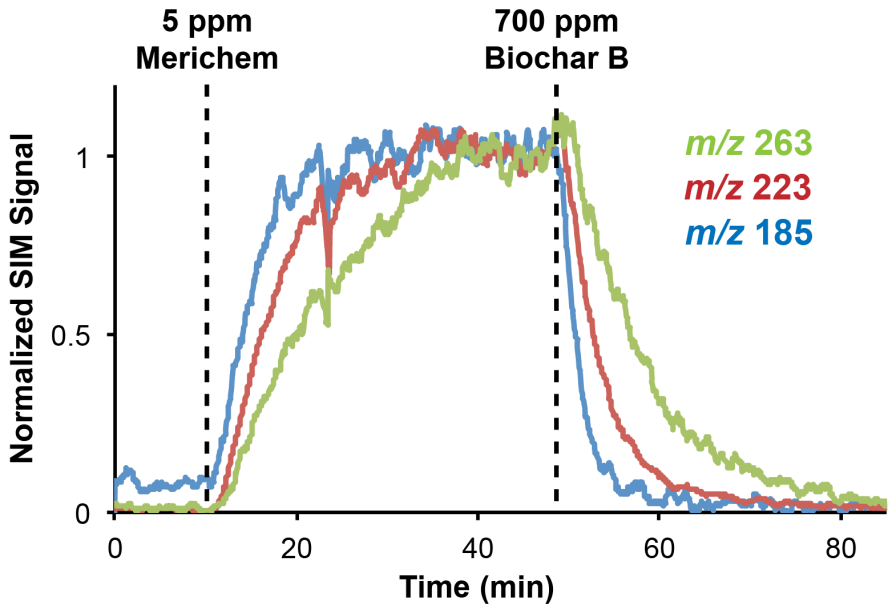

Figure 41: Ion chronogram for 5 ppm Merichem solution with medium loading of biochar B added at 50 min, monitored at three SIM *m/z* (Datafile: DLMIMS_131)

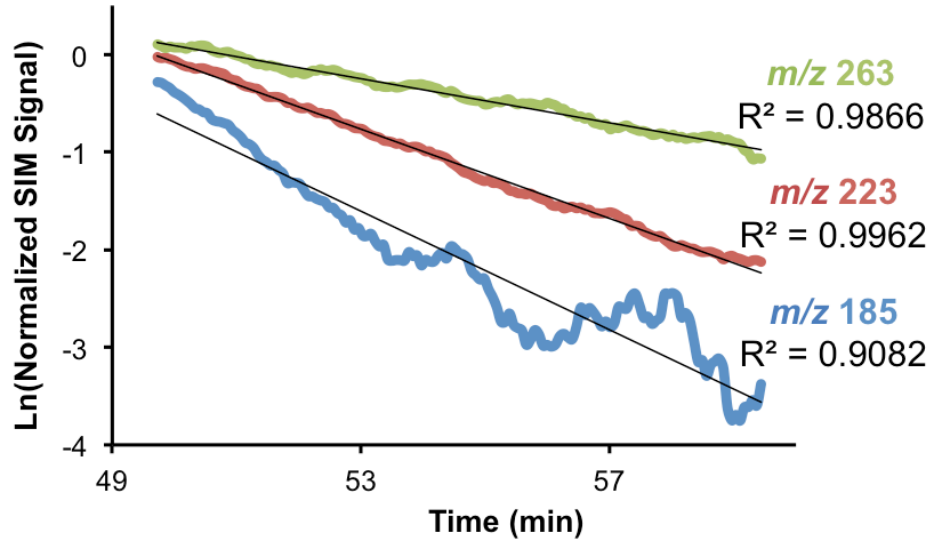

Figure 42: First order kinetic plots for $t_{10\text{-}90}$ region of adsorption decay curves for a 5 ppm Merichem solution monitored at three SIM *m/z* (Datafile: DLMIMS_131)

As evidenced by Fig. 42, the decays of all three SIM experiments seem to follow first-order kinetics, as they exhibit linear trends (equations and R^2 values shown in figure) when their natural logarithm is taken and best-fit lines found for the data. Indeed, any single mass in a NA spectrum can be followed as it exhibits decay due to adsorption, and higher- and lower-mass decays compared for different biochars. A closer look at the kinetics of the non-steady state regions of compound rise earlier in the chronogram also reveals correspondingly slower kinetics for the larger masses. This is explained by Eqn. 2 from section 1.3.1, where risetime is shown to be proportional to the diffusivity (D) of the compound in the PDMS membrane. For compounds with larger molar volumes, the diffusivity is smaller because of more steric hindrance when passing through the PDMS material, making their risetimes proportionally larger. Table 16 collects some rate constants from an adsorption experiment with a medium loading of biochar B, where as SIM *m/z* increases, the rate constants for both rise and decay can both be seen to decrease, indicating both slower transport across the membrane and probably slower adsorption kinetics to the biochar, governed by diffusion in aqueous solution. As a note, because each *m/z* in a NA spectrum obtained on a low-resolution MS can represent a whole class of compounds that appear at the same nominal mass, the observed kinetics in these experiments represents a weighted average.

Table 16: Comparison of rise and decay rate constants ($t_{10\text{-}90}$) for adsorption of 5 ppm Merichem by medium loading of biochar B, monitored at three SIM channels

SIM (*m/z*)	k_{rise} (min^{-1})	k_{decay} (min^{-1})	k_{rise} / k_{decay}
185	0.25	0.48	0.52
223	0.19	0.23	0.81
263	0.092	0.11	0.81

Datafile: DLMIMS_131

Similar data was collected for an experiment with a low loading of biochar B added to a 5 ppm Merichem solution, revealing more kinetic differences between low and high masses. For example, it seems that biochar B more rapidly adsorbs lower mass NAs over higher mass NAs, as indicated by the decay curves of SIM signals at *m/z* 263, 223, and 185 in Fig. 43. Following that, the 10-90% natural logarithm-transformed signals are displayed in Fig. 44 to obtain decay constants, collected in Table 17.

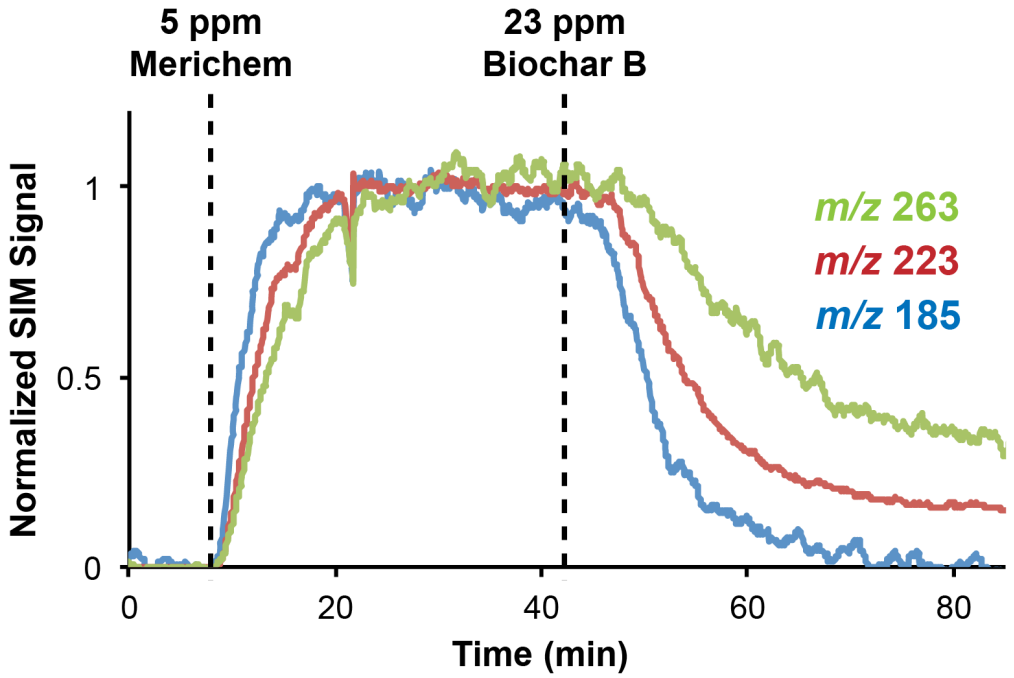

Figure 43: Ion chronogram for 5 ppm Merichem solution with low loading of biochar B added at 50 min, monitored at three SIM *m/z* (Datafile: DLMIMS_131)

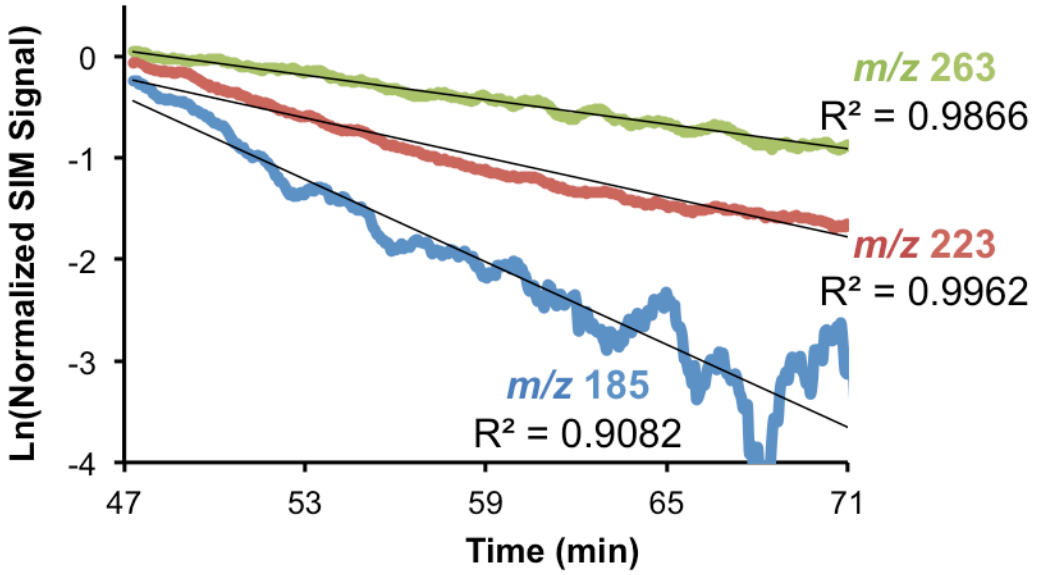

Figure 44: First order kinetic plots for $t_{10\text{-}90}$ region of adsorption decay curves for a 5 ppm Merichem solution monitored at three SIM *m/z* (Datafile: DLMIMS_131)

Similar trends to the medium loading experiments can be observed in the resulting data from the low loading experiment, collected in Table 17. Signal rise times decrease as SIM *m/z* increases, and decay constants exhibit the same trend.

Table 17: Comparison of rise and decay rate constants ($t_{10\text{-}90}$) for adsorption of 5 ppm Merichem by low loading of biochar B, monitored at three SIM channels

SIM (*m/z*)	k_{rise} (min^{-1})	k_{decay} (min^{-1})	k_{rise} / k_{decay}
185	0.44	0.30	1.4
223	0.26	0.23	1.1
263	0.19	0.11	1.7

Datafile: DLMIMS_131

However, there exists the potential for the kinetic resolution of these experiments to be limited by membrane transport (i.e. a process can only be monitored as fast as the reactants can permeate through the membrane). Because the rate constant k_{decay} represents a combination of adsorption and membrane transport kinetics, care must be taken when interpreting decay data where k_{decay} is very close to k_{rise}. In the case of Table 16, it is likely that the adsorption process is faster than the mass transport kinetics of analyte through the membrane. The rate constants for decay are not interpretable considering their approach of membrane kinetic limits. In addition, we observe relative standard deviations for rate constants in these experiments on the order of 20-30%, prompting further experimentation to properly investigate these perceived trends.

4.3.5 Multi-Loading Experiments

Several experiments were carried out where increased loadings of adsorbent were added to a stirred NA mixture to investigate the dependence of $[NA]_T^{free}$ on the mass of adsorbent added. These experiments were conducted at controlled temperature (34 ± 1 ºC), and without the use of the internal standard correction or acceptor phase base addition techniques. Fig. 45 shows a chronogram from one of these experiments, where successive loadings of biochar B are added to a buffered solution of 4 ppm Merichem, monitored at three characteristic masses (*m/z* 213, 237, and 251) in fullscan mode. Four

adsorbent loadings were added to the solution, generating four 'steady-state' regions after decay was (mostly) complete.

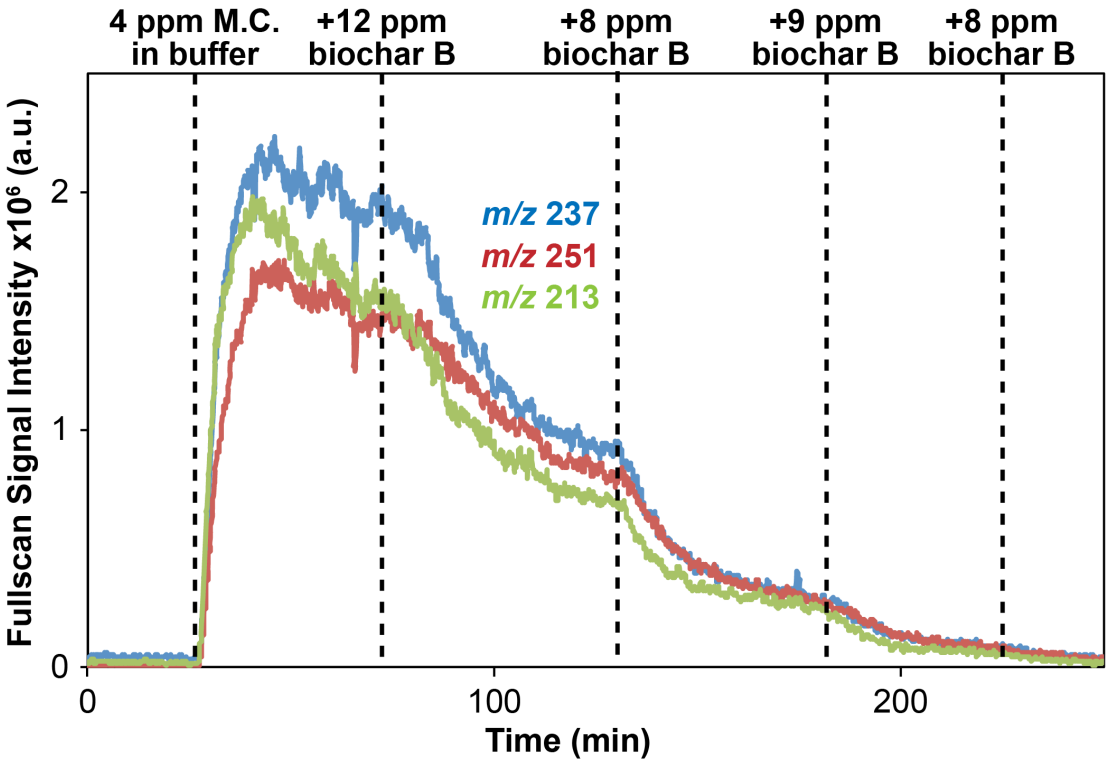

Figure 45: Chronogram for experiment where multiple loadings of biochar B are added to a stirred solution of 4 ppm Merichem in buffer, monitored at *m/z* 213, 237 and 251 extracted from the fullscan of Merichem. Final [biochar] = 33.1 ppm (Datafile: DLMIMS_133)

When averaged data from the 'steady-state' regions after the decays resulting from each biochar loading is used to calculate the free concentrations of each Merichem isomer class (*m/z* 213, 237 and 251), the dependence of $[NA]^{free}$ on mass loading of biochar can be investigated (Fig. 46). This calculation for $[NA]^{free}$ for one such isomer class (*m/z* 251) is demonstrated in Eqn. 11. The CP-MIMS signal for each isomer class represents the free concentration of that class in solution at any given point in time, and can be related to concentration via the signal intensity of the isomer class resulting from the initial 4.1 ppm Merichem spike (a 1 point calibration).

Equation 11: $$[NA]^{free} = Signal\ Int.^{m}/_{z}\ 251 \times \frac{4.1\ ppm\ [NA]_T\ as\ M.C.}{Initial\ Signal\ Int.\ for\ ^{m}/_{z}\ 251}$$

Fig. 46 illustrates that the concentration of free naphthenic acid decreases as the mass loading of adsorbent increases. It seems that there is a linear relationship between $[NA]^{free}$ and the mass of added biochar B for the Merichem fullscan TIC, while the individual isomer classes are not described by a linear fit. It should be noted that Fig. 46 represents preliminary work, and an in-depth interpretation of this data is not possible due to several experimental oversights. For example, the free concentrations obtained after adsorbent loading were not given sufficient time to reach steady-state (as seen in Fig. 45), and therefore the values for each point in Fig. 46 do not necessarily represent the full adsorption capacity of the biochar. Future experiments should either allow time to let each decay signal stabilize before the next loading is added, or the vessel containing sample/adsorbent should be moved offline to fully react for several hours/overnight and subsequently measured again by CP-MIMS after the adsorption process has reached equilibrium. If linear, the relationship between $[NA]^{free}$ and the mass of added adsorbent could be used to characterize the adsorption capability of a particular adsorbent, for both $[NA]_T^{free}$ and individual concentrations of isomer class components in a complex OSPW.

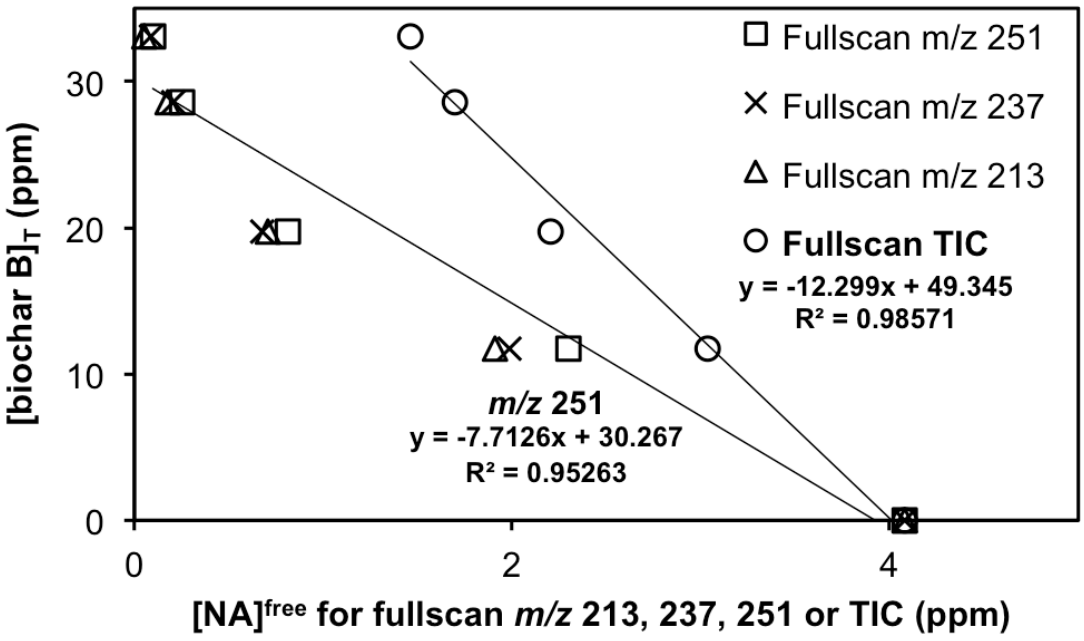

Figure 46: Dependence of $[NA]^{free}$ on mass of biochar B added, monitored with fullscan *m/z* 213, 237, 251 and TIC. The total free concentration of NAs for either fullscan *m/z* 213, 237, 251 or the TIC is plotted versus the total mass of biochar B added (Datafile: DLMIMS_133)

A more common method for characterizing adsorbents is to generate isotherm plots, which can be used to classify adsorbent/adsorbate behavior with common isotherm fits [such as Langmuir or Brunauer–Emmett–Teller (BET)], as well as generate characteristic K_d values that measure adsorbent effectiveness. A single experiment was performed to attempt to generate one such plot, and was performed by adding increasing amounts of Merichem NAs to a buffered solution already containing a low loading of biochar B. This was done in part to solve the problem of mixing very small doses of adsorbent into the NA solution (as in previous experiments), where it was often very difficult to quantitatively transfer a small weighed aliquot of the electrostatictically-sensitive biochar to the sample vessel. Fig. 47 displays the chronogram for an experiment involving several injections of concentrated Merichem into a sample vessel containing buffered solution (pH = 3.6) and biochar B (~25 ppm), monitored at three representative isomer classes (*m/z* 213, 237 and 251) as SIM experiments. With each injection of Merichem, a region of non-steady state rise due to the step increase in NA concentration occurs, quickly followed by a decay region as the biochar adsorbs the NA components in the solution. Thus, the resulting peak shape is the consequence of two competing processes (membrane permeation and adsorption kinetics).

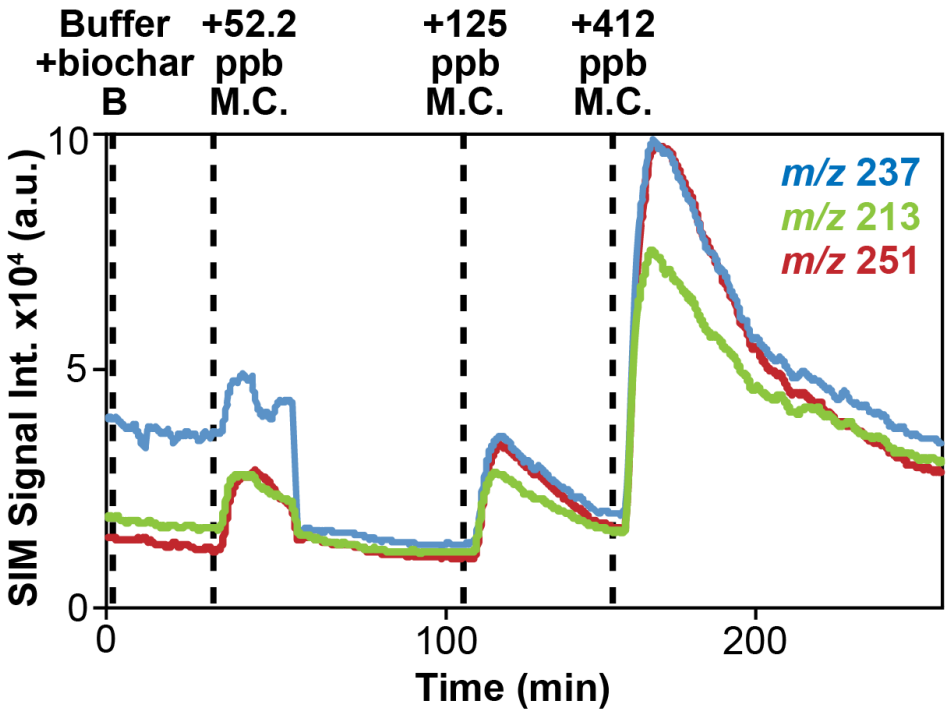

Figure 47: Chronogram for multi-loading experiment where Merichem is added in concentrated doses to a stirred solution of buffer and biochar B (~25 ppm), monitored at SIMs *m/z* 213, 237, and 251. Final $[NA]_T$ as Merichem is 589 ppb (Datafile: DLMIMS_135)

The data from this multi-loading experiment was worked up as isotherm plots for all three SIM *m/z* (the experiment was conducted at constant temperature, T = 34 ºC). If averaged data from the 'steady-state' regions (after the decays resulting from each Merichem spike and subsequent adsorption to the biochar) is used to calculate the free concentrations of the Merichem isomer classes (*m/z* 213, 237 and 251), the dependence of $[NA]^{free}$ on mass loading of biochar can be investigated. These calculations are accomplished via Eqns. 12 and 13, where again, the CP-MIMS signal for each isomer class represents the free concentration of that class in solution at any given point in time, and can be related to concentration via the 1 point calibration from the previous multi-loading experiment (performed ~1 week beforehand).

Equation 12: $$[NA]^{free}_{m/z\,251}(ppm) = Signal\ Int.^{m}/_{z}\ 251 \times \frac{4.1\ ppm\ [NA]_T\ as\ M.C.}{Initial\ Signal\ Int.\ for\ ^{m}/_{z}\ 251}$$

Equation 13: $[NA]^{ads}_{m/z\ 251}\ \left(\frac{mg}{kg}\right) = \frac{\left([NA]_T\ (\frac{mg}{kg}) - [NA]^{free}_{m/z\ 251}(\frac{mg}{kg})\right) \times Mass\ Solution\ (kg)}{Mass\ Biochar\ (kg)}$

Fig. 48 shows the results, where the free concentrations for each isomer class ($[NA]^{free}$, ppm) are plotted versus the mass of each isomer class adsorbed ($[NA]^{ads}$, mg isomer class / kg adsorbent), and lines of best fit, equations, and R^2 values are displayed.

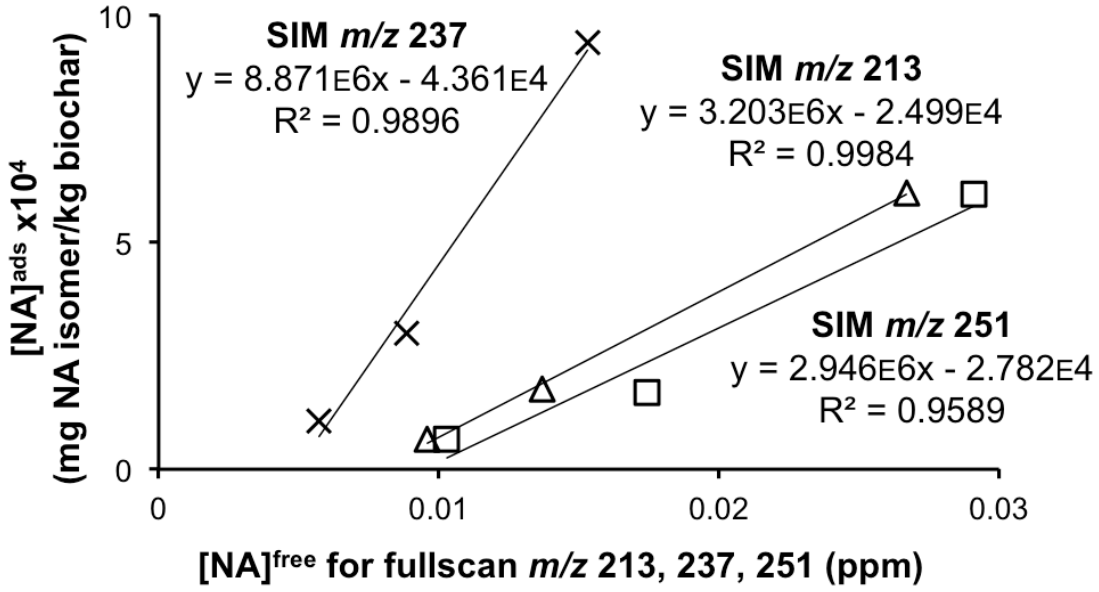

Figure 48: Isotherm plots for three SIM *m/z* from Merichem fullscan. Free concentrations of Merichem isomer classes at *m/z* 213, 237 and 251 are plotted against the adsorbed concentrations of the same isomers in mg isomer/kg biochar added (DLMIMS_135)

While overinterpreting Fig. 48 would be inappropriate considering that signals were not allowed to fully reach steady-state, good linearity was achieved for all three *m/z* on the isotherm plot, with R^2 values > 0.95. This experiment demonstrates the capability of CP-MIMS to rapidly characterize adsorbents through the construction of isotherm plots, with the ability to target specific isomer classes within a complex mixture to assess adsorbent effectiveness for each.

4.4 Conclusions and Future Directions

4.4.1 Conclusions

CP-MIMS has been demonstrated as an effective tool for rapidly screening NAs within complex samples, with a wealth of fullscan mass spectral data providing in-depth sample information within minutes. Furthermore, the ability to dynamically monitor processes allows researchers to observe mass profile changes over time, and characterize the effectiveness of potential adsorbents in complex, heterogeneous samples. The data obtained from multi-loading adsorption experiments allows for the generation of adsorption isotherms and a more complete characterization of NA adsorption behavior with activated biochars, or indeed any adsorbent imaginable. These studies will assist decision-makers in the oil sands to screen potential adsorbents for effectiveness in remediating NA-contaminated waters by providing kinetic information detailing the specific behavior of adsorbents as they interact with the various components of complex NA mixtures. Futhermore, the continuous monitoring capabilities demonstrated here can be applied to the monitoring of other dynamic processes such as natural weathering and attenuation, advanced oxidation, or other treatment processes.

4.4.2 Screening of Adsorbents

The qualitative studies performed in this thesis demonstrate ‘proof-of-concept’ for several possible avenues of research and future directions. With regard to the screening of adsorbents for their effectiveness in removing NAs from contaminated samples, there is further work to be done in testing a wider variety of adsorbents at different concentration levels. In addition to a wide variety of commercially available activated biochars, there are classes of compounds such as the cyclodextrins that have proven effective at removing NAs.[103, 104] A more extensive survey of some of these materials would be in order for a future project. Even with the two biochars studied from Layzell et al., there is further work to be done in developing adsorption isotherms to better characterize these materials. Further experimental modifications may be needed to address some of the

challenges faced here, including achieving sufficient mixing of the adsorbent into the NA mixture to prevent the biochars from floating on the surface of the solution, the stirbar, and the CP-MIMS probe itself. Ideally, a more robust and well-mixed experimental setup with pre-wetted adsorbents should be developed before continuing these experiments. Another possible variant would be to immobilize the biochar in a column and monitor the concentration of eluent as it 'breaks through' after reaching its adsorption capacity.

4.4.3 Kinetic Data and Adsorption Isotherms

Kinetic data obtained with CP-MIMS is limited by membrane transport kinetics, so that monitoring any processes occurring faster than the rate of compound diffusion across the membrane is not possible. All the experimental work for this thesis was conducted with a 170 μm-thick membrane, but there are a variety of thinner membranes that could allow a greater spectrum of kinetic processes to be observed.[60] These include a thin-film composite membrane (0.5 μm PDMS film deposited on a 263 μm OD and 209 μm ID polypropylene support, neoMecs Inc., Eden Prairie, MN, USA) and 35 μm PDMS membranes (237 μm OD and 167 μm ID, Permselect, MedArray Inc., MI, USA) previously characterized by our group.[49] In general, recent progress in material science should allow for a greater variety of membrane materials and thicknesses in future studies, with the opportunity to tune both the selectivity and the response time of CP-MIMS to develop a more versatile real-time, on-line, direct sampling analytical technique.

Future experiments should further explore characterization of adsorbents through the construction of adsorption isotherm plots once a more robust and reproducible experimental setup is developed for the CP-MIMS multi-loading experiments, and sufficient time is allowed for all signals to reach steady-state before data is interpreted.

Concluding Remarks

This thesis demonstrated the ability of CP-MIMS to rapidly assess quantitative concentrations as well as monitor mass profile changes during adsorption phenomena for naphthenic acids in complex oil sands process water samples. Through comparison studies, it was shown that the CP-MIMS technique was able to perform measurements comparable in precision and 'accuracy' to two other published methods, despite the lack of true analytical standards and the variety in units of quantitation among current analytical NA methodologies. Above and beyond this, CP-MIMS measurements were made in real-time in complex samples with little to no sample preparation (at most, a quick pH adjustment) and no chromatography. Many applications are anticipated. Remote deployment in the field to make on-site measurements at industrial oil sands sites is a possibility if CP-MIMS is paired with a portable instrument (such as a single quadrupole mass spectrometer). Much more accurate and specific quantitation is anticipated for pairing of CP-MIMS with high resolution mass spectrometers such as FT-ICR[49] or orbitrap[47] instruments, in tandem with the improvements made in this thesis. Such instruments will allow for targeting of specific compound classes within NAFC mixtures, including determination of molecular formulae for many mixture components.

With real-time analysis made possible by the membrane interface, it will be possible to observe detailed changes in NA mixture composition at high resolution during processes such as pH change[49] and adsorption. This thesis explored applications of the existing CP-MIMS technique paired with nominal resolution mass spectrometry to screen biochars for their ability to adsorb NAs, including the construction of adsorption isotherms from multi-loading experiments. The kinetic data resulting from these studies was used to produce decay constants for isomer classes within a NA mixture and characterize the adsorption behavior for several biochars. At high mass resolution, molecular formulae could be assigned to these isomer classes, providing specific information on which mixture components are selected for adsorption by a particular adsorbent.

Recent developments in ionization sources have led to significant progress in opening up the field of mass spectrometry to new analyte classes, particularly when working at atmospheric pressure with a liquid sample as in CP-MIMS or LC-MS techniques. Ionization sources such as APPI, APCI, and direct EI have recently been characterized for analysis of naphthenic acid fraction components,[4] larger biomolecules such as pharmaceuticals,[59] and non-polar analytes such as PAHs.[105] CP-MIMS is amenable to pairing with all of these sources, and is currently being adapted by our group for use with lower-flow sources such as nano-flow ESI and DEI.[105]

CP-MIMS stands to benefit from innovations in mass spectrometry (higher resolving power as well as greater portability) as well as innovations at the membrane level, as progress is made in materials science. PDMS is primarily selective for relatively small, hydrophobic molecules, but there are membrane materials selective for other classes of molecules, including ions,[65] and carriers and channels can be used within membranes to enhance selectivity. As described earlier, different membrane thicknesses can also significantly change the response time of a membrane for certain analytes, and in particular, can speed up analysis for large molecules that would otherwise experience an unusably long signal response time with thicker membranes.

While the body of literature concerning both quantitative and qualitative analyses of naphthenic acids continues to grow, rapid screening techniques such as CP-MIMS still represent a relatively small portion of the field. These techniques are often overlooked due to their semi-quantitative nature, and are thus often deemed unfit for cases where defendable, reliable data is required. It is anticipated that work such as that presented in this thesis will emphasize the utility of techniques that offer real time, direct sampling with the ability to achieve quantitative results that compare well with benchtop methods, and yet involve little to no sample preparation steps or chromatography. Additionally, with the ability to deploy in the field, techniques such as CP-MIMS can be used to garner measurements of analytes in complex matrices when, and where, they are needed.

Bibliography

1. J. W. Martin, X. M. Han, K. M. Peru and J. V. Headley, Comparison of high- and low-resolution electrospray ionization mass spectrometry for the analysis of naphthenic acid mixtures in oil sands process water, *Rapid Communications in Mass Spectrometry*, 2008, **22**, 1919-1924.

2. Alberta, *Facts about Alberta's oil sands and its industry*, http://history.alberta.ca/oilsands/docs/facts_sheets09.pdf, Accessed March 15, 2016.

3. Alberta, *Oil Sands*, http://www.energy.alberta.ca/ourbusiness/oilsands.asp, Accessed March 15, 2016.

4. M. P. Barrow, M. Witt, J. V. Headley and K. M. Peru, Athabasca oil sands process water: Characterization by atmospheric pressure photoionization and electrospray ionization Fourier transform ion cyclotron resonance mass spectrometry, *Analytical Chemistry*, 2010, **82**, 3727-3735.

5. NormanEinstein, *Athabasca Oil Sands map.png*, http://commons.wikimedia.org/wiki/File:Athabasca_Oil_Sands_map.png, Accessed March 15, 2016.

6. CBS, *Surprise in Keystone XL pipeline controversy*, http://www.cbsnews.com/news/keystone-xl-pipeline-company-asks-u-s-to-suspend-application-review, Accessed March 15, 2016.

7. Phys.org, *Key facts about controversial Keystone XL pipeline*, http://phys.org/news/2015-11-key-facts-controversial-keystone-xl.html, Accessed March 15, 2016.

8. G. Steward, *First Nations bear the risks of oilsands development*, http://www.thestar.com/news/atkinsonseries/2015/08/28/first-nations-bear-the-risks-of-oilsands-development.html, Accessed March 14, 2016.

9. J. Rodriguez-Estival and J. E. G. Smits, Small mammals as sentinels of oil sands related contaminants and health effects in northeastern Alberta, Canada, *Ecotoxicology and Environmental Safety*, 2016, **124**, 285-295.

10. L. Cruz-Martinez, K. J. Fernie, C. Soos, T. Harner, F. Getachew and J. E. G. Smits, Detoxification, endocrine, and immune responses of tree swallow nestlings naturally exposed to air contaminants from the Alberta oil sands, *Science of the Total Environment*, 2015, **502**, 8-15.

11. M. S. Ross, A. S. Pereira, J. Fennell, M. Davies, J. Johnson, L. Sliva and J. W. Martin, Quantitative and qualitative analysis of naphthenic acids in natural waters surrounding the Canadian oil sands industry, *Environmental Science & Technology*, 2012, **46**, 12796-12805.

12. J. V. Headley, M. P. Barrow, K. M. Peru, B. Fahlman, R. A. Frank, G. Bickerton, M. E. McMaster, J. Parrott and L. M. Hewitt, Preliminary fingerprinting of Athabasca oil sands polar organics in environmental samples using electrospray ionization Fourier transform ion cyclotron resonance mass spectrometry, *Rapid Communications in Mass Spectrometry*, 2011, **25**, 1899-1909.

13. J. V. Headley, K. M. Peru and M. P. Barrow, Advances in mass spectrometric characterization of naphthenic acids fraction compounds in oil sands environmental samples and crude oil—a review, *Mass Spectrometry Reviews*, 2015, **35**, 311-328.

14. K. L. Goff, J. V. Headley, J. R. Lawrence and K. E. Wilson, Assessment of the effects of oil sands naphthenic acids on the growth and morphology of Chlamydomonas reinhardtii using microscopic and spectromicroscopic techniques, *Science of the Total Environment*, 2013, **442**, 116-122.

15. R. A. Frank, R. Kavanagh, B. K. Burnison, G. Arsenault, J. V. Headley, K. M. Peru, G. Van Der Kraak and K. R. Solomon, Toxicity assessment of collected fractions from an extracted naphthenic acid mixture, *Chemosphere*, 2008, **72**, 1309-1314.

16. E. K. Quagraine, J. V. Headley and H. G. Peterson, Is biodegradation of bitumen a source of recalcitrant naphthenic acid mixtures in oil sands tailing pond waters?, *Journal of Environmental Science and Health Part A - Toxic/Hazardous Substances & Environmental Engineering*, 2005, **40**, 671-684.

17. S. D. Melvin, C. M. Lanctot, P. M. Craig, T. W. Moon, K. M. Peru, J. V. Headley and V. L. Trudeau, Effects of naphthenic acid exposure on development and liver metabolic processes in anuran tadpoles, *Environmental Pollution*, 2013, **177**, 22-27.

18. J. V. Headley, K. M. Peru, M. P. Barrow and P. J. Derrick, Characterization of naphthenic acids from Athabasca oil sands using electrospray ionization: The significant influence of solvents, *Analytical Chemistry*, 2007, **79**, 6222-6229.

19. J. M. E. Ahad, H. Pakdel, M. M. Savard, A. I. Calderhead, P. R. Gammon, A. Rivera, K. M. Peru and J. V. Headley, Characterization and quantification of mining-related "naphthenic acids" in groundwater near a major oil sands tailings pond, *Environmental Science & Technology*, 2013, **47**, 5023-5030.

20. R. A. Frank, J. W. Roy, G. Bickerton, S. J. Rowland, J. V. Headley, A. G. Scarlett, C. E. West, K. M. Peru, J. L. Parrott, F. M. Conly and L. M. Hewitt, Profiling oil sands mixtures from industrial developments and natural groundwaters for source identification, *Environmental Science & Technology*, 2014, **48**, 2660-2670.

21. B. Wittmeier, *Energy regulator now says 122 birds confirmed dead at tailings ponds in Athabasca oilsands*, http://www.edmontonjournal.com/energy+regulator+says+birds+confirmed+dead

+tailings+ponds+athabasca+oilsands/10356200/story.html, Accessed March 14, 2016.

22. S. McCarthy, *Canadian government approves Enbridge's controversial Northern Gateway pipeline*, http://www.theglobeandmail.com/report-on-business/industry-news/energy-and-resources/northern-gateway-decision/article19180594, Accessed March 14, 2016.

23. D. M. Grewer, R. F. Young, R. M. Whittal and P. M. Fedorak, Naphthenic acids and other acid-extractables in water samples from Alberta: What is being measured?, *Science of the Total Environment*, 2010, **408**, 5997-6010.

24. S. J. Rowland, C. E. West, D. Jones, A. G. Scarlett, R. A. Frank and L. M. Hewitt, Steroidal aromatic 'naphthenic acids' in oil sands process-affected water: Structural comparisons with environmental estrogens, *Environmental Science & Technology*, 2011, **45**, 9806-9815.

25. P. Brunswick, D. Y. Shang, G. van Aggelen, R. Hindle, L. M. Hewitt, R. A. Frank, M. Haberl and M. Kim, Trace analysis of total naphthenic acids in aqueous environmental matrices by liquid chromatography/mass spectrometry-quadrupole time of flight mass spectrometry direct injection, *Journal of Chromatography A*, 2015, **1405**, 49-71.

26. V. V. Rogers, K. Liber and M. D. MacKinnon, Isolation and characterization of naphthenic acids from Athabasca oil sands tailings pond water, *Chemosphere*, 2002, **48**, 519-527.

27. J. V. Headley, K. M. Peru, M. H. Mohamed, R. A. Frank, J. W. Martin, R. R. O. Hazewinkel, D. Humphries, N. P. Gurprasad, L. M. Hewitt, D. C. G. Muir, D. Lindeman, R. Strub, R. F. Young, D. M. Grewer, R. M. Whittal, P. M. Fedorak, D. A. Birkholz, R. Hindle, R. Reisdorph, X. Wang, K. L. Kasperski, C. Hamilton, M. Woudneh, G. Wang, B. Loescher, A. Farwell, D. G. Dixon, M. Ross, A. D. S. Pereira, E. King, M. P. Barrow, B. Fahlman, J. Bailey, D. W. McMartin, C. H. Borchers, C. H. Ryan, N. S. Toor, H. M. Gillis, L. Zuin, G. Bickerton, M.

McMaster, E. Sverko, D. Shang, L. D. Wilson and F. J. Wrona, Chemical fingerprinting of naphthenic acids and oil sands process waters—A review of analytical methods for environmental samples, *Journal of Environmental Science and Health Part A - Toxic/Hazardous Substances & Environmental Engineering*, 2013, **48**, 1145-1163.

28. J. V. Headley, M. P. Barrow, K. M. Peru and P. J. Derrick, Salting-out effects on the characterization of naphthenic acids from Athabasca oil sands using electrospray ionization, *Journal of Environmental Science and Health Part A - Toxic/Hazardous Substances & Environmental Engineering*, 2011, **46**, 844-854.

29. J. Martin, personal communication, 2016.

30. Thomson-Reuters, *Web of Science*, http://webofknowledge.com, Accessed March 15, 2016.

31. J. V. Headley, K. M. Peru and M. P. Barrow, Mass spectrometric characterization of naphthenic acids in environmental samples: A review, *Mass Spectrometry Reviews*, 2009, **28**, 121-134.

32. R. Hindle, M. Noestheden, K. Peru and J. Headley, Quantitative analysis of naphthenic acids in water by liquid chromatography-accurate mass time-of-flight mass spectrometry, *Journal of Chromatography A*, 2013, **1286**, 166-174.

33. X. M. Han, M. D. MacKinnon and J. W. Martin, Estimating the in situ biodegradation of naphthenic acids in oil sands process waters by HPLC/HRMS, *Chemosphere*, 2009, **76**, 63-70.

34. X. Wang and K. L. Kasperski, Analysis of naphthenic acids in aqueous solution using HPLC-MS/MS, *Analytical Methods*, 2010, **2**, 1715-1722.

35. D. Y. Shang, M. Kim, M. Haberl and A. Legzdins, Development of a rapid liquid chromatography tandem mass spectrometry method for screening of trace naphthenic acids in aqueous environments, *Journal of Chromatography A*, 2013, **1278**, 98-107.

36. A. S. Pereira, S. Bhattacharjee and J. W. Martin, Characterization of oil sands process-affected waters by liquid chromatography orbitrap mass spectrometry, *Environmental Science & Technology*, 2013, **47**, 5504-5513.

37. A. S. Pereira, M. D. S. Islam, M. G. El-Din and J. W. Martin, Ozonation degrades all detectable organic compound classes in oil sands process-affected water; an application of high-performance liquid chromatography/orbitrap mass spectrometry, *Rapid Communications in Mass Spectrometry*, 2013, **27**, 2317-2326.

38. A. Nyakas, J. Han, K. M. Peru, J. V. Headley and C. H. Borchers, Comprehensive analysis of oil sands processed water by direct-infusion Fourier-transform ion cyclotron resonance mass spectrometry with and without offline UHPLC sample prefractionation, *Environmental Science & Technology*, 2013, **47**, 4471-4479.

39. S. J. Rowland, A. G. Scarlett, D. Jones, C. E. West and R. A. Frank, Diamonds in the rough: Identification of individual naphthenic acids in oil sands process water, *Environmental Science & Technology*, 2011, **45**, 3154-3159.

40. C. E. West, J. Pureveen, A. G. Scarlett, S. K. Lengger, M. J. Wilde, F. Korndorffer, E. W. Tegelaar and S. J. Rowland, Can two-dimensional gas chromatography/mass spectrometric identification of bicyclic aromatic acids in petroleum fractions help to reveal further details of aromatic hydrocarbon biotransformation pathways?, *Rapid Communications in Mass Spectrometry*, 2014, **28**, 1023-1032.

41. M. P. Barrow, K. M. Peru and J. V. Headley, An added dimension: GC atmospheric pressure chemical ionization FTICR MS and the Athabasca oil sands, *Analytical Chemistry*, 2014, **86**, 8281-8288.

42. X. Ortiz, K. J. Jobst, E. J. Reiner, S. M. Backus, K. M. Peru, D. W. McMartin, G. O'Sullivan, V. Y. Taguchi and J. V. Headley, Characterization of naphthenic acids by gas chromatography-Fourier transform ion cyclotron resonance mass spectrometry, *Analytical Chemistry*, 2014, **86**, 7666-7673.

43. M. S. MacLennan, C. Tie, D. D. Y. Chen, K. M. Peru and J. V. Headley, Capillary electrophoresis-mass spectrometry technology for analysis of naphthenic acids fraction compounds in oil sands process water, *97th Canadian Chemistry Conference and Exhibition*, Vancouver, Canada, 2014.

44. M. R. Noestheden, J. V. Headley, K. M. Peru, M. P. Barrow, L. L. Burton, T. Sakuma, P. Winkler and J. L. Campbell, Rapid characterization of naphthenic acids using differential mobility spectrometry and mass spectrometry, *Environmental Science & Technology*, 2014, **48**, 10264-10272.

45. J. V. Headley, K. M. Peru, S. A. Armstrong, X. Han, J. W. Martin, M. M. Mapolelo, D. F. Smith, R. P. Rogers and A. G. Marshall, Aquatic plant-derived changes in oil sands naphthenic acid signatures determined by low-, high- and ultrahigh-resolution mass spectrometry, *Rapid Communications in Mass Spectrometry*, 2009, **23**, 515-522.

46. J. V. Headley, K. M. Peru, A. Janfada, B. Fahlman, C. Gu and S. Hassan, Characterization of oil sands acids in plant tissue using Orbitrap ultra-high resolution mass spectrometry with electrospray ionization, *Rapid Communications in Mass Spectrometry*, 2011, **25**, 459-462.

47. T. Leshuk, T. Wong, S. Linley, K. M. Peru, J. V. Headley and F. Gu, Solar photocatalytic degradation of naphthenic acids in process-affected water, *Chemosphere*, 2016, **144**, 1854-1861.

48. Merichem, *Product safety summary - naphthenic acid*, http://www.merichem.com/naphthenic-acid, Accessed March 15, 2016.

49. K. D. Duncan, D. R. Letourneau, G. W. Vandergrift, K. Jobst, E. Reiner, C. G. Gill and E. T. Krogh, A semi-quantitative approach for the rapid screening and mass profiling of naphthenic acids directly in contaminated aqueous samples, *Journal of Mass Spectrometry*, 2016, **51**, 44-52.

50. M. B. Woudneh, M. Coreen Hamilton, J. P. Benskin, G. Wang, P. McEachern and J. R. Cosgrove, A novel derivatization-based liquid chromatography tandem mass spectrometry method for quantitative characterization of naphthenic acid isomer profiles in environmental waters, *Journal of Chromatography A*, 2013, **1293**, 36-43.

51. H. Malle and J. Simser, *Naphthenic acids interlaboratory calibration study – revised report*, Burlington, Ontario, 2012.

52. R. A. Ketola, M. Ojala, V. Komppa, T. Kotiaho, J. Juujarvi and J. Heikkonen, A non-linear asymmetric error function-based least mean square approach for the analysis of multicomponent mass spectra measured by membrane inlet mass spectrometry, *Rapid Communications in Mass Spectrometry*, 1999, **13**, 654-662.

53. R. C. Johnson, R. G. Cooks, T. M. Allen, M. E. Cisper and P. H. Hemberger, Membrane introduction mass spectrometry: Trends and applications, *Mass Spectrometry Reviews*, 2000, **19**, 1-37.

54. N. G. Davey, E. T. Krogh and C. G. Gill, Membrane introduction mass spectrometry (MIMS), *Trends in Analytical Chemistry*, 2011, **30**, 1477-1485.

55. G. Hoch and B. Kok, A mass spectrometer inlet system for sampling gases dissolved in liquid phases, *Archives of Biochemistry and Biophysics*, 1963, **101**, 160-170.

56. R. J. Bell, N. G. Davey, M. Martinsen, C. Collin-Hansen, E. T. Krogh and C. Gill, A field-portable membrane introduction mass spectrometer for real-time quantitation and spatial mapping of atmospheric and aqueous contaminants, *Journal of the American Society for Mass Spectrometry*, 2015, **26**, 212-223.

57. R. J. Bell, R. T. Short, F. H. W. Van Amerom and R. H. Byrne, Calibration of an in situ membrane inlet mass spectrometer for measurements of dissolved gases and volatile organics in seawater, *Environmental Science & Technology*, 2007, **41**, 8123-8128.

58. N. G. Davey, C. T. E. Fitzpatrick, J. M. Etzkorn, M. Martinsen, R. S. Crampton, G. D. Onstad, T. V. Larson, M. G. Yost, E. T. Krogh, M. Gilroy, K. H. Himes, E. T. Saganic, C. D. Simpson and C. G. Gill, Measurement of spatial and temporal variation in volatile hazardous air pollutants in Tacoma, Washington, using a mobile membrane introduction mass spectrometry (MIMS) system, *Journal of Environmental Science and Health Part A - Toxic/Hazardous Substances & Environmental Engineering*, 2014, **49**, 1199-1208.

59. K. D. Duncan, M. D. Willis, E. T. Krogh and C. G. Gill, A miniature condensed-phase membrane introduction mass spectrometry (CP-MIMS) probe for direct and on-line measurements of pharmaceuticals and contaminants in small, complex samples, *Rapid Communications in Mass Spectrometry*, 2013, **27**, 1213-1221.

60. M. D. Willis, K. D. Duncan, E. T. Krogh and C. G. Gill, Delicate polydimethylsiloxane hollow fibre membrane interfaces for condensed phase membrane introduction mass spectrometry (CP-MIMS), *Rapid Communications in Mass Spectrometry*, 2014, **28**, 671-681.

61. S. Bauer, Membrane introduction mass spectrometry: An old method that is gaining new interest through recent technological advances, *Trends in Analytical Chemistry*, 1995, **14**, 202-213.

62. S. Bauer and D. Solyom, Determination of volatile organic compounds at the parts per trillion level in complex aqueous matrixes using membrane introduction mass spectrometry, *Analytical Chemistry*, 1994, **66**, 4422-4431.

63. S. J. Bauer and R. G. Cooks, MIMS for trace-level determination of organic analytes in online process monitoring and environmental analysis, *American Laboratory*, 1993, **25**, 36-51.

64. K. D. Duncan, E. P. B. McCauley, E. T. Krogh and C. G. Gill, Characterization of a condensed-phase membrane introduction mass spectrometry (CP-MIMS) interface using a methanol acceptor phase coupled with electrospray ionization for the continuous on-line quantitation of polar, low-volatility analytes at trace levels

in complex aqueous samples, *Rapid Communications in Mass Spectrometry*, 2011, **25**, 1141-1151.

65. M. Gernatova, P. Janderka, A. Marcinkova and P. Ostrizek, Use of Nafion as a membrane separator in membrane introduction mass spectrometry, *European Journal of Mass Spectrometry*, 2009, **15**, 571-577.

66. E. T. Krogh and C. G. Gill, Membrane introduction mass spectrometry (MIMS): A versatile tool for direct, real-time chemical measurements, *Journal of Mass Spectrometry*, 2014, **49**, 1205-1213.

67. V. Lopez-Avila, J. Benedicto, H. Prest and S. Bauer, Direct analysis of MTBE in water using automated membrane-introduction mass spectrometry, *Spectroscopy*, 1999, **14**, 37.

68. N. Musilova-Kebrlova and P. Janderka, Analysis of mixtures of organic volatile compound in water by MIMS: Semiquantitative evaluation of data, *Collection of Czechoslovak Chemical Communications*, 2009, **74**, 581-597.

69. R. Rios, L. L. da Rocha, T. G. Vieira, R. M. Lago and R. Augusti, On-line monitoring by membrane introduction mass spectrometry of chlorination of organics in water: Mechanistic and kinetic aspects of chloroform formation, *Journal of Mass Spectrometry*, 2000, **35**, 618-624.

70. M. Schluter and T. Gentz, Application of membrane inlet mass spectrometry for online and in situ analysis of methane in aquatic environments, *Journal of the American Society for Mass Spectrometry*, 2008, **19**, 1395-1402.

71. R. Sparrapan, M. N. Eberlin and R. M. Alberici, Quantitation of trace phenolic compounds in water by trap-and-release membrane introduction mass spectrometry after acetylation, *Rapid Communications in Mass Spectrometry*, 2008, **22**, 4105-4108.

72. E. VanHassel and M. E. Bier, An electrospray membrane probe for the analysis of volatile and semi-volatile organic compounds in water, *Rapid Communications in Mass Spectrometry*, 2007, **21**, 413-420.

73. M. Soni, S. Bauer, J. W. Amy, P. Wong and R. G. Cooks, Direct determination of organic compounds in water at parts-per-quadrillion levels by membrane introduction mass spectrometry, *Analytical Chemistry*, 1995, **67**, 1409-1412.

74. P. S. H. Wong, N. Srinivasan, N. Kasthurikrishnan, R. G. Cooks, J. A. Pincock and J. S. Grossert, On-line monitoring of the photolysis of benzyl acetate and 3,5-dimethoxybenzyl acetate by membrane introduction mass spectrometry, *Journal of Organic Chemistry*, 1996, **61**, 6627-6632.

75. A. J. Thompson, J. M. Etzkorn, D. M. van Pel, E. T. Krogh, D. R. Drakeford and C. G. Gill, Membrane introduction tandem mass spectrometry (MIMS-MS/MS) as a real-time monitor for biogenic volatile organic compound (BVOC) emissions from plants, *Canadian Journal of Analytical Sciences and Spectroscopy*, 2008, **53**, 75-81.

76. J. T. Borges, R. Sparrapan, J. R. Guimaraes, M. N. Eberlin and R. Augusti, Chloroform formation by chlorination of aqueous algae suspensions: Online monitoring via membrane introduction mass spectrometry, *Journal of the Brazilian Chemical Society*, 2008, **19**, 950-955.

77. L. L. da Rocha, R. Rios, R. M. Lago and R. Augusti, Membrane introduction mass spectrometry applied to the monitoring of chloroform degradation by hypochloride in acidic aqueous medium, *Journal of the Brazilian Chemical Society*, 2005, **16**, 270-274.

78. D. R. Letourneau, C. G. Gill and E. T. Krogh, Photosensitized degradation kinetics of trace halogenated contaminants in natural waters using membrane introduction mass spectrometry as an in situ reaction monitor, *Photochemical & Photobiological Sciences*, 2015, **14**, 2108-2118.

79. J. H. L. Nelson, D. A. Friesen, C. G. Gill and E. T. Krogh, On-line measurement of oxidative degradation kinetics for trace gasoline contaminants in aqueous solutions and natural water by membrane introduction tandem mass spectrometry, *Journal of Environmental Science and Health Part A - Toxic/Hazardous Substances & Environmental Engineering*, 2010, **45**, 1720-1731.

80. R. Augusti, A. Dias, L. Rocha and R. Lago, Kinetics and mechanism of benzene derivative degradation with Fenton's reagent in aqueous medium studied by MIMS, *The Journal of Physical Chemistry A*, 1998, **102**, 10723-10727.

81. A. E. Burgos, R. D. Sinisterra, R. Augusti and R. M. Lago, Application of the MIMS technique to study the stability constants of small organic guest molecules into cyclodextrin hosts in aqueous medium, *Journal of Inclusion Phenomena and Macrocyclic Chemistry*, 2003, **45**, 149-154.

82. H. Frandsen, C. Janfelt and F. R. Lauritsen, Fast and direct screening of polyaromatic hydrocarbon (PAH)-contaminated sand using a miniaturized membrane inlet mass spectrometer (mini-MIMS), *Rapid Communications in Mass Spectrometry*, 2007, **21**, 1574-1578.

83. R. M. Lago, A. C. B. Silva, A. C. M. Teixeira and R. Augusti, Application of membrane introduction mass spectrometry to the study of adsorption of organic compounds on activated carbon and solid phase extraction experiments, *Analyst*, 2003, **128**, 884-888.

84. D. Lloyd, K. L. Thomas, G. Cowie, J. D. Tammam and A. G. Williams, Direct interface of chemistry to microbiological systems: membrane inlet mass spectrometry, *Journal of Microbiological Methods*, 2002, **48**, 289-302.

85. M. E. G. Moral, C. K. Tu, N. G. J. Richards and D. N. Silverman, Membrane inlet for mass spectrometric measurement of catalysis by enzymatic decarboxylases, *Analytical Biochemistry*, 2011, **418**, 73-77.

86. M. Willis, The investigation of mass transport of environmental contaminants in polymers using membrane introduction mass spectrometry (MIMS), Vancouver Island University, 2011.

87. M. A. LaPack, J. C. Tou and C. G. Enke, Membrane mass spectrometry for the direct trace analysis of volatile organic compounds in air and water, *Analytical Chemistry*, 1990, **62**, 1265-1271.

88. K. D. Duncan, G. W. Vandergrift, E. T. Krogh and C. G. Gill, Ionization suppression effects with condensed phase membrane introduction mass spectrometry: methods to increase the linear dynamic range and sensitivity, *Journal of Mass Spectrometry*, 2015, **50**, 437-443.

89. J. V. Headley, K. M. Peru, D. W. McMartin and M. Winkler, Determination of dissolved naphthenic acids in natural waters by using negative-ion electrospray mass spectrometry, *Journal of Aoac International*, 2002, **85**, 182-187.

90. J. D. Hunter, Matplotlib: A 2D graphics environment, *Computing in Science & Engineering*, 2007, **9**, 90-95.

91. P. J. Quinlan and K. C. Tam, Water treatment technologies for the remediation of naphthenic acids in oil sands process-affected water, *Chemical Engineering Journal*, 2015, **279**, 696-714.

92. J. V. Headley, J. L. Du, K. M. Peru and D. W. McMartin, Electrospray ionization mass spectrometry of the photodegradation of naphthenic acids mixtures irradiated with titanium dioxide, *Journal of Environmental Science and Health Part A - Toxic/Hazardous Substances & Environmental Engineering*, 2009, **44**, 591-597.

93. K. M. Peru, personal communication, 2016.

94. S. Kim, P. A. Thiessen, E. E. Bolton, J. Chen, G. Fu, A. Gindulyte, L. Han, J. He, S. He, B. A. Shoemaker, J. Wang, B. Yu, J. Zhang and S. H. Bryant, PubChem substance and compound databases, *Nucleic Acids Research*, 2016, **4**, 1202-1213.

95. M. J. Avery, Quantitative characterization of differential ion suppression on liquid chromatography/atmospheric pressure ionization mass spectrometric bioanalytical methods, *Rapid Communications in Mass Spectrometry*, 2003, **17**, 197-201.

96. C. C. Lo, B. G. Brownlee and N. J. Bunce, Mass spectrometric and toxicological assays of Athabasca oil sands naphthenic acids, *Water Research*, 2006, **40**, 655-664.

97. J. M. Etzkorn, N. G. Davey, A. J. Thompson, A. S. Creba, C. W. LeBlanc, C. D. Simpson, E. T. Krogh and C. G. Gill, The Use of MIMS-MS-MS in Field Locations as an On-Line Quantitative Environmental Monitoring Technique for Trace Contaminants in Air and Water, *Journal of Chromatographic Science*, 2009, **47**, 57-66.

98. M. P. Barrow, J. V. Headley, K. M. Peru and P. J. Derrick, Data visualization for the characterization of naphthenic acids within petroleum samples, *Energy & Fuels*, 2009, **23**, 2592-2599.

99. B. Zhao, R. Currie and H. Mian, *Catalogue of analytical methods for naphthenic acids related to oil sands operations*, Oil Sands Research and Information Network, University of Alberta, School of Energy and the Environment Edmonton, Alberta, 2012.

100. F. S. Azad, J. Abedi and S. Iranmanesh, Removal of naphthenic acids using adsorption process and the effect of the addition of salt, *Journal of Environmental Science and Health Part A - Toxic/Hazardous Substances & Environmental Engineering*, 2013, **48**, 1649-1654.

101. S. E. Ruzin, *Plant Microtechnique and Microscopy*, Oxford University Press, University of California, Berkeley, 1999.

102. D. B. Layzell, personal communication, 2015.

103. M. H. Mohamed, L. D. Wilson, J. V. Headley and K. M. Peru, Investigation of the sorption properties of beta-cyclodextrin-based polyurethanes with phenolic dyes and naphthenates, *Journal of Colloid and Interface Science*, 2011, **356**, 217-226.

104. M. H. Mohamed, L. D. Wilson and J. V. Headley, Design and characterization of novel beta-cyclodextrin based copolymer materials, *Carbohydrate Research*, 2011, **346**, 219-229.

105. V. Termopoli, G. Famiglini, P. Palma, A. Cappiello, G. W. Vandergrift, E. T. Krogh and C. G. Gill, Condensed Phase Membrane Introduction Mass Spectrometry with Direct Electron Ionization: On-line Measurement of PAHs in Complex Aqueous Samples, *Journal of the American Society for Mass Spectrometry*, 2016, **27**, 301-308.

Appendix A: Supplementary Data

Table 18: Merichem top 30 *m/z* with intensities from fullscan at pH 4, $[NA]_T$ = 4 ppm

Mass	Absolute counts	% of total
237.21	7.87E+05	8.6
213.22	6.78E+05	7.4
251.21	6.36E+05	7.0
223.21	5.96E+05	6.5
249.21	4.83E+05	5.3
225.2	4.30E+05	4.7
211.21	4.05E+05	4.4
235.21	3.87E+05	4.2
263.22	3.28E+05	3.6
239.16	3.11E+05	3.4
209.19	2.99E+05	3.3
265.21	2.87E+05	3.2
197.18	2.55E+05	2.8
199.2	2.10E+05	2.3
277.21	1.56E+05	1.7
253.12	1.53E+05	1.7
261.22	1.51E+05	1.7
221.2	1.45E+05	1.6
185.18	1.42E+05	1.6
247.2	1.32E+05	1.4
279.24	1.17E+05	1.3
183.17	1.10E+05	1.2
157.09	1.03E+05	1.1
267.17	9.98E+04	1.1
275.19	9.84E+04	1.1
227.18	9.55E+04	1.0
273.19	9.34E+04	1.0
195.17	9.01E+04	1.0
259.19	7.40E+04	0.8
171.15	7.27E+04	0.8
TOTALS:	7.92E+06	87

Datafile: Merichem pH 4 sorted by intensity

Table 19: Quantitation of OSPW and SW samples as Merichem and PyBA equivalents, with and without I.S. and pH correction techniques, compared to results from AXYS

	CP-MIMS						AXYS	
Sample[a]	**$[NA]_T$ as Merichem (ppm)**				**$[NA]_T$ as PyBA (ppm)**		**$[NA]_T$ as M.C. (ppm)[51]**	**$[NA]_T$ as PyBA (ppm)**
	D.L.=0.1 ppm				*DL<0.01 ppm*			
	I.S., pH	***pH, no I.S.***	***I.S., no pH***	***No I.S., no pH***	***I.S., pH***	***I.S., no pH***		
OSPW1	38.6	11.0	22.0	0.1	19.5	17.0	-	25.9
OSPW2	443	572	389	510	196	200	-	150.6
OSPW3	26.7	7.2	19.9	0.1	17.6	19.4	-	-
OSPW4	0.2	0.0	0.1	-0.1	0.3	0.4	-	-
OSPW5	0.2	0.0	-0.1	-0.2	0.2	0.1	-	-
OSPW6	0.9	0.4	1.0	0.4	0.5	0.6	-	-
OSPW7	69.4	18.1	61.9	10.9	37.9	41.3	56.0	-
OSPW8	3.8	-3.0	5.0	-6.8	6.2	10.8	56.9	-
OSPW9	95.2	42.7	91.2	37.1	43.0	48.6	57.1	-
SW1	0.2	0.0	0.3	-0.1	0.2	0.3	-	-
SW2	-0.1	-0.1	-0.3	-0.3	0.0	0.0	-	-

[a] n=1 for all samples, except OSPW2 (n=3)

Datafile: Initial Comparison of OSPWs by CP-MIMS

Table 20: Parametric study with various amounts of two bases added to CP-MIMS acceptor phase to improve ionization of carboxylic acids. Four model compounds are presented at low concentration (8-11 ppb), and all data represents improvement factors from experiments performed with no base added

		CARBOXYLATED SPECIES		***HYDROXYLATED SPECIES***	
	BASE	**4tBCHCA**	**LA**	**NP**	**TC**
In MeOH	0.1% NH_4OH	0.5	0.2	0.1	0.1
	0.2% NH_4OH	0.3	0.0	0.1	0.0
	0.1% NH_4Ac	0.0	0.0	0.0	0.1
	0.2% NH_4Ac	0.0	0.0	0.0	0.1
In H_2O	0.05% NH_4OH	0.7	0.7	0.6	1.2
	0.1% NH_4OH	**2.6**	**1.9**	**2.1**	**1.8**
	0.2% NH_4OH	1.5	0.5	1.1	0.7
	0.1% NH_4Ac	0.0	0.0	0.0	0.0
	0.2% NH_4Ac	0.0	0.1	0.0	0.1
Just H_2O	5% H_2O	1.0	0.6	0.6	0.7
	10% H_2O	1.2	0.7	0.5	0.9
	15% H_2O	0.9	0.4	0.1	0.6
	20% H_2O	0.4	0.0	0.0	0.2

Datafiles: DLMIMS_146-155

Table 21: Calibration curve data (1-2300 ppb) for top 30 Merichem *m/z* chosen for targeted SIM method

m/z	Abundance in Merichem fullscan spectrum (%)	Equation of line in 1-2300 ppb Merichem calibration curve[a]	R^2
157	1.2	y = 0.0016x - 0.012	0.99458
183	1.0	y = 0.0015x + 0.0084	0.97836
185	1.7	y = 0.0016x + 0.029	0.98058
195	1.0	y = 0.0011x + 0.014	0.99382
197	3.2	y = 0.0027x + 0.047	0.98413
199	2.2	y = 0.0020x + 0.021	0.96841
209	3.2	y = 0.0029x + 0.056	0.98633
211	4.6	y = 0.0034x + 0.058	0.97153
213	6.4	y = 0.0050x + 0.10	0.96681
221	1.7	y = 0.0013x + 0.020	0.98732
223	5.8	y = 0.0048x + 0.073	0.97432
225	4.7	y = 0.0030x + 0.046	0.95818
227	1.7	y = 0.00080x + 0.020	0.93230
235	3.8	y = 0.0029x + 0.035	0.97358
237	7.5	y = 0.0053x + 0.073	0.95860
239	3.8	y = 0.0020x + 0.046	0.93667
247	1.1	y = 0.0010x - 0.021	0.96944
249	5.1	y = 0.0039x + 0.038	0.85632
251	7.3	y = 0.0041x + 0.096	0.93031
253	2.6	y = 0.0011x + 0.050	0.90694
259	0.6	y = 0.00045x + 0.0029	0.97596
261	1.2	y = 0.0010x - 0.020	0.93735
263	1.2	y = 0.0020x + 0.054	0.92425
265	0.5	y = 0.0017x + 0.084	0.88643
267	0.5	y = 0.00047x + 0.027	0.87790
273	0.9	y = 0.00050x + 0.0046	0.95979
275	0.7	y = 0.00061x + 0.010	0.88178
277	1.7	y = 0.00082x + 0.047	0.87192
279	1.5	y = 0.00061x + 0.045	0.84663
287	0.6	y = 0.00032x + 0.0056	0.93949

[a] Slopes in units of (ppb DA / ppb $[NA]_T$ as Merichem)
Datafile: DLMIMS_159

Appendix B: Fullscan Mass Spectra

Note: All fullscan mass spectra were captured from *m/z* 100-600, using a unit-resolution Waters-Micromass Quattro LC with ESI ionization source as per mass spectrometry conditions outlined in section 2.2.3. All samples were adjusted to pH < 4 and analyzed at concentrations well within the CP-MIMS LDR (0.1-3 ppm $[NA]_T$ as Merichem).

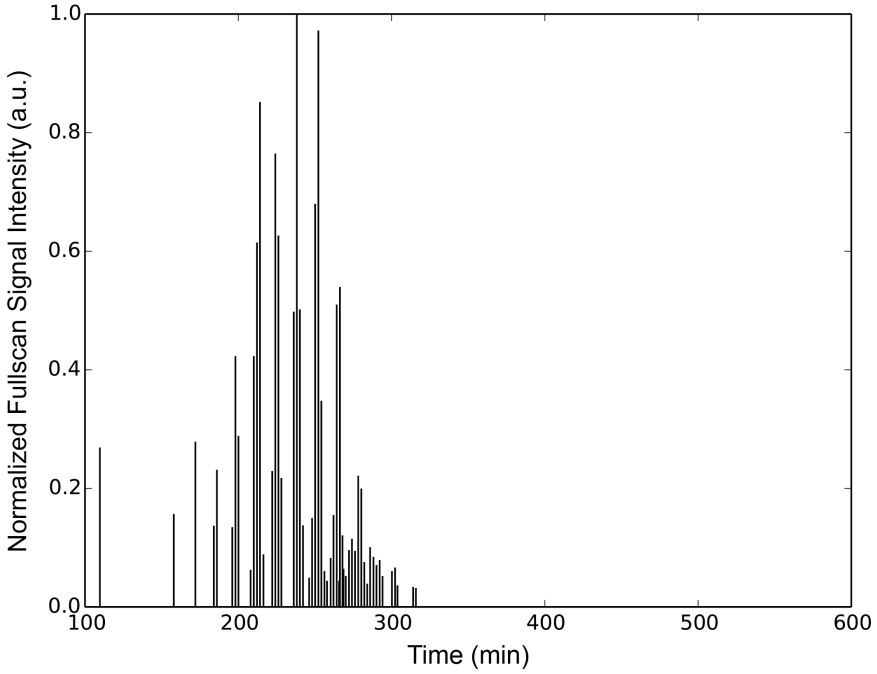

Figure 49: Merichem fullscan mass spectrum, dilution = 5,000,000X, $[NA]_T$ = 0.20 ppm as M.C. Datafile: DLMIMS_156

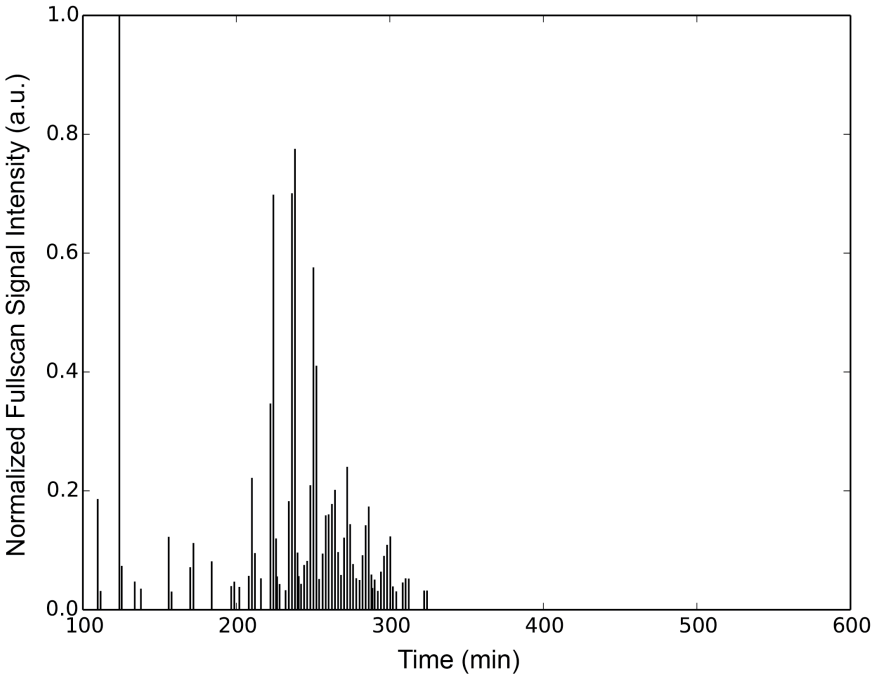

Figure 50: LVE1 fullscan mass spectrum, dilution = 1,082X, $[NA]_T$ = 2.5 ppm as LVE1 NAFCs (Environment Canada).[93] Datafile: DLMIMS_183

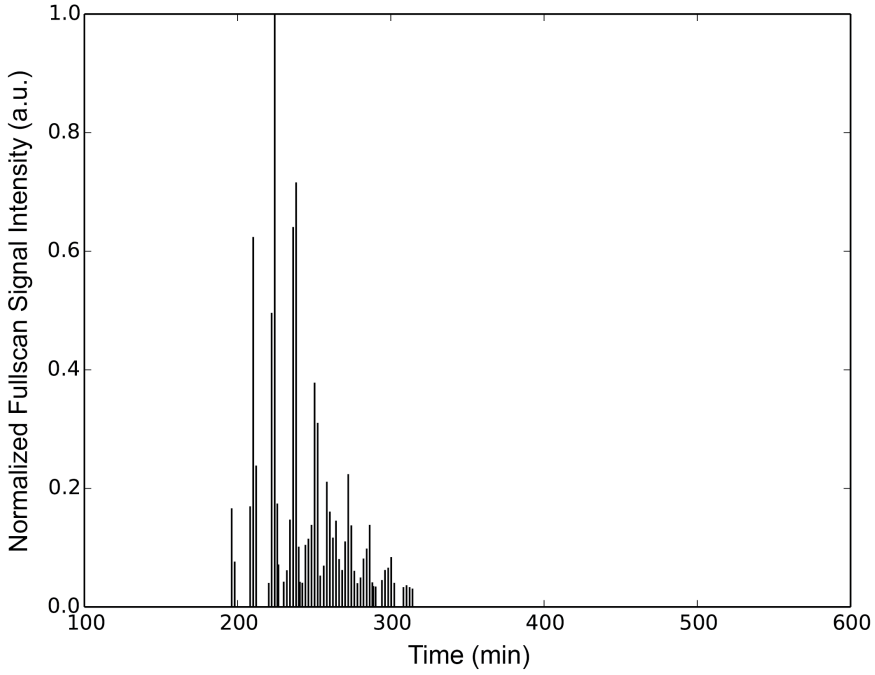

Figure 51: LVE2 fullscan mass spectrum, dilution = 1,157X, $[NA]_T$ = 6.9 ppm as LVE2 NAFCs (Environment Canada).[93] Datafile: DLMIMS_184

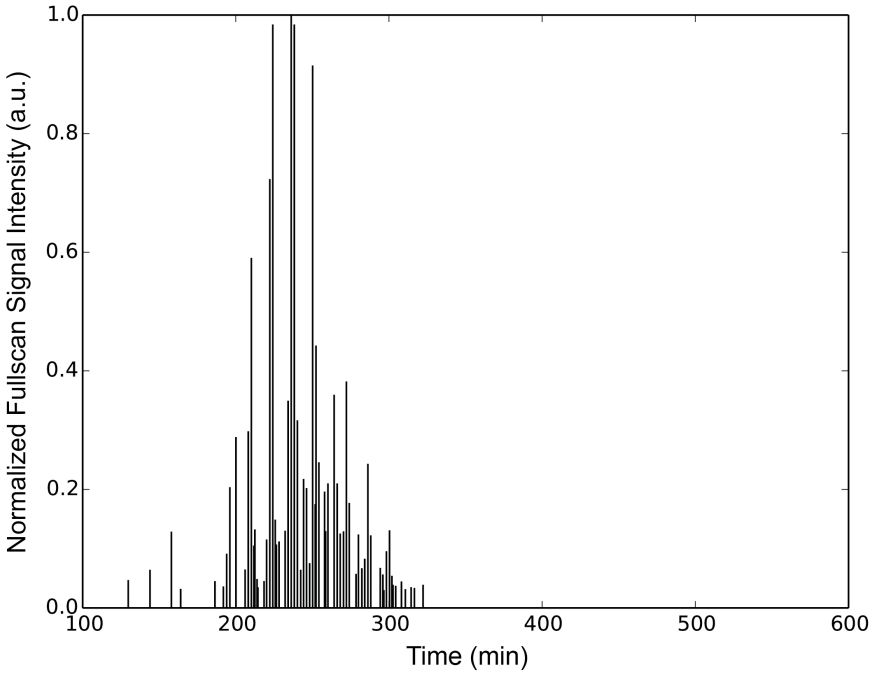

Figure 52: OSPW1 fullscan mass spectrum, dilution = 61.2X, $[NA]_T$ = 0.25 ppm as M.C. Datafile: DLMIMS_165

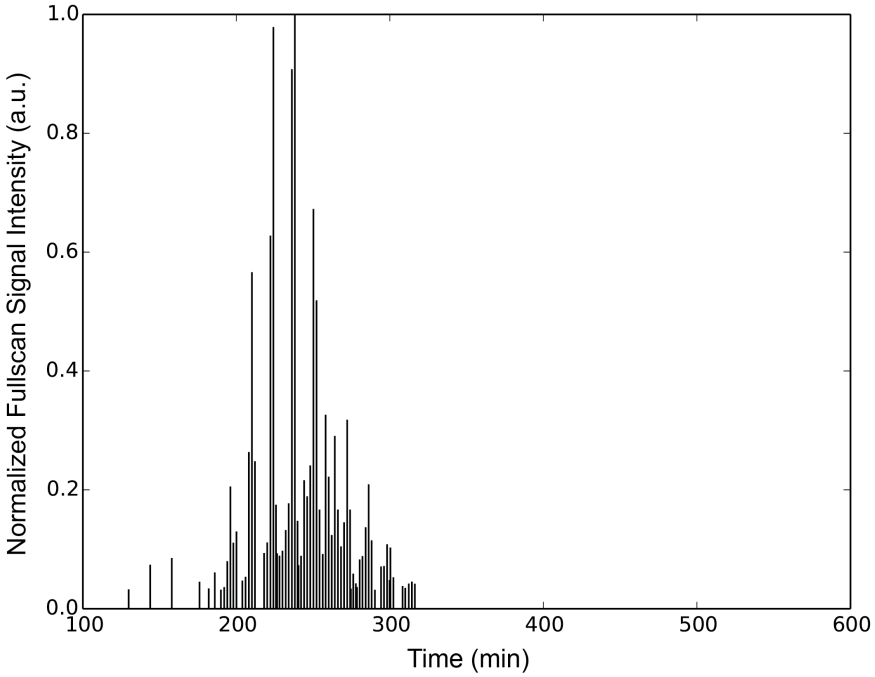

Figure 53: OSPW2 fullscan mass spectrum, dilution = 132X, $[NA]_T$ = 0.56 ppm as M.C. Datafile: DLMIMS_160

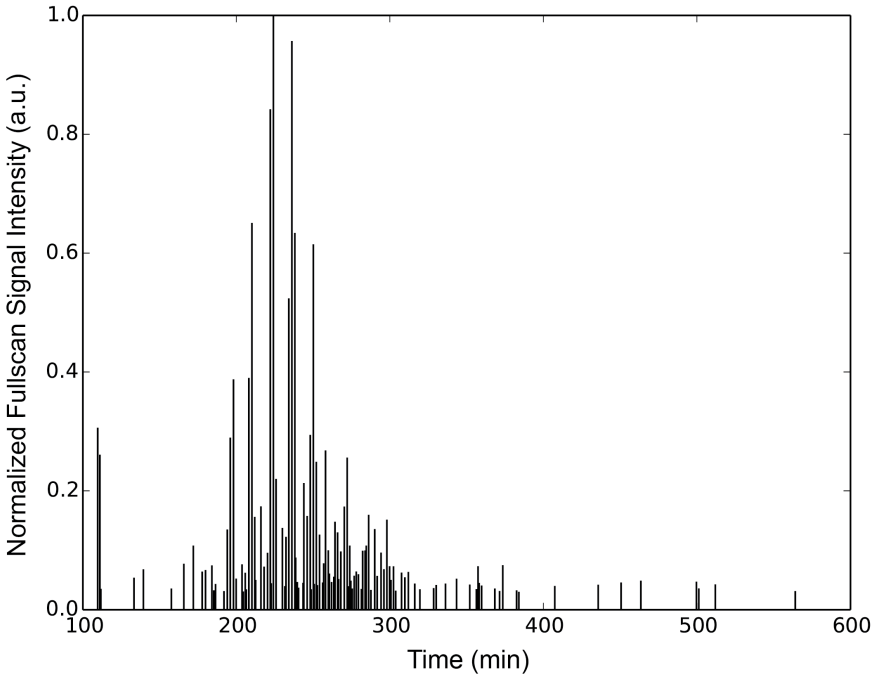

Figure 54: OSPW3 fullscan mass spectrum, dilution = 48.5X, $[NA]_T$ = 0.31 ppm as M.C. Datafile: DLMIMS_174

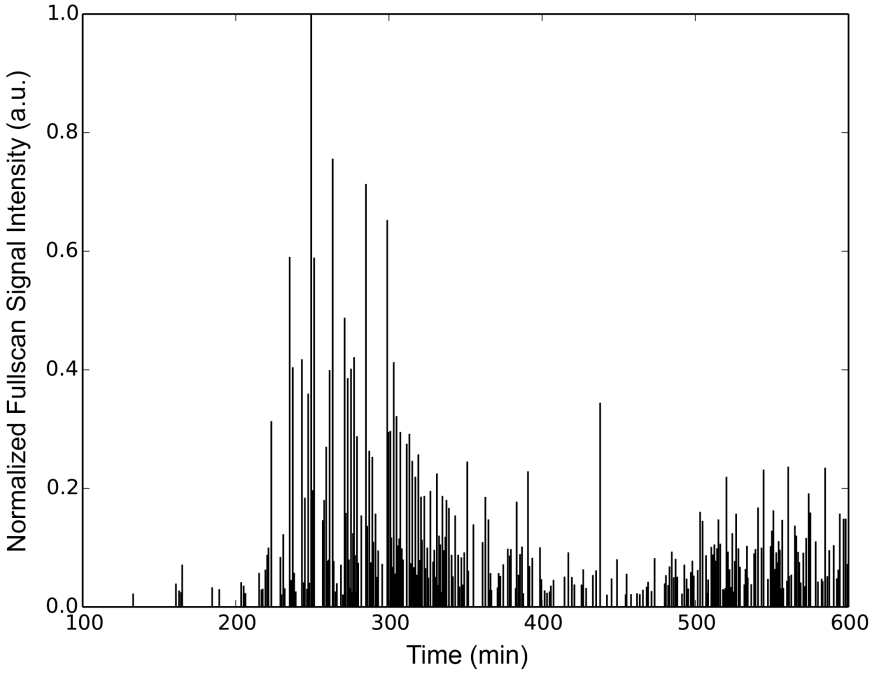

Figure 55: OSPW4 fullscan mass spectrum, undiluted, $[NA]_T$ = ~0.1 ppm as M.C. Datafile: DLMIMS_078

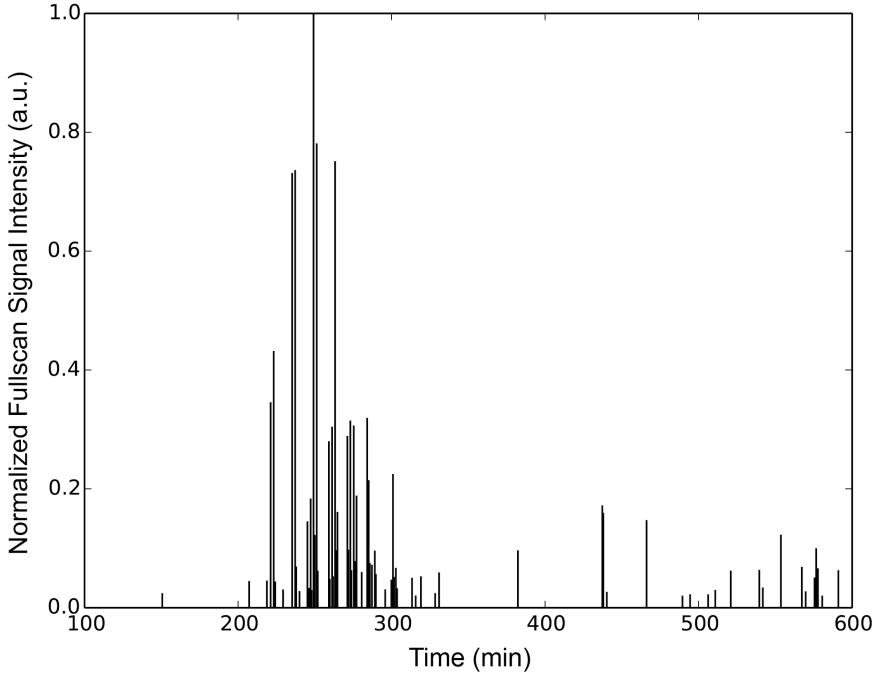

Figure 56: OSPW5 fullscan mass spectrum, undiluted, $[NA]_T$ < 0.1 ppm as M.C. (below CP-MIMS detection limits). Datafile: DLMIMS_079

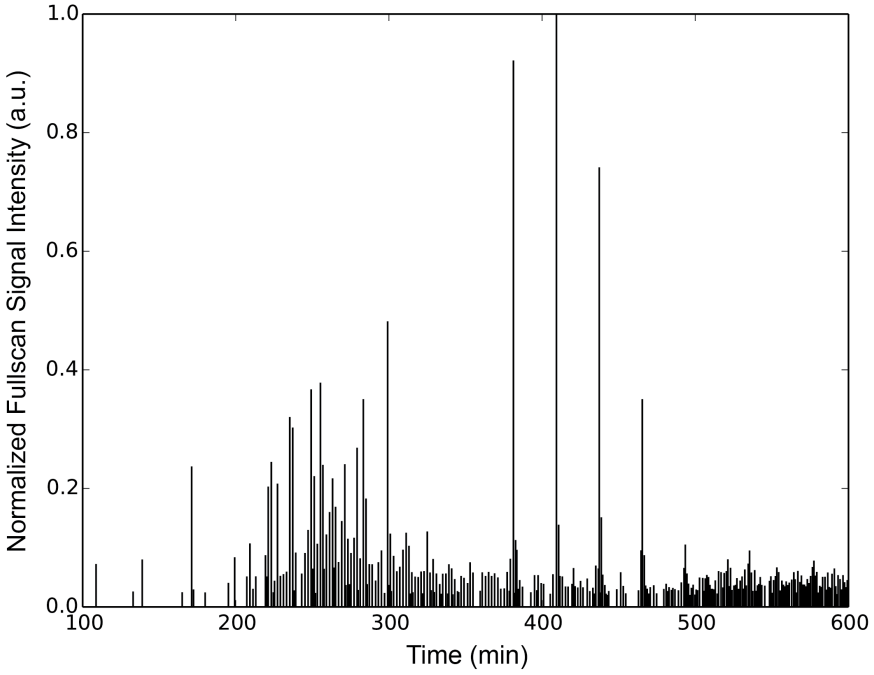

Figure 57: OSPW6 fullscan mass spectrum, undiluted, $[NA]_T$ = 1.0 ppm as M.C. Datafile: DLMIMS_080

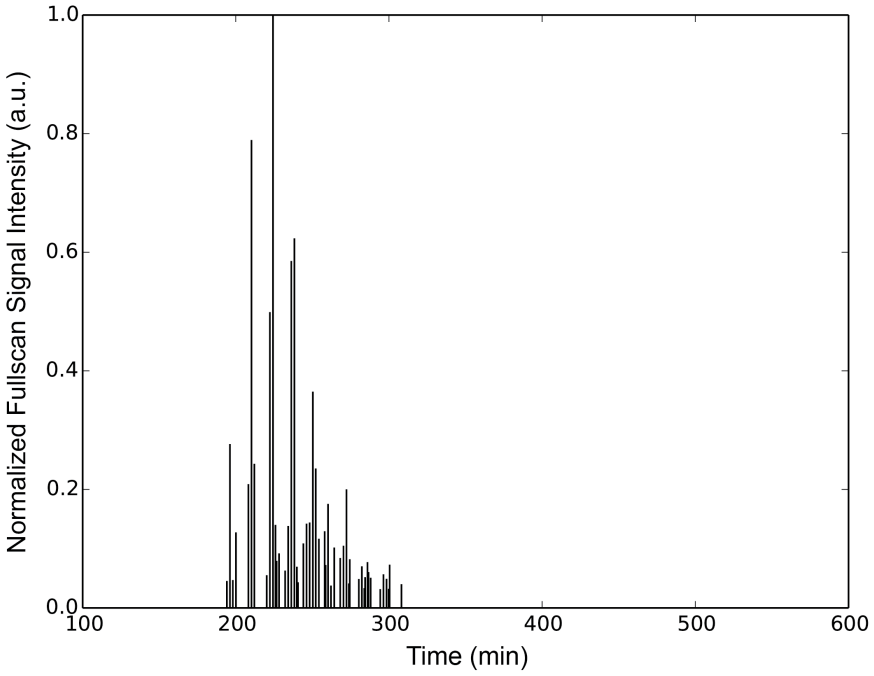

Figure 58: OSPW7 fullscan mass spectrum, dilution = 51.2X, $[NA]_T$ = 0.82 ppm as M.C. Datafile: DLMIMS_170

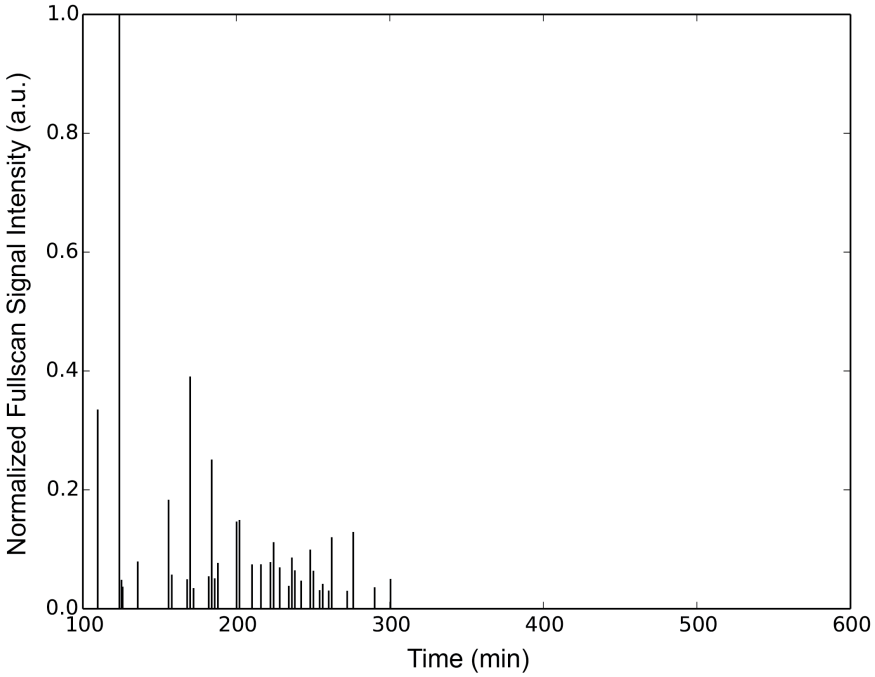

Figure 59: OSPW8 fullscan mass spectrum, dilution = 51.2X, $[NA]_T$ = 0.14 ppm as M.C. Datafile: DLMIMS_170

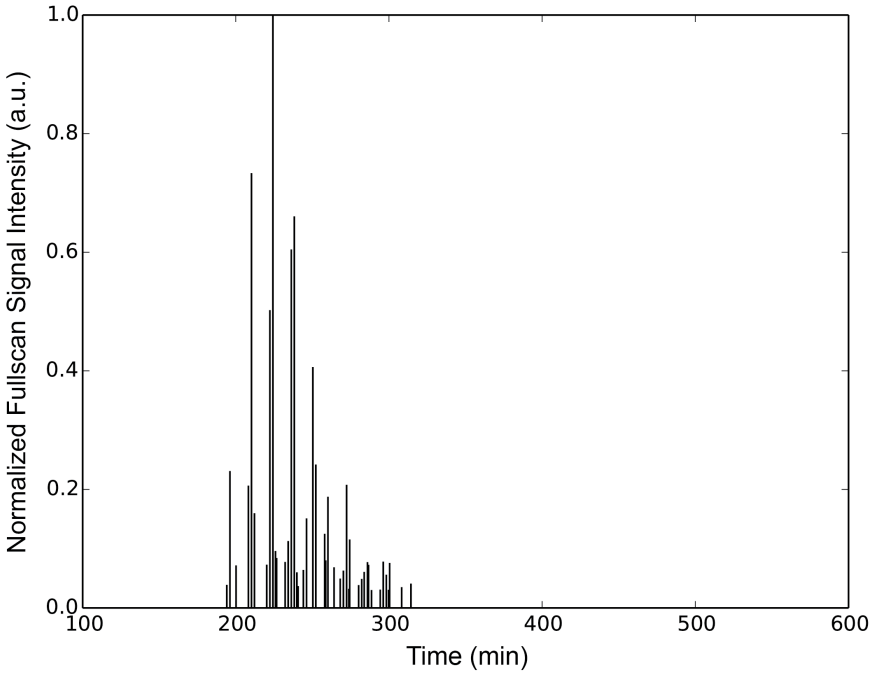

Figure 60: OSPW9 fullscan mass spectrum, dilution = 50.7X, $[NA]_T$ = 0.36 ppm as M.C. Datafile: DLMIMS_170

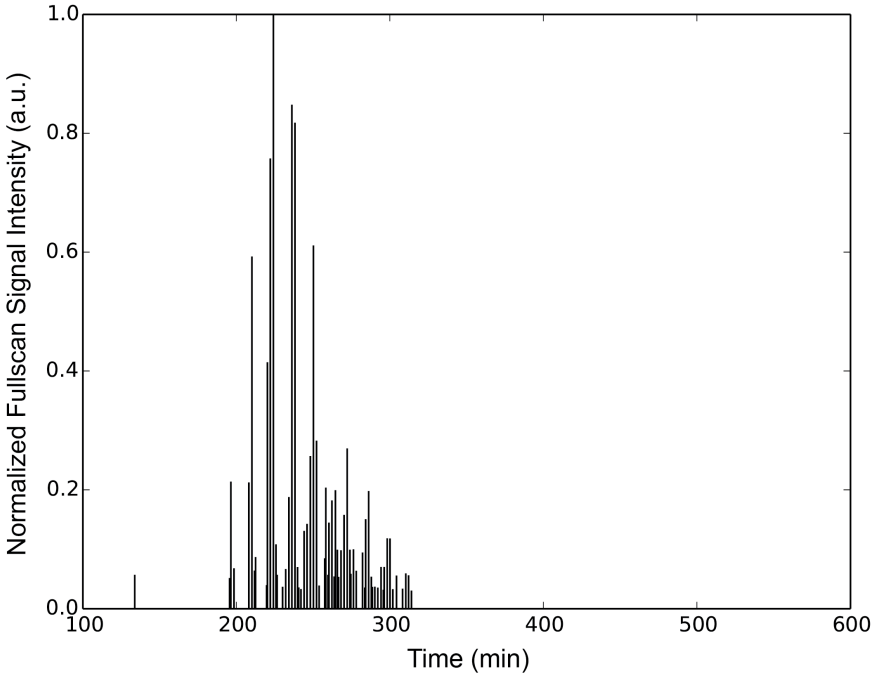

Figure 61: OSPW10 fullscan mass spectrum, dilution = 6.0X, $[NA]_T$ = 4.3 ppm as M.C. Datafile: DLMIMS_186

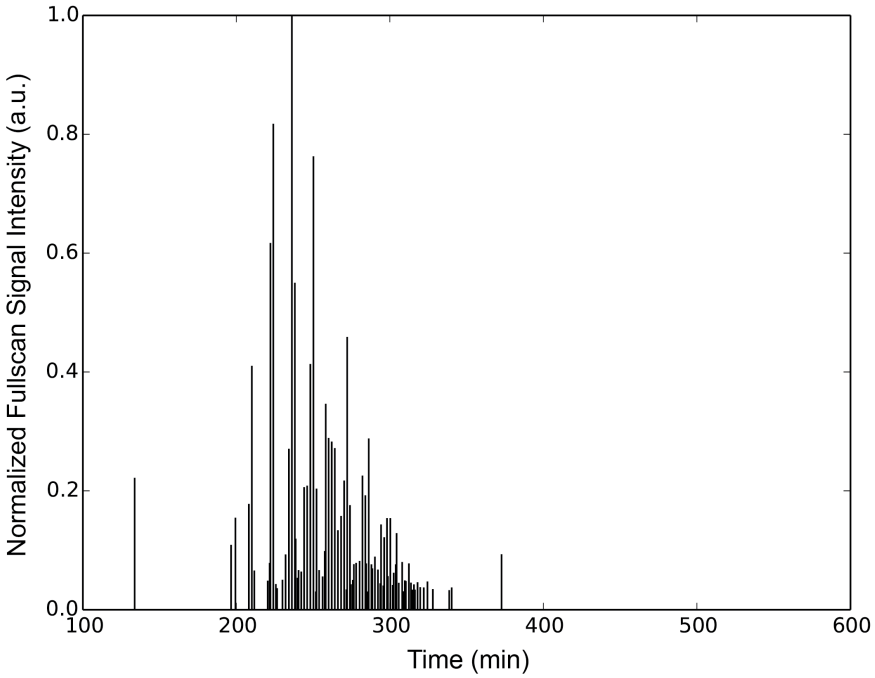

Figure 62: OSPW11 fullscan mass spectrum, dilution = 6.0X, $[NA]_T$ = 2.8 ppm as M.C. Datafile: DLMIMS_186

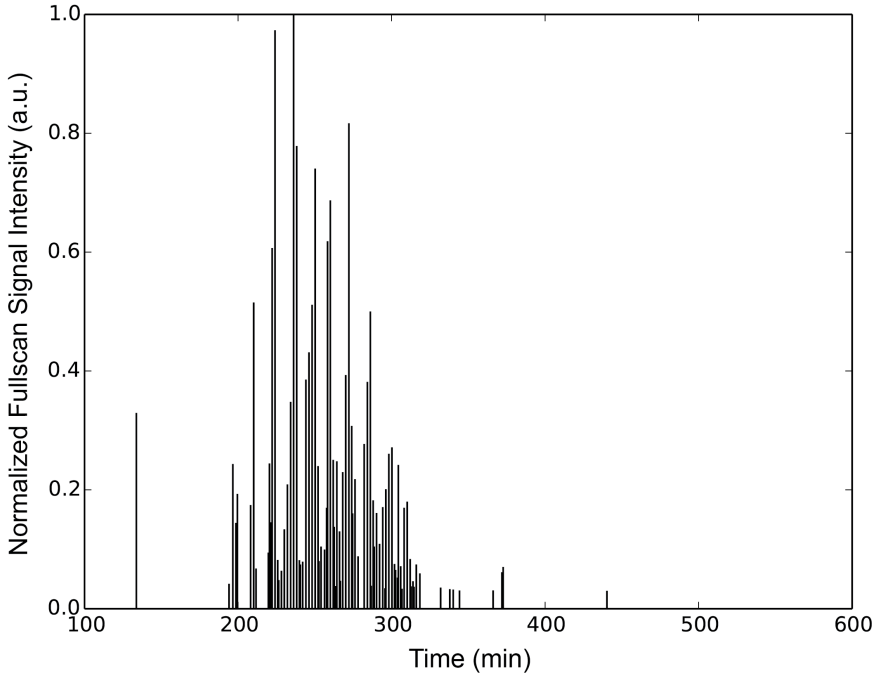

Figure 63: OSPW12 fullscan mass spectrum, dilution = 7.2X, $[NA]_T$ = 3.2 ppm as M.C. Datafile: DLMIMS_186

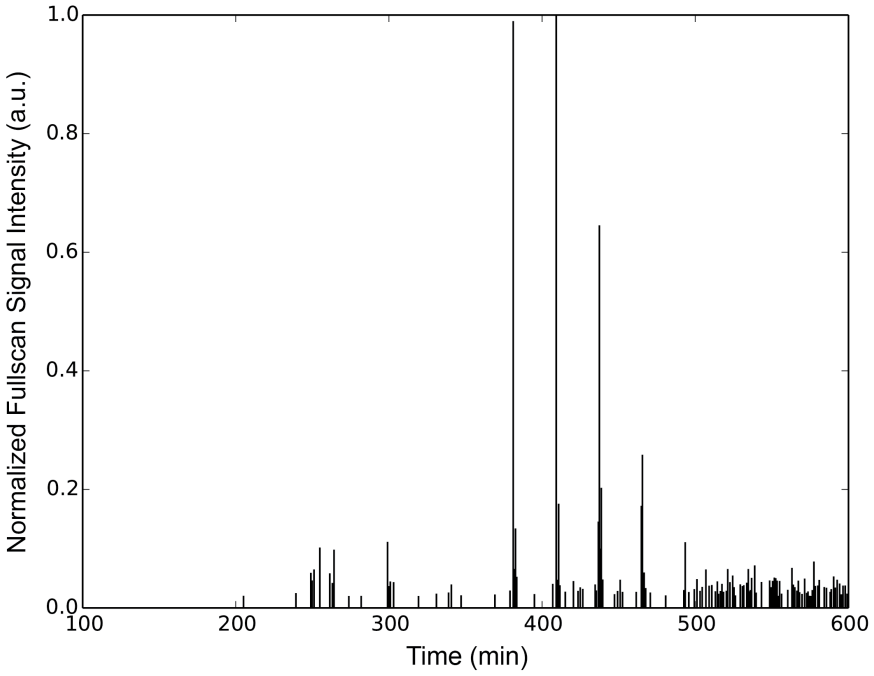

Figure 64: SW1 fullscan mass spectrum, undiluted, $[NA]_T$ = 0.30 ppm as M.C. Datafile: DLMIMS_081

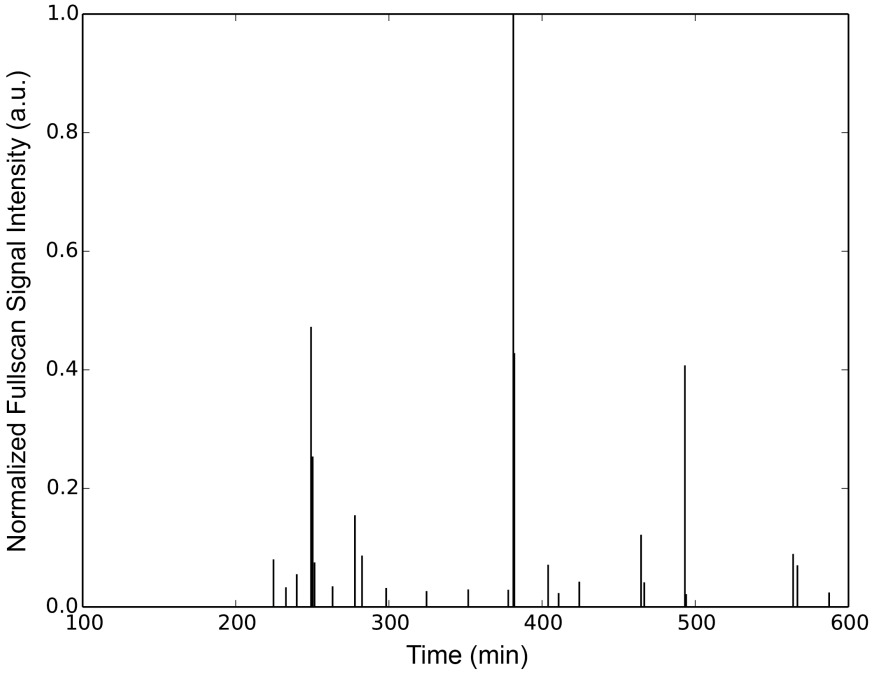

Figure 65: SW2 fullscan mass spectrum, undiluted, $[NA]_T$ < 0.1 ppm as M.C. (below CP-MIMS detection limits). Datafile: DLMIMS_082

Appendix C: Sample Workflow and Calculations for Quantitation of NAs by CP-MIMS

Data Extraction and Averaging

Raw chronogram data is exported from MassLynx™ software, copied into Excel as time (minutes) vs. mass spectrometer counts (intensity), and plotted on a graph to visualize, as seen below in Fig. 66.

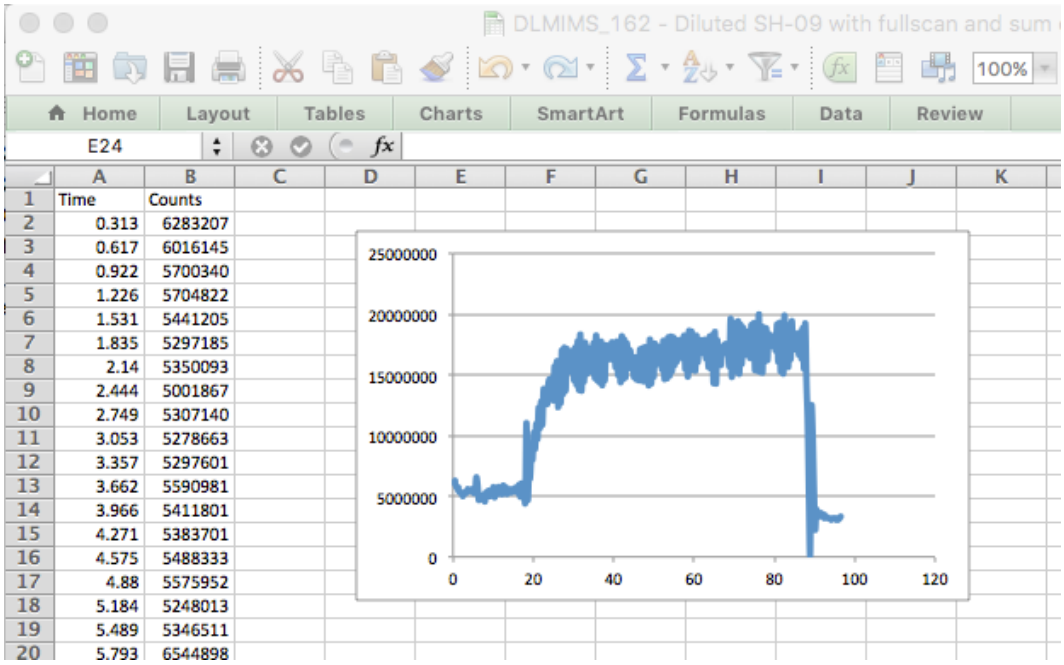

Figure 66: Raw fullscan TIC data for an OSPW quantitation experiment copied into Excel

Data for both the fullscan TIC (above) and SIM experiments for 30 *m/z* are copied into Excel in this fashion, and then averaged (10-pt boxcar) and baseline subtracted, as shown below for the internal standard SIM (decanoic acid at *m/z*=171) in Fig 67. The graph is updated to show the averaging and baseline subtraction. At t~15 minutes, decanoic acid is injected into the acceptor phase at 10 ppb, causing a rise to steady-state, and at t~85 minutes, it is rinsed out (end of the experiment).

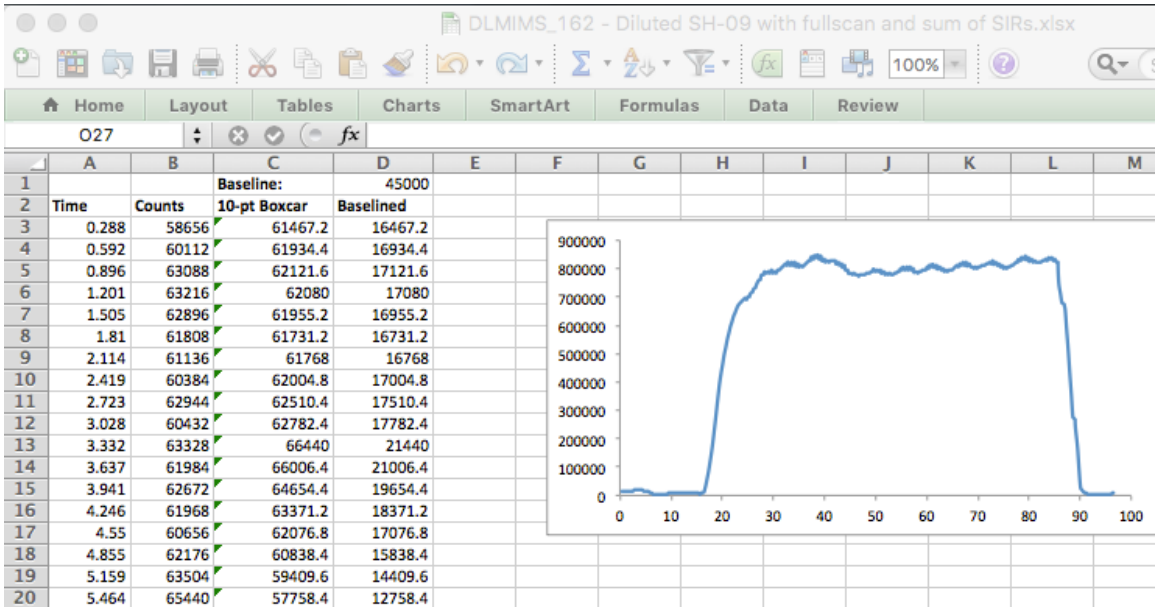

Figure 67: Averaged, baseline subtracted data for the DA internal standard

Each of the 30 SIMs are processed in a similar fashion. Fig. 68 presents example data for SIM *m/z*=237. At t~25 min, baseline is established. At t~43 min, the CP-MIMS probe is immersed in the OSPW being analyzed (at pH=4) and a rise to steady-state is observed. At t~85 min, the probe is rinsed.

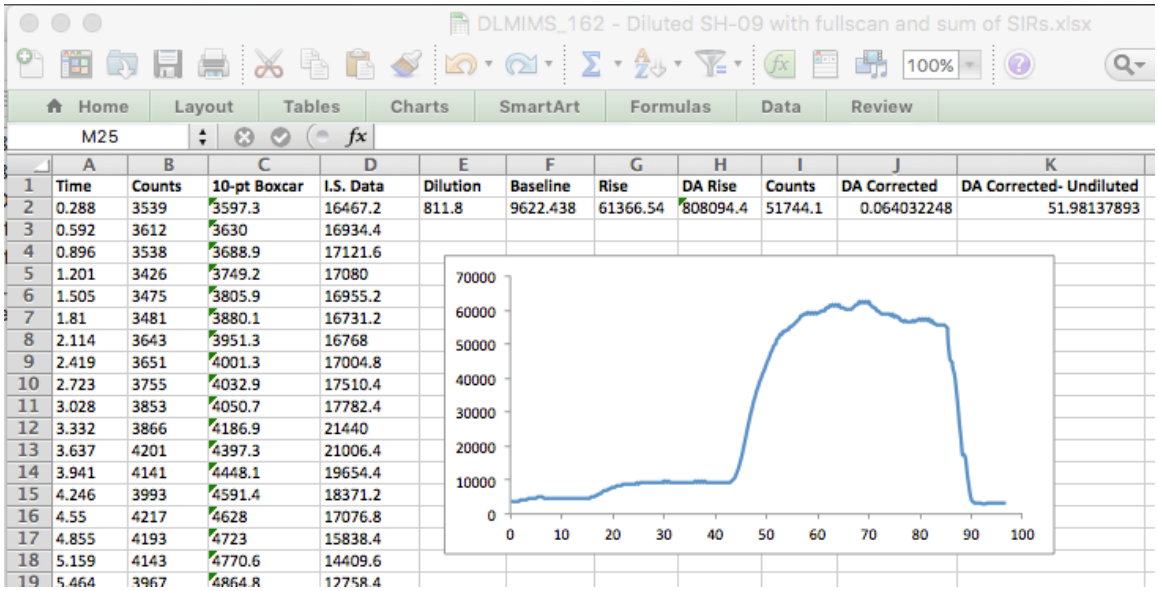

Figure 68: Processed data for one of 30 SIMs (*m/z*=237) collected for an OSPW quantitation experiment

Averaged, baseline-subtracted data for the internal standard is shown (copied from column D in Fig. 67), and baseline (35-40 min) and rise (65-70 min) regions are established based on ~5 minutes of steady-state signal. Data from these 5 minute windows is averaged and presented in columns F and G. The dilution of the sample is noted in column E.

Internal Standard Correction

The internal standard data from column D is averaged over the same 5 minute window as was used for the steady-state "rise" region of the OSPW being analyzed (65-70 min) and shown in column H (Fig. 69). The OSPW signal is baseline corrected ('rise' – 'baseline', or column G – column F), resulting in the "counts" in column I. Column I is then divided by column H (DA signal), giving the "DA corrected" signal in column J. This value is multiplied by the dilution factor from column E to give the "DA corrected-undiluted" signal in column K, and finally is multiplied by the DA concentration (10 ppb +/- 1 ppb) to give a final signal in units of ppb DA (column L).

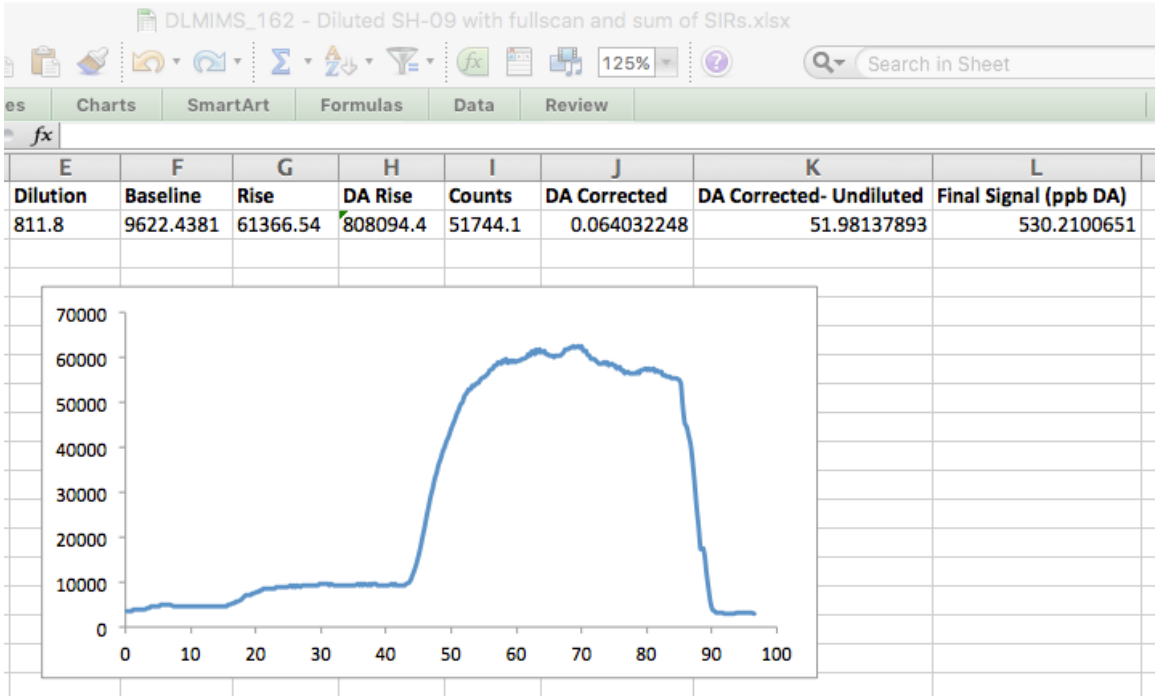

Figure 69: Data processing for SIM *m/z*=237

Quantitation with Direct Merichem Calibration

The final signal from the previous section is one of 30 (for each SIM *m/z*) that are summed to give the total DA-corrected signal for the OSPW being analyzed. This summed signal, with units of ppb DA, can be converted to equivalents of other external calibrants for comparisons with other units of quantitation, as elaborated upon in Chapter 3 of this thesis. One such calibration can be made with Merichem by constructing a calibration curve in a separate experiment (as described in detail in section 3.4.2). In fact, multiple direct Merichem calibration curves were run (*n=4*) from 1-2300 ppb $[NA]_T$ as M.C., and the slopes and intercepts of the best-fit lines found and averaged. The data in the Merichem calibrations was processed exactly as described previously – 30 SIM experiments were summed and DA corrected to give final signals in units of ppb DA. When plotted in a calibration curve, this gave units of ppb DA for the y-axis and units of ppb $[NA]_T$ as M.C. for the x-axis. The averaged slope and intercept values for four Merichem calibration curves were used to calibrate the OSPW signal obtained in the last section. Technically, only the diluted OSPW signal was processed with the Merichem calibration curve, as it falls within the calibration range (1-2300 ppb). For example:

Slope = 0.083515 (ppb DA/ppb M.C.)
Y-intercept = 1.7396 ppb DA
Summed, diluted OSPW signal from previous section = 5.9034 ppb DA

Equation 14: $$\frac{5.9034\ ppb\ DA - 1.7396\ ppb\ DA}{0.083515\ \frac{ppb\ DA}{ppb\ M.C.}} = 70.661\ ppb\ M.C.$$

This value is then multiplied by the dilution factor for the OSPW analyzed (in this case, the sample was 811.8X diluted) to give the final signal for the OSPW in units of ppb $[NA]_T$ as equivalents of Merichem:

Equation 15: $$70.661\ ppb\ M.C. \times 811.8 = \mathbf{57363\ ppb}\ [\boldsymbol{NA}]_{\boldsymbol{T}}\ \boldsymbol{as\ M.C.}$$

Quantitation with Standard Addition of PyBA

A second method of quantitation utilized in this thesis (and well described in section 3.4.1 previously) was a standard addition of PyBA, performed directly in the OSPW sample being analyzed. PyBA was monitored with a SIM experiment at *m/z*=287, and the standard addition (usually ~30 ppb final concentration of PyBA) was performed after a steady-state signal had been achieved for the OSPW at pH 4, as shown in Figure 27. Because SIM *m/z*=287 was a part of the 30 SIM experiments selected for the targeted SIM quantitation (and was a common peak in most OSPW samples), the data for *m/z* 287 before the standard addition was added (i.e., before t~70 min) was exported and processed just like the other 30 SIM experiments, as described earlier in this Appendix.

Fig. 70 shows the processed data for the SIM at *m/z*=287. At t~70 min, a large signal due to the ~30 ppb standard addition of PyBA is visible in the chronogram. This signal was processed separately from the earlier data. Cell E4 contains the final PyBA concentration after dilution in the sample (calculated from the known concentration of PyBA injected and the mass of the sample vial + OSPW solution). Cell F4 is the averaged steady-state signal before the standard addition from 65-70 min (essentially the same as the steady-state signal resulting from the OSPW at pH=4 from 60-65 min). Cell G4 is the steady-state signal after the PyBA signal has risen and stabilized (~80-85 min). Cell H4 is the averaged DA signal over the same time period (~80-85 min). Cell I4 is the baseline-corrected signal for the standard addition (cell G4 – cell F4), which is then corrected to the internal standard by dividing by cell H4 and multiplying by the DA concentration, resulting in the DA corrected signal (cell J4) with units of ppb DA. The final concentration of the PyBA standard addition is then divided by this corrected signal to produce the ratio in cell K4, which has units of [PyBA] (ppb) per signal at *m/z* 287 (ppb DA).

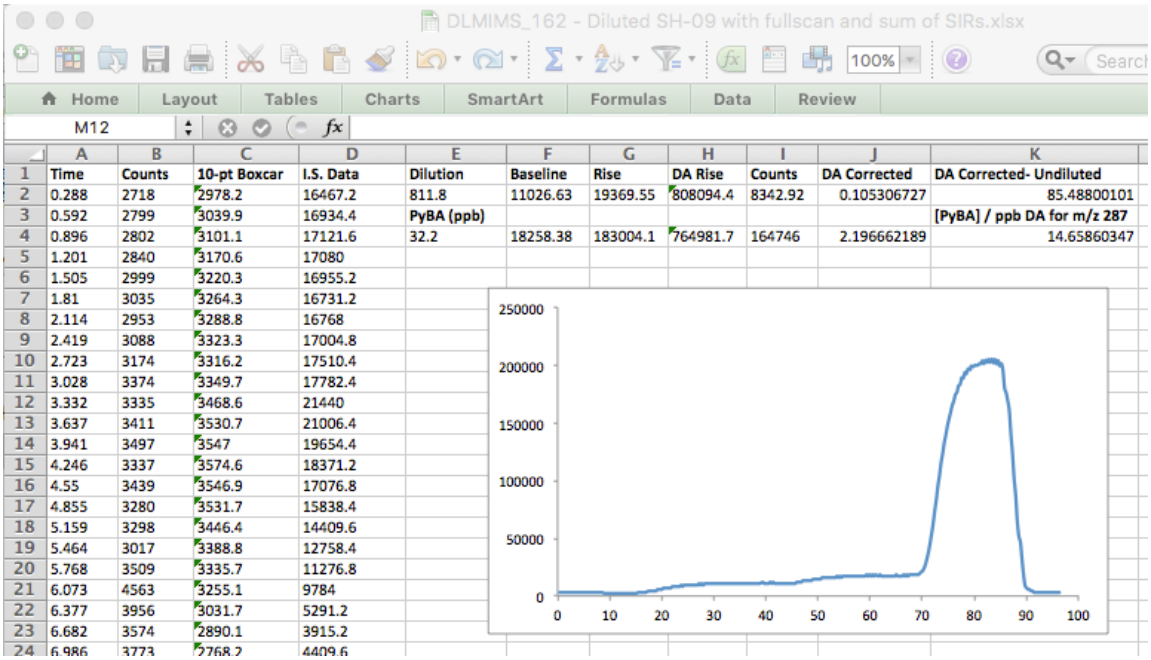

	A	B	C	D	E	F	G	H	I	J	K
1	Time	Counts	10-pt Boxcar	I.S. Data	Dilution	Baseline	Rise	DA Rise	Counts	DA Corrected	DA Corrected- Undiluted
2	0.288	2718	2978.2	16467.2	811.8	11026.63	19369.55	808094.4	8342.92	0.105306727	85.48800101
3	0.592	2799	3039.9	16934.4	PyBA (ppb)						[PyBA] / ppb DA for m/z 287
4	0.896	2802	3101.1	17121.6	32.2	18258.38	183004.1	764981.7	164746	2.196662189	14.65860347
5	1.201	2840	3170.6	17080							
6	1.505	2999	3220.3	16955.2							
7	1.81	3035	3264.3	16731.2							
8	2.114	2953	3288.8	16768							
9	2.419	3088	3323.3	17004.8							
10	2.723	3174	3316.2	17510.4							
11	3.028	3374	3349.7	17782.4							
12	3.332	3335	3468.6	21440							
13	3.637	3411	3530.7	21006.4							
14	3.941	3497	3547	19654.4							
15	4.246	3337	3574.6	18371.2							
16	4.55	3439	3546.9	17076.8							
17	4.855	3280	3531.7	15838.4							
18	5.159	3298	3446.4	14409.6							
19	5.464	3017	3388.8	12758.4							
20	5.768	3509	3335.7	11276.8							
21	6.073	4563	3255.1	9784							
22	6.377	3956	3031.7	5291.2							
23	6.682	3574	2890.1	3915.2							
24	6.986	3773	2768.2	4409.6							

Figure 70: Processed data for SIM *m/z*=287

This ratio can be applied to the OSPW signal (in units of ppb DA), giving the equivalent concentration of PyBA (in ppb) that would result in the same magnitude of signal at *m/z*=287. For example, the summed, diluted OSPW signal from the previous sections can be quantified via this standard addition, as shown below in Equation 16:

Equation 16: $$5.9034\ ppb\ DA \times \frac{14.659\ ppb\ PyBA}{ppb\ DA\ (m/z\ 287)} = 86.536\ ppb\ [NA]_T\ as\ PyBA$$

After the dilution of the sample is taken into account, the final quantitative value can be calculated as follows:

Equation 17: $$86.536\ ppb\ M.C. \times 811.8 = \mathbf{70250\ ppb}\ \mathbf{[NA]_T\ as\ PyBA}$$